

# Cross sections of $\alpha$ -induced reactions for targets with masses $A \approx 20 - 50$ at low energies

Peter Mohr<sup>1,2a</sup>

<sup>1</sup> Diakonie-Klinikum, D-74523 Schwäbisch Hall, Germany

<sup>2</sup> Institute for Nuclear Research ATOMKI, H-4001 Debrecen, Hungary

Received: date / Revised version: date

**Abstract.** A simple reduction scheme using so-called reduced energies  $E_{\text{red}}$  and reduced cross sections  $\sigma_{\text{red}}$  allows the comparison of heavy-ion induced reaction cross sections for a broad range of masses of projectile and target and over a wide energy range. A global behavior has been found for strongly bound projectiles whereas much larger reduced cross sections have been observed for weakly bound and halo projectiles. It has been shown that this simple reduction scheme works also well for  $\alpha$ -particle induced reactions on heavy target nuclei, but very recently significant deviations have been seen for  $\alpha+^{33}\text{S}$  and  $\alpha+^{23}\text{Na}$ . Motivated by these unexpected discrepancies, the present study analyses  $\alpha$ -induced reaction cross sections for targets with masses  $A \approx 20 - 50$ . The study shows that the experimental data for  $\alpha$ -induced reactions on nuclei with  $A \approx 20 - 50$  deviate slightly from the global behavior of reduced cross sections. However, in general the deviations evolve smoothly towards lower masses. The only significant outliers are the recent data for  $^{33}\text{S}$  and  $^{23}\text{Na}$  which are far above the general systematics, and some very old data may indicate that  $^{36}\text{Ar}$  and  $^{40}\text{Ar}$  are below the general trend. As expected, also the doubly-magic  $^{40}\text{Ca}$  nucleus lies slightly below the results for its neighboring nuclei. Overall, the experimental data are nicely reproduced by a statistical model calculation utilizing the simple  $\alpha$ -nucleus potential by McFadden and Satchler. Simultaneously with the deviation of reduced cross sections  $\sigma_{\text{red}}$  from the general behavior, the outliers  $^{23}\text{Na}$ ,  $^{33}\text{S}$ ,  $^{36}\text{Ar}$ , and  $^{40}\text{Ar}$  also show significant disagreement between experiment and statistical model calculation.

**PACS.** 25.55.-e 3H-, 3He-, and 4He-induced reactions – 24.10.Pa Thermal and statistical models

## 1 Introduction

The cross sections of  $\alpha$ -induced reactions play an important role in nuclear astrophysics. Stellar evolution and nucleosynthesis depend on the Maxwellian-averaged cross sections or reaction rates  $N_A \langle \sigma v \rangle$ . Some prominent examples in the mass range under study are the  $^{18}\text{Ne}(\alpha, p)^{21}\text{Na}$  reaction which is important for the break-out from hot CNO-cycles to the so-called rapid proton capture process (*rp*-process) [1,2], the  $^{22}\text{Ne}(\alpha, n)^{25}\text{Mg}$  reaction which is an important neutron source in the slow neutron capture process (*s*-process) [3,4,5], the  $^{23}\text{Na}(\alpha, p)^{26}\text{Mg}$  reaction which affects the production of galactic  $^{26}\text{Al}$  [6], and the  $^{40}\text{Ca}(\alpha, \gamma)^{44}\text{Ti}$  and  $^{44}\text{Ti}(\alpha, p)^{47}\text{V}$  reactions which govern the production and destruction of the tracer radionuclide  $^{44}\text{Ti}$  in core-collapse supernovae [7,8]. Beyond stellar evolution and nucleosynthesis,  $\alpha$ -induced reactions are also relevant for radionuclide production by energetic solar particles. It has been shown recently that  $\alpha$ -induced reactions may significantly contribute to the production of positron emitters [9], and the abundance of the radionu-

clide  $^{36}\text{Cl}$  may even be dominated by this scenario instead of stellar nucleosynthesis [10].

In addition to the astrophysical motivation,  $\alpha$ -induced reactions can also be used for analytical purposes. The thin-layer activation analysis technique has been suggested for the measurement of vanadium and chromium contents by  $(\alpha, X)$  reactions on  $^{\text{nat}}\text{V}$  and  $^{\text{nat}}\text{Cr}$  [11,12]. The concentration of sulfur which is an important element for material deterioration can be measured using the  $^{32}\text{S}(\alpha, p)^{35}\text{Cl}$  reaction [13]. At slightly higher energies  $\alpha$ -induced reactions are used for the production of important tracer elements. For biological and medical studies  $^{43}\text{K}$  can be produced by  $^{40}\text{Ar}(\alpha, p)^{43}\text{K}$  [14], and  $^{30}\text{P}$  can be made from  $^{27}\text{Al}(\alpha, n)^{30}\text{P}$  [15]. The behavior of aluminum in bio- and eco-systems can be traced by  $^{29}\text{Al}$  which is produced by the  $^{26}\text{Mg}(\alpha, p)^{29}\text{Al}$  reaction [16].

For heavy nuclei it has been found that the total reaction cross section  $\sigma_{\text{reac}}$  follows a general trend in the mass range around  $A \approx 90 - 150$  [17,18]. This trend becomes nicely visible when so-called reduced cross sections  $\sigma_{\text{red}}$  are plotted versus the reduced energy  $E_{\text{red}}$  as suggested by [19]. However, very recently huge discrepancies have been found for the light nuclei  $^{23}\text{Na}$  and  $^{33}\text{S}$  where much larger values for  $\sigma_{\text{red}}$  have been observed; a detailed dis-

<sup>a</sup> Email: [WidmaierMohr@t-online.de](mailto:WidmaierMohr@t-online.de); [mohr@atomki.mta.hu](mailto:mohr@atomki.mta.hu)

cussion of  $\alpha$ -induced reactions of  $^{33}\text{S}$  was provided recently in [20].

Cross sections for intermediate mass and heavy targets are usually calculated within the statistical model (StM). The basic prerequisite of the StM is a sufficiently high level density in the compound nucleus at the excitation energy  $E^* = E_{\text{c.m.}} + S_\alpha$  where  $E_{\text{c.m.}}$  is the energy in the center-of-mass system and  $S_\alpha$  is the separation energy of the  $\alpha$ -particle in the compound nucleus. This prerequisite is certainly fulfilled for heavy nuclei, but it will be shown that the experimental cross sections in the lower mass range under study can also be nicely reproduced by StM calculations.

For heavy nuclei  $\alpha$ -induced cross sections are typically very well reproduced by StM calculations at energies above the Coulomb barrier. This finding is almost independent of the chosen parameterization of the underlying  $\alpha$ -nucleus potential. At low energies the application of the widely used  $\alpha$ -nucleus potential by McFadden and Satchler [21] typically overestimates the experimental cross sections. This general behavior of the McFadden/Satchler potential extends down to at least  $^{64}\text{Zn}$  [22] and  $^{58}\text{Ni}$  [23]. Much efforts have been done in the last decade to provide improved  $\alpha$ -nucleus potentials (e.g., [18, 24, 25, 26, 27]).

Contrary to this general behavior for heavy nuclei, StM calculations underestimate the experimental results for  $^{23}\text{Na}$  and  $^{33}\text{S}$ . However, for the even lighter target  $^{18}\text{Ne}$  and the  $^{18}\text{Ne}(\alpha, p)^{21}\text{Na}$  reaction it was found that StM calculations are – at least on average – in reasonable agreement with experimental results although the excitation function is governed by many resonances which cannot be reproduced by the StM [28]. It is the main scope of the present study to analyze the mass region around  $A \approx 20 - 50$  and search for systematic trends for the cross sections of  $\alpha$ -induced reactions. For this purpose all available reaction data in the EXFOR database [29] are reviewed and compared to StM calculations. It will be shown that there is a smooth trend of increasing reduced cross sections  $\sigma_{\text{red}}$  with decreasing mass  $A$  with two exceptionally large  $\sigma_{\text{red}}$  values for  $^{23}\text{Na}$  and  $^{33}\text{S}$  and perhaps exceptionally low  $\sigma_{\text{red}}$  values for  $^{36}\text{Ar}$  and  $^{40}\text{Ar}$  (based on very few data points from an experiment in the 1950s).

The paper is organized as follows. Sec. 2 provides general information on reduced energies  $E_{\text{red}}$  and reduced cross sections  $\sigma_{\text{red}}$  (Sec. 2.1), on the  $\alpha$ -nucleus potential which is the essential ingredient for the StM (Sec. 2.2), and on the statistical model itself (Sec. 2.3). Sec. 3 briefly discusses experimental techniques for the determination of the relevant cross sections. Results for nuclei with  $A \approx 20 - 50$  are presented in Sec. 4. For each nucleus under study the available experimental data are reviewed and compared to a theoretical prediction from the StM, and the reduced cross section is shown. The results are discussed in Sec. 5, and finally conclusions are drawn in Sec. 6. A list of all nuclei under study is provided in Table 1 which includes the residual nuclei and the reaction  $Q$ -values for the  $(\alpha, \gamma)$ ,  $(\alpha, n)$ , and  $(\alpha, p)$  reactions. The  $Q$ -value data are taken from nuclear masses in the latest AME2012 evaluation [30, 31].

## 2 General considerations

### 2.1 Reduced energy $E_{\text{red}}$ and reduced cross section

$\sigma_{\text{red}}$

A simple reduction scheme for the comparison of heavy-ion induced reactions has been suggested by Gomes *et al.* [19]. The so-called reduced cross sections  $\sigma_{\text{red}}$  and reduced energies  $E_{\text{red}}$  are defined by:

$$E_{\text{red}} = \frac{(A_P^{1/3} + A_T^{1/3})E_{\text{c.m.}}}{Z_P Z_T} \quad (1)$$

$$\sigma_{\text{red}} = \frac{\sigma_{\text{reac}}}{(A_P^{1/3} + A_T^{1/3})^2} \quad (2)$$

The reduced energy  $E_{\text{red}}$  takes into account the different heights of the Coulomb barrier in the systems under consideration, whereas the reduced reaction cross section  $\sigma_{\text{red}}$  scales the measured total reaction cross section  $\sigma_{\text{reac}}$  according to the geometrical size of the projectile-plus-target system. It is found that the reduced cross sections  $\sigma_{\text{red}}$  show a very similar behavior for a broad range of projectiles and targets over a wide energy range. Significantly higher values of  $\sigma_{\text{red}}$  are found for weakly bound projectiles (like e.g.  $^{6,7}\text{Li}$ ) or halo projectiles (e.g.  $^6\text{He}$ ), see [32, 33]. Results for  $\alpha$ -induced reactions on heavy target nuclei fit into the systematics of heavy-ion induced reactions [17, 18]. Results are shown in Fig. 1.

The experimental  $\sigma_{\text{red}}$  data for  $^{34}\text{S}$  and  $^{50}\text{Cr}$  have been derived from the experimental angular distributions of Bredbecka *et al.* [34] by phase shift fits according to [35] (see Figs. 2 and 3). The data point for  $^{44}\text{Ti}$  at  $E_{\text{red}} \approx 2.52$  MeV has been taken from the analysis of elastic  $^{44}\text{Ti}(\alpha, \alpha)^{44}\text{Ti}$  scattering in [36]; it is hardly visible because it overlaps with a data point for  $^{34}\text{S}$ . The low-energy data points for  $^{44}\text{Ti}$  will be explained later (Sec. 4.7). As can be seen from Fig. 1, the  $\sigma_{\text{red}}$  values for lighter targets seem to be close above the general systematics with increasing differences towards lower energies and lower masses.

Interestingly, the relation between the reduced energy  $E_{\text{red}}$  and the most effective energy for the determination of astrophysical reaction rates (the so-called Gamow window) is practically independent of the target mass  $A_T$  and target charge number  $Z_T$  for  $\alpha$ -induced reactions. In the mass range under study the Gamow window is found at  $E_{\text{red}} \approx 0.29$  MeV for  $T_9 = 1$  (where  $T_9$  is the temperature in Giga-Kelvin); the variation between  $^{21}\text{Ne}$  ( $E_{\text{red}} = 0.293$  MeV) and  $^{51}\text{V}$  ( $E_{\text{red}} = 0.279$  MeV) is practically negligible (and even for heavy nuclei like  $^{208}\text{Pb}$  a close value of  $E_{\text{red}} = 0.264$  MeV is found for  $T_9 = 1$ ).  $T_9 = 2$  corresponds to  $E_{\text{red}} \approx 0.45$  MeV, and  $T_9 = 3$  corresponds to  $E_{\text{red}} \approx 0.59$  MeV for all nuclei under study in this work. Further details on the relation between the Gamow window and the corresponding reduced energy  $E_{\text{red}}$  will be given in [37].

**Table 1.**  $Q$ -values of  $\alpha$ -induced reactions (taken from AME2012 [30,31]). Stable residual nuclei are underlined.

Section	target	Z	N	$(\alpha,\gamma)$		$(\alpha,n)$		$(\alpha,p)$	
				residual	$Q$ (MeV)	residual	$Q$ (MeV)	residual	$Q$ (MeV)
4.2	$^{50}\text{Cr}$	24	26	$^{54}\text{Fe}$	+8.417	$^{53}\text{Fe}$	-4.961	$^{53}\text{Mn}$	-0.437
4.3	$^{51}\text{V}$	23	28	$^{55}\text{Mn}$	+7.933	$^{54}\text{Mn}$	-2.294	$^{54}\text{Cr}$	-0.134
4.4	$^{50}\text{V}$	23	27	$^{54}\text{Mn}$	+8.758	$^{53}\text{Mn}$	-0.181	$^{53}\text{Cr}$	+1.198
4.5	$^{48}\text{Ti}$	22	26	$^{52}\text{Cr}$	+9.351	$^{51}\text{Cr}$	-2.687	$^{51}\text{V}$	-1.152
4.6	$^{46}\text{Ti}$	22	24	$^{50}\text{Cr}$	+8.560	$^{49}\text{Cr}$	-4.441	$^{49}\text{V}$	-1.030
4.7	$^{44}\text{Ti}$	22	22	$^{48}\text{Cr}$	+7.698	$^{47}\text{Cr}$	-8.634	$^{47}\text{V}$	-0.407
4.8	$^{45}\text{Sc}$	21	24	$^{49}\text{V}$	+9.315	$^{48}\text{V}$	-2.241	$^{48}\text{Ti}$	+2.257
4.9	$^{48}\text{Ca}$	20	28	$^{52}\text{Ti}$	+7.669	$^{51}\text{Ti}$	-0.139	$^{49}\text{Sc}$	-5.860
4.10	$^{42}\text{Ca}$	20	22	$^{46}\text{Ti}$	+8.005	$^{45}\text{Ti}$	-5.185	$^{45}\text{Sc}$	-2.340
4.11	$^{40}\text{Ca}$	20	20	$^{44}\text{Ti}$	+5.127	$^{43}\text{Ti}$	-11.172	$^{43}\text{Sc}$	-3.522
4.12	$^{41}\text{K}$	19	22	$^{45}\text{Sc}$	+7.937	$^{44}\text{Sc}$	-3.390	$^{44}\text{Ca}$	+1.045
4.13	$^{40}\text{K}$	19	21	$^{44}\text{Sc}$	+6.705	$^{43}\text{Sc}$	-2.994	$^{43}\text{Ca}$	+0.009
4.14	$^{39}\text{K}$	19	20	$^{43}\text{Sc}$	+4.806	$^{42}\text{Sc}$	-7.332	$^{42}\text{Ca}$	-0.124
4.15	$^{40}\text{Ar}$	18	22	$^{44}\text{Ca}$	+8.854	$^{43}\text{Ca}$	-2.277	$^{43}\text{K}$	-3.329
4.16	$^{36}\text{Ar}$	18	18	$^{40}\text{Ca}$	+7.040	$^{39}\text{Ca}$	-8.595	$^{39}\text{K}$	-1.288
4.17	$^{37}\text{Cl}$	17	20	$^{41}\text{K}$	+6.223	$^{40}\text{K}$	-3.872	$^{40}\text{Ar}$	-1.586
4.18	$^{35}\text{Cl}$	17	18	$^{39}\text{K}$	+7.219	$^{38}\text{K}$	-5.859	$^{38}\text{Ar}$	+0.837
4.19	$^{34}\text{S}$	16	18	$^{38}\text{Ar}$	+7.208	$^{37}\text{Ar}$	-4.630	$^{37}\text{Cl}$	-3.034
4.20	$^{33}\text{S}$	16	17	$^{37}\text{Ar}$	+6.787	$^{36}\text{Ar}$	-2.001	$^{36}\text{Cl}$	-1.928
4.21	$^{32}\text{S}$	16	16	$^{36}\text{Ar}$	+6.641	$^{35}\text{Ar}$	-8.615	$^{35}\text{Cl}$	-1.866
4.22	$^{31}\text{P}$	15	16	$^{35}\text{Cl}$	+6.998	$^{34}\text{Cl}$	-5.647	$^{34}\text{S}$	+0.627
4.23	$^{30}\text{Si}$	14	16	$^{34}\text{S}$	+7.924	$^{33}\text{S}$	-3.494	$^{33}\text{P}$	-2.960
4.24	$^{29}\text{Si}$	14	15	$^{33}\text{S}$	+7.116	$^{32}\text{S}$	-1.526	$^{32}\text{P}$	-2.454
4.25	$^{28}\text{Si}$	14	14	$^{32}\text{S}$	+6.948	$^{31}\text{S}$	-8.097	$^{31}\text{P}$	-1.916
4.26	$^{27}\text{Al}$	13	14	$^{31}\text{P}$	+9.669	$^{30}\text{P}$	-2.643	$^{30}\text{Si}$	+2.372
4.27	$^{26}\text{Mg}$	12	14	$^{30}\text{Si}$	+10.643	$^{29}\text{Si}$	+0.034	$^{29}\text{Al}$	-2.874
4.28	$^{25}\text{Mg}$	12	13	$^{29}\text{Si}$	+11.127	$^{28}\text{Si}$	+2.654	$^{28}\text{Al}$	-1.206
4.29	$^{24}\text{Mg}$	12	12	$^{28}\text{Si}$	+9.984	$^{27}\text{Si}$	-7.196	$^{27}\text{Al}$	-1.601
4.30	$^{23}\text{Na}$	11	12	$^{27}\text{Al}$	+10.092	$^{26}\text{Al}$	-2.966	$^{26}\text{Mg}$	+1.821
4.31	$^{22}\text{Ne}$	10	12	$^{26}\text{Mg}$	+10.615	$^{25}\text{Mg}$	-0.478	$^{25}\text{Na}$	-3.531
4.32	$^{21}\text{Ne}$	10	11	$^{25}\text{Mg}$	+9.886	$^{24}\text{Mg}$	+2.555	$^{24}\text{Na}$	-2.178
4.33	$^{20}\text{Ne}$	10	10	$^{24}\text{Mg}$	+9.317	$^{23}\text{Mg}$	-7.215	$^{23}\text{Na}$	-2.376
4.34	$^{18}\text{Ne}$	10	8	$^{22}\text{Mg}$	+8.142	$^{21}\text{Mg}$	-11.242	$^{21}\text{Na}$	+2.638
4.35	$^{19}\text{F}$	9	10	$^{23}\text{Na}$	+10.467	$^{22}\text{Na}$	-1.952	$^{22}\text{Ne}$	+1.673

## 2.2 $\alpha$ -nucleus potential

For heavy nuclei it has been found that total reaction cross sections  $\sigma_{\text{reac}}$  and thus reduced cross sections  $\sigma_{\text{red}}$  can be reproduced by almost any reasonable  $\alpha$ -nucleus potential at energies above the Coulomb barrier. The reason for this universal behavior is discussed in detail in [38,39]. As an example the reduced cross sections for  $^{140}\text{Ce}$  are calculated from three global  $\alpha$ -nucleus potentials. The dashed green line in Fig. 1 shows the result from the ATOMKI-V1 potential which was derived from elastic scattering data in the mass range  $A \approx 90 - 150$  [18]. The red dash-dotted line is calculated from the many-parameter potential by Avrigeanu *et al.* in the version of [26] which was derived from elastic scattering and reaction data in a similar mass range, and the blue dotted line corresponds to the old and very simple 4-parameter potential by McFadden and Satchler [21]. It is obvious that the results are very similar above  $E_{\text{red}} \approx 0.8\text{MeV}$ , but at lower energies significant discrepancies appear. As a typical result for heavy

nuclei it has been found that the McFadden/Satchler potential strongly overestimates experimental cross sections at low energies. This may be a consequence of the missing energy dependence of the imaginary part of the McFadden/Satchler potential, and noticeable improvements have been achieved by adding such an energy dependence (e.g., [40,41]). The ATOMKI-V1 potential has also a slight trend to overestimate experimental cross sections at low energies [18,39], and the Avrigeanu potential [26,27] typically slightly underestimates experimental data at very low energies.

As the ATOMKI-V1 potential and the Avrigeanu potential have not been optimized for the mass range under study in this work, reduced cross sections  $\sigma_{\text{red}}$  for the nuclei  $^{51}\text{V}$ ,  $^{36}\text{Ar}$ , and  $^{21}\text{Ne}$  have been calculated from the McFadden/Satchler potential (full black lines in Fig. 1). It will be shown later that the McFadden/Satchler potential gives excellent predictions in the whole mass range  $A \approx 20 - 50$ . The shown calculations for  $^{51}\text{V}$ ,  $^{36}\text{Ar}$ , and  $^{21}\text{Ne}$  indicate a slightly increased reduced cross section

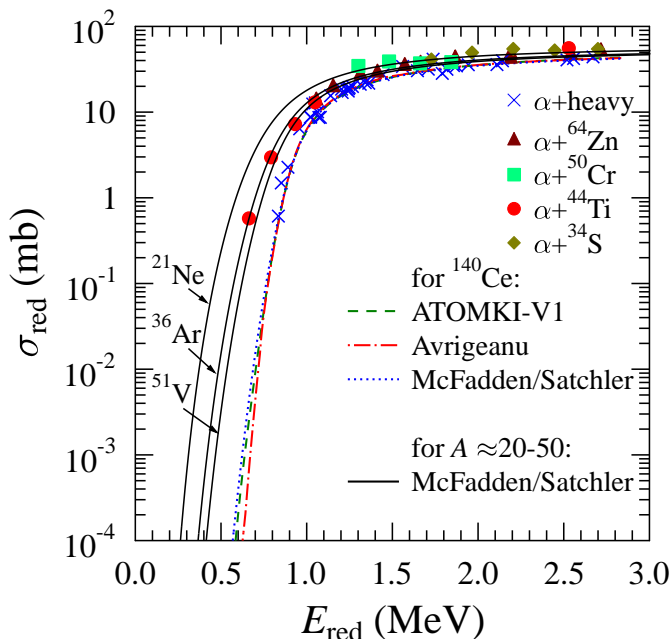


**Fig. 1.** Reduced cross section  $\sigma_{\text{red}}$  versus reduced energy  $E_{\text{red}}$  for  $\alpha$ -induced reactions on heavy nuclei. Data from elastic ( $\alpha, \alpha$ ) scattering of heavy target nuclei have been taken from [17, 18] and are shown as blue crosses. Slightly higher values for  $\sigma_{\text{red}}$  are found for  $^{64}\text{Zn}$  and for the mass range of this work ( $^{50}\text{Cr}$ ,  $^{44}\text{Ti}$  and  $^{34}\text{S}$ ). The dashed, dash-dotted, and dotted lines show calculations for a heavy target nucleus ( $^{140}\text{Ce}$ ) using three different  $\alpha$ -nucleus potentials (data taken from [39]). The full lines show calculations for  $^{21}\text{Ne}$ ,  $^{36}\text{Ar}$ , and  $^{51}\text{V}$ , i.e. in the full mass range of this study, using the  $\alpha$ -nucleus potential of McFadden and Satchler [21].

$\sigma_{\text{red}}$  at higher energies above  $E_{\text{red}} \approx 1.5$  MeV, as compared to the global systematics of heavy-ion induced reactions. At energies below  $E_{\text{red}} \approx 1.5$  MeV the  $\sigma_{\text{red}}$  for  $A \approx 20 - 50$  are significantly increased, and this increase becomes more pronounced for lighter targets. In the detailed study of the available experimental data in the  $A \approx 20 - 50$  mass range this trend will be confirmed for most nuclei under study (see Sec. 4).

### 2.3 Statistical model

Reaction cross sections of  $\alpha$ -induced reactions for heavy nuclei can be calculated using the StM [42]. In particular, this model has been widely applied for the calculation of reaction cross sections and stellar reaction rates in nuclear astrophysics [43] using the TALYS [44] and NON-SMOKER [45] codes. The applicability of the StM to  $\alpha$ -induced reactions in the mass range  $A \approx 20 - 50$  may be limited because the level density in the compound nucleus may be not sufficiently high. In such cases the cross section will be dominated by individual resonances instead of many overlapping resonances. Consequently, the StM model will not be able to predict the detailed shape of the excitation function, but nevertheless the StM should

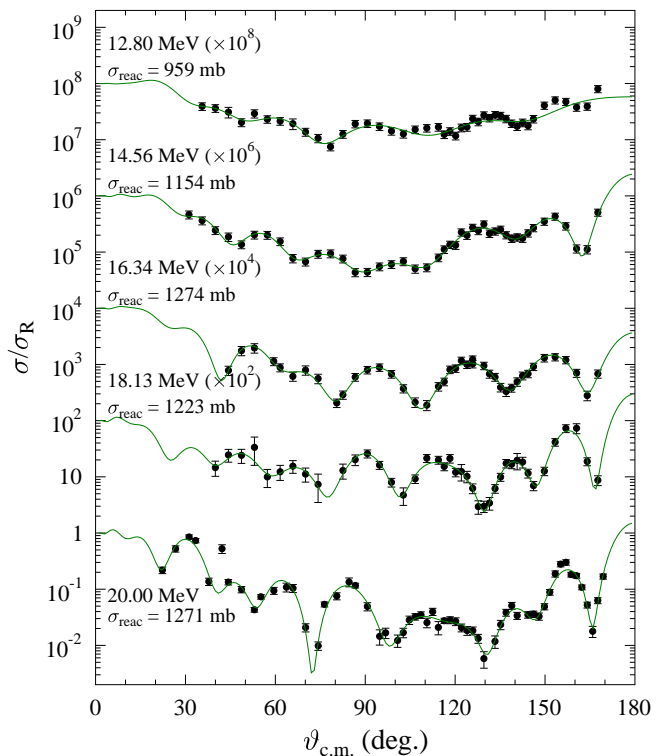


**Fig. 2.**  $^{34}\text{S}(\alpha, \alpha)^{34}\text{S}$  elastic scattering: experimental data [34] and a phase shift fit to determine the total reaction cross section  $\sigma_{\text{reac}}$  using the method from [35].

be able to reproduce the general trend of the energy dependence of the cross section. E.g., such a behavior has been found for the  $^{18}\text{Ne}(\alpha, p)^{21}\text{Na}$  reaction, see [28] and Sec. 4.34. Further details on the applicability of the StM are given in [46] (see Fig. 8 of [46] for  $\alpha$ -induced reactions).

In a schematic notation the reaction cross section in the StM is proportional to

$$\sigma(\alpha, X) \sim \frac{T_{\alpha,0} T_X}{\sum_i T_i} = T_{\alpha,0} \times b_X \quad (3)$$

with the transmission coefficients  $T_i$  into the  $i$ -th open channel and the branching ratio  $b_X = T_X / \sum_i T_i$  for the decay into the channel  $X$ . The  $T_i$  are calculated from global optical potentials (particle channels) and from the gamma-ray strength function for the photon channel. For details of the definition of  $T_i$ , see [43].  $T_{\alpha,0}$  refers to the entrance channel where the target nucleus is in its ground state under laboratory conditions. The calculation of stellar reaction rates  $N_A \langle \sigma v \rangle$  requires further modification of Eq. (3) [43].

It is typical for  $\alpha$ -induced reactions on heavy nuclei that  $T_\alpha$  (and thus  $T_{\alpha,0}$ ) is much smaller than the other  $T_i$ . A simple qualitative explanation is the high Coulomb barrier in the  $\alpha$  channel. In the neutron channel a Coulomb barrier is completely missing, and in the proton channel the barrier is much lower. As a consequence, the cross section in the StM in Eq. (3) factorizes into a production cross section of the compound nucleus which is proportional to  $T_{\alpha,0}$ , and a decay branching ratio  $b_X = T_X / \sum_i T_i$  practi-

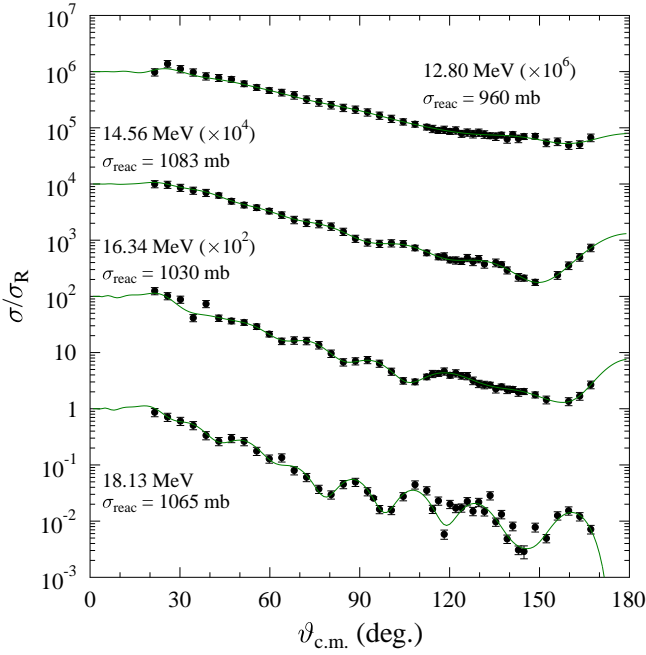


**Fig. 3.**  $^{50}\text{Cr}(\alpha,\alpha)^{50}\text{Cr}$  elastic scattering: experimental data [34] and a phase shift fit to determine the total reaction cross section  $\sigma_{\text{reac}}$  using the method from [35].

cally independent of  $T_\alpha$  because  $T_\alpha$  only marginally contributes to the sum  $\sum_i T_i$  in the above nominator of  $b_X$ . The production cross section is thus entirely defined by the underlying  $\alpha$ -nucleus potential whereas the branching ratio  $b_X$  does practically not depend on the chosen  $\alpha$ -potential but on all the other ingredients of the StM (optical potentials for the other channels, gamma-ray strength functions, level densities). Consequently, the cross sections of  $\alpha$ -induced reactions are sensitive to the  $\alpha$ -nucleus potential, but in addition each individual  $(\alpha,p)$ ,  $(\alpha,n)$ , or  $(\alpha,\gamma)$  reaction has further and sometimes complicated sensitivities to the other ingredients. A quantitative estimate whether a calculated reaction cross is sensitive to a particular ingredient, is the so-called sensitivity (as defined e.g. in [47]). As the  $\alpha$ -nucleus potential affects directly the production cross section, the sensitivity on the  $\alpha$ -nucleus potential is typically close to 1 for all  $(\alpha,X)$  reactions at energies around or below the Coulomb barrier.

The present study focuses on the deviation of the  $\sigma_{\text{red}}$  values for  $\alpha$ -induced reactions for  $A \approx 20 - 50$  from the universal trend of heavy-ion induced reactions. This deviation mainly appears for reduced energies below  $E_{\text{red}} \approx 1$  MeV. At these energies typically at least one particle channel (proton or neutron channel) is open, and this open channel dominates the sum  $\sum_i T_i$  because  $T_\alpha$  is suppressed by the Coulomb barrier and  $T_\gamma$  is usually much smaller than  $T_X$  into particle channels. For particle channels this means that Eq. (3) simplifies to

$$\sigma(\alpha, X) \sim \frac{T_{\alpha,0} T_X}{\sum_i T_i} \approx T_{\alpha,0} \times \frac{T_X}{T_p + T_n} \quad (4)$$

Furthermore, because of the different  $Q$ -values of the  $(\alpha,p)$  and  $(\alpha,n)$  reactions, often one channel is strongly dominating. In such cases  $b_X = T_X/(T_p + T_n) \approx 1$  for the dominating channel, and the  $(\alpha,X)$  cross section is almost identical to the total reaction cross section  $\sigma_{\text{reac}}$ . Consequently, it is sufficient to measure the total reaction cross section of the dominating particle channel for these particular nuclei to determine the total reaction cross section  $\sigma_{\text{reac}}$  and the reduced cross section  $\sigma_{\text{red}}$ .

### 3 Experimental techniques

Total reaction cross sections  $\sigma_{\text{reac}}$  of  $\alpha$ -induced reactions at higher energies far above the Coulomb barrier have been determined from transmission data, see e.g. [48]. At lower energies  $\sigma_{\text{reac}}$  can be derived from the analysis of elastic scattering angular distributions, and it has been shown recently that the result from elastic scattering is in agreement with the sum of the cross sections of all open channels [22]. As pointed out above, in many cases one particular open channel is dominating, and then it is sufficient to measure the total  $(\alpha,p)$  or total  $(\alpha,n)$  cross section to obtain an excellent estimate of the total reaction cross section  $\sigma_{\text{reac}}$ .

#### 3.1 Activation

Activation is a reliable and widely used technique for the measurement of total  $(\alpha,p)$  or  $(\alpha,n)$  cross sections. A large fraction of the  $(\alpha,p)$  and  $(\alpha,n)$  data for targets with  $A \approx 20 - 50$  has been measured by activation. However, activation experiments are obviously limited to reactions with unstable residual nuclei. In a usual activation experiment many targets are irradiated at different energies, and the excitation function is derived from the activation yields. In several cases the so-called ‘‘stacked-foil’’ technique was applied which allows the determination of excitation functions within a very limited beamtime because many target foils are stacked behind each other and irradiated simultaneously. As will be shown below, this technique provides good results at energies close to the projectile energy before the stack of foils. However, the results for the lowest energies are often not reliable, probably because of uncertainties in foil thickness and resulting energy loss and straggling of the projectiles.

Various techniques can be used to determine the number of produced radioactive nuclei. The chosen technique depends on the half-life and the decay properties of the respective nucleus. In most cases  $\gamma$ -rays following the  $\beta^+$ - or  $\beta^-$ -decay of the mother nuclide are detected using high-resolution germanium detectors. In some cases without detectable  $\gamma$ -ray branch, X-rays can be measured (following e.g. electron capture from the  $K$ -shell). Also a direct detection of electrons from  $\beta^-$ -decay or positrons from  $\beta^+$ -decay is possible. Finally, for long half-lives the accelerator mass spectrometry technique allows to count few nuclei with otherwise unrivaled sensitivity.

### 3.2 Direct neutron measurements

#### 3.2.1 Neutron counting

As an alternative to activation, the total cross section of  $(\alpha, n)$  reactions can be measured by neutron thermalization and counting. In practice, this technique is widely used, but experiments have to be done very carefully because minor build-up of carbon on the target may lead to a significant neutron yield from the  $^{13}\text{C}(\alpha, n)^{16}\text{O}$  background reaction. Highly enriched (and thus expensive) targets are required to avoid neutron yields from other (more neutron-rich) isotopes.

#### 3.2.2 Time-of flight measurements

A direct neutron detection using the time-of-flight (TOF) technique is also possible. However, these experiments determine the differential cross section  $d\sigma/d\Omega$  of a particular  $n_i$  channel at the detector angle  $\vartheta$  (where  $n_0$  stands for the ground state of the residual nucleus,  $n_1$  for the first excited state, etc.). There are two basic problems to determine the total  $(\alpha, n)$  cross section from such data. First, the integration of the differential cross section requires the knowledge of the full angular distribution (i.e., measurements at many angles), and second, all exit channels  $n_i$  have to be summed up properly. Here weak channels may be overlooked.

### 3.3 Direct proton measurements

Similar problems appear in direct measurements of  $(\alpha, p)$  cross sections. Again, the angular distribution has to be integrated correctly, and all channels  $p_i$  have to be summed up. This summation is even more critical for  $(\alpha, p)$  reactions because relatively high-lying final states lead to small proton energies which may be difficult to detect (of course depending on the target thickness).

### 3.4 Target thickness

The target thickness is a very important experimental parameter. The experimental yield is given by the average cross section over the energy interval  $[E_\alpha, E_\alpha - \Delta E]$  where  $\Delta E$  is the energy loss of the  $\alpha$  projectile in the target. A precise determination of the cross section  $\sigma(E)$  clearly asks for a thin target, i.e. a small energy loss  $\Delta E$ . However, for the application of the StM a sufficient number of resonances must lie within the corresponding interval of excitation energies in the compound nucleus. There is no problem for heavy target nuclei which have high level densities, and any realistic target is sufficiently thick for the applicability of the StM. However, at the lower end of the mass range  $A \approx 20 - 50$  the level density may be too low, in particular for very thin targets. As a consequence, the experimental data for a thin target will be governed by individual resonances, and the StM will not

be able to reproduce the details of the excitation function. Experimental data for a thick target will average over the individual resonances, leading to a smooth energy dependence of the excitation function. Such a behavior will be nicely illustrated e.g. for the target  $^{27}\text{Al}$  (see Sec. 4.26).

### 3.5 (Infinitely) Thick-target yields

In principle, it is possible to derive reaction cross sections from thick-target yield curves by differentiation. However, in practice this leads to significant uncertainties. If the thick-target yield curve is measured with large energy steps (e.g.,  $E_2 \gg E_1$ ), the resulting cross section is averaged over a broad energy interval  $E_2 - E_1$ . Smaller energy steps reduce this uncertainty; but at the same time the yields  $Y(E_2)$  and  $Y(E_1)$  become more and more similar, and the cross section has to be derived from the difference  $Y(E_2) - Y(E_1)$  which is a small number. The uncertainty in the difference of two quite similar numbers is further amplified if yield curves are not available numerically and have to be re-digitized from figures. Therefore, thick-target yield curves are not considered in this work.

One exception is made for the data by Roughton *et al.* [49] because these data allow to include the doubly-magic nucleus  $^{48}\text{Ca}$  in this study. Roughton *et al.* have measured thick-target yield curves for 36 nuclear reactions in relatively small energy steps. The data are available numerically from Table II in [49], and the conversion from the given thick-target yield to cross sections is precisely defined in Eq. (3) of an earlier study of proton-induced reactions [50]; it is based on the energy-loss formulae given in [51]. The resulting cross sections are in reasonable agreement with other available data as long as the energy difference between two subsequent yields is sufficiently large. As expected, for very small energy differences the uncertainty of the derived average cross section increases dramatically. Surprisingly it turns out that practically all of these cross sections from small energy differences are much lower than other experimental data. Despite of these obvious inconsistencies, this allows at least to determine a good estimate of the  $^{48}\text{Ca}(\alpha, n)^{51}\text{Ti}$  cross section from Roughton *et al.* [49]. However, because of the above inconsistencies in the Roughton *et al.* data, in most cases the data are only shown in the cross section plots without further discussion in the text (with the same symbol “star” and same color “olive-green” in all figures), and the data are omitted in the plots of reduced cross sections (see Sec. 4.1).

### 3.6 Elastic scattering

The determination of total reaction cross sections  $\sigma_{\text{reac}}$  from elastic scattering can be done under two prerequisites. First, the deviation of the elastic scattering cross section from the Rutherford cross section of point-like charges has to exceed the experimental uncertainty. Thus, at energies below the Coulomb barrier experimental data with very small uncertainties are required. Second, full angular distributions must be available. Often total reaction

cross sections are determined by fits of an optical potential; but it should be kept in mind that the choice of the parametrization of the optical potential already restricts the model space, and thus the derived  $\sigma_{\text{reac}}$  may become model-dependent. Such a model dependence should always be checked by a model-independent phase shift analysis. In the present work the formalism of Chiste *et al.* [35] was applied for this purpose.

For completeness it should also be noted that the parameters of optical potentials are not very well constrained from elastic scattering below the Coulomb barrier. So-called continuous and discrete ambiguities are often found (see e.g. [52]). However, although the parameters of the optical potential may remain uncertain, the resulting angular distributions are more or less similar. It remains then possible to determine total cross sections  $\sigma_{\text{reac}}$  from elastic scattering even at low energies where it is impossible to determine the parameters of the optical potential [39].

### 3.7 Availability of experimental data

Fortunately, nowadays many experimental data are provided by the EXFOR database [29] which is a great facilitation for a literature overview. However, it has to be kept in mind that the quality of the data in EXFOR depends sensitively on the data source. Newer data are often provided by the authors of the experimental paper. For earlier papers the original data are only available if the data are listed in a table in the paper (or in an underlying thesis or laboratory report; however, the latter are often not easily accessible). If original data are not available, the EXFOR editors have often re-digitized experimental data from figures. In such cases significant uncertainties arise from the digitization procedure which may exceed the experimental uncertainties of the original data. This holds in particular for small figures in logarithmic scale.

The determination of total reaction cross sections  $\sigma_{\text{reac}}$  from elastic scattering is particularly sensitive to the available data quality because the experimental  $(\alpha, \alpha)$  angular distribution must be fitted in an optical model calculation or phase shift analysis. In many cases re-digitized data in EXFOR are listed without experimental error bars; then assumptions on the uncertainties have to be made for the fitting procedure. Fortunately, for the phase shift fits shown above in Figs. 2 and 3 the original data of Bredbecka *et al.* [34] could be restored, and these original data were sent to EXFOR to replace the previously available re-digitized data.

## 4 Results

### 4.1 General remarks on the presentation of results

The results for  $\alpha$ -induced reactions for nuclei in the  $A \approx 20 - 50$  mass range will be presented in the following way. For each nucleus the available data at EXFOR will be briefly described. A comparison is made between the

experimental  $(\alpha, p)$  and  $(\alpha, n)$  cross sections and predictions from the StM. Here I use the TALYS code [44] with standard parameters except the  $\alpha$ -nucleus potential where the potential by McFadden/Satchler is selected. As the  $\alpha$ -nucleus potential is the essential ingredient in most cases (see discussion above), NON-SMOKER [45] calculations lead to very similar results because the McFadden/Satchler potential is the default option in NON-SMOKER.

In practically all cases the  $(\alpha, \gamma)$  cross section is much smaller than the  $(\alpha, p)$  or  $(\alpha, n)$  cross section. Thus,  $(\alpha, \gamma)$  cross sections will be shown only in few cases; an explanation will be given in the respective sections for these special cases.

For some nuclei under study only very few or even no  $(\alpha, p)$  or  $(\alpha, n)$  data are available in literature. For these nuclei it was attempted to obtain further information on the total reaction cross section  $\sigma_{\text{reac}}$  from the analysis of elastic scattering angular distributions. In practice, this analysis can only be performed at energies around or above the Coulomb barrier whereas at very low energies below the Coulomb barrier the elastic scattering cross section approaches the Rutherford cross section of point-like charges.

For each nucleus under study the available data for the  $(\alpha, p)$  and  $(\alpha, n)$  reactions (and also the  $(\alpha, \gamma)$  data and total reaction cross sections  $\sigma_{\text{reac}}$  from elastic scattering) will be shown in a first figure. In this figure also a comparison with a calculation in the StM will be made. The energy in all these figures is  $E_\alpha$  in the laboratory system; for experiments in inverse kinematics, the corresponding energy  $E_\alpha$  is calculated from the given energy of the heavy projectile.

In addition to the comparison of reaction cross sections, reduced cross sections  $\sigma_{\text{red}}$  are shown versus the reduced energy  $E_{\text{red}}$  in a second figure for each nucleus under study. In these  $\sigma_{\text{red}}$  figures the experimental data are shown together with the three calculations of  $\sigma_{\text{red}}$  from the total reaction cross section  $\sigma_{\text{reac}}$  for  $^{21}\text{Ne}$ ,  $^{36}\text{Ar}$ , and  $^{51}\text{V}$  (these calculations have already been shown as full lines in Fig. 1). The purpose of this presentation is to show how the experimental data for nuclei with  $A \approx 20 - 50$  move smoothly with decreasing  $A$  from the calculation for  $^{51}\text{V}$  to the calculation for  $^{21}\text{Ne}$  with the few noticeable exceptions of  $^{40}\text{Ar}$ ,  $^{36}\text{Ar}$ ,  $^{33}\text{S}$ , and  $^{23}\text{Na}$  (as already mentioned in the introduction). For this purpose the scale of all graphs with  $\sigma_{\text{red}}$  versus  $E_{\text{red}}$  is exactly the same to guide the eye, and the systematics for  $\alpha$ -induced reaction cross sections for heavy targets (see Fig. 1) is repeated in each graph with small blue crosses.

In general, experimental data for  $(\alpha, n)$  reactions will be shown as open symbols, and  $(\alpha, p)$  reactions will be shown as full symbols. Exceptions will be indicated in the figure captions.

For several nuclei under study, data in the book of Levkovskij [53] are referenced in EXFOR. Often significant deviations to other available data sets are found for the Levkovskij data. As the book [53] is not available to the author of this study, it is not possible to trace back

to the origin of these discrepancies. The data of [53] are omitted in the following graphs.

## 4.2 $^{50}\text{Cr}$

The  $^{50}\text{Cr}(\alpha,n)^{53}\text{Fe}$  and  $^{50}\text{Cr}(\alpha,p)^{53}\text{Mn}$  reactions can both be measured by activation. However, the half-life of  $^{53}\text{Mn}$  is extremely long ( $T_{1/2} = 3.74 \times 10^6$  years), and no activation data are available for the proton channel. Because of the strongly negative  $Q$ -value of the  $(\alpha,n)$  reaction and  $Q \approx -0.44$  MeV for the  $(\alpha,p)$  reaction, the  $(\alpha,p)$  channel is dominating at low energies, but at energies above about 6 – 7 MeV the  $(\alpha,n)$  cross section also contributes significantly to the total reaction cross section  $\sigma_{\text{reac}}$ .

A detailed study of both  $\alpha$ -induced reactions on  $^{50}\text{Cr}$  has been done by Morton *et al.* [54]. The excitation function of the  $^{50}\text{Cr}(\alpha,p)^{53}\text{Mn}$  reaction has been measured using a silicon detector at the angle of  $\vartheta = 125^\circ$ . The measured protons have been grouped into  $p_0$ ,  $p_1$ ,  $p_{2-4}$ ,  $p_{5-7}$ ,  $p_{8-15}$ , and  $p_{16-28}$ . Corrections for the angular distributions have been taken from StM calculations; however, these corrections remain relatively small because of the chosen angle. The total  $(\alpha,p)$  cross section is determined by the sum over the above proton groups. The result is shown in Fig. 4.

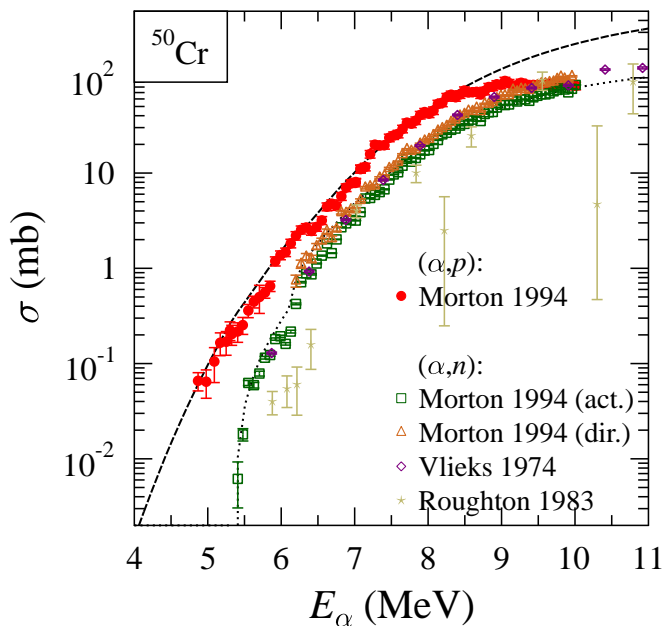


**Fig. 4.** Cross sections of the  $^{50}\text{Cr}(\alpha,n)^{53}\text{Fe}$  and  $^{50}\text{Cr}(\alpha,p)^{53}\text{Mn}$  reactions. The  $(\alpha,n)$  data are shown with open symbols and dotted line, the  $(\alpha,p)$  data are shown with full symbols and dashed line. (The same style will be used in all following figures except explicitly noted.) The experimental data have been taken from [54,55,49]. Further discussion see text.

The experimental  $^{50}\text{Cr}(\alpha,p)^{53}\text{Mn}$  cross section is compared to a StM calculation using the code TALYS with

default parameters and the  $\alpha$ -nucleus potential by McFadden and Satchler [21] (dashed line in Fig. 4). It can be seen that the agreement is excellent at low energies whereas above about 8 MeV the calculation is higher than the experimental data. As the StM calculations are typically very stable and reliable at higher energies, this deviation may indicate that the summation over the proton groups ( $p_{0-28}$ ) is insufficient at the highest energies. Alternatively, the uncertainty of the correction on the angular distribution of the proton groups increases with energy [54]; this uncertainty may be larger than estimated by the authors.

The  $^{50}\text{Cr}(\alpha,n)^{53}\text{Fe}$  reaction has been measured by Morton *et al.* using two independent techniques. Neutrons were counted directly with  $^3\text{He}$ -filled proportional counters, and activation was observed with a germanium detector by detection of the 378 keV  $\gamma$ -ray in the decay of  $^{53}\text{Fe} \rightarrow ^{53}\text{Mn}$ . Both data sets show the same energy dependence, but unfortunately the two data sets deviate by about 20% in their absolute scale. The reason for this discrepancy remains unclear. An earlier experiment by Vlieks *et al.* [55] has measured the induced activity by positron counting. These earlier data are in better agreement with the direct neutron data by Morton *et al.* [54]. As a similar experiment has been done by the same authors on  $^{51}\text{V}(\alpha,n)^{54}\text{Mn}$  (see next Sec. 4.3) where direct neutron counting and activation are in excellent agreement, the discrepancy observed for the  $^{50}\text{Cr}(\alpha,n)^{53}\text{Fe}$  re-

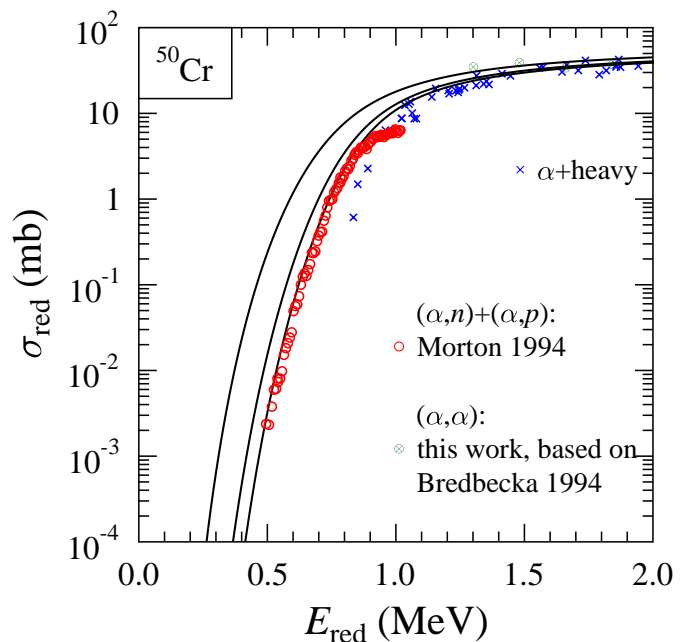


**Fig. 5.** Reduced cross section  $\sigma_{\text{red}}$  versus reduced energy  $E_{\text{red}}$  for  $\alpha$ -induced reactions on  $^{50}\text{Cr}$ . The experimental data have been taken from [54]. In addition, the result of a reanalysis of the elastic scattering data of [34] is shown. Data points from elastic scattering on heavy ( $A > 60$ ) target nuclei are repeated from Fig. 1 (blue crosses). As a guide to the eye, the calculations for  $^{21}\text{Ne}$ ,  $^{36}\text{Ar}$ , and  $^{51}\text{V}$  are also repeated from Fig. 1 (full black lines). Further discussion see text.

action is probably the consequence of an incorrect decay branching of the analyzed 378 keV  $\gamma$ -ray. Morton *et al.* have used  $42 \pm 8\%$ ; the present ENSDF evaluation recommends  $42 \pm 3\%$  [56], and good agreement between direct neutron counting and activation would be obtained for a branching of about 34%.

It is obvious from Fig. 4 that the StM calculations reproduce the experimental data of both reactions very well. In particular at low energies the agreement is excellent, and a possible explanation for the deviation at higher energies in the  $^{50}\text{Cr}(\alpha,p)^{53}\text{Mn}$  channel has already been given above.

For the determination of the total reaction cross section  $\sigma_{\text{reac}}$  and the reduced cross section  $\sigma_{\text{red}}$ , the  $(\alpha,p)$  and  $(\alpha,n)$  data of Morton *et al.* [54] were summed. The result is shown in Fig. 5. In addition, the data from elastic  $^{50}\text{Cr}(\alpha,\alpha)^{50}\text{Cr}$  scattering (see Fig. 3) are shown. The  $\sigma_{\text{red}}$  data are slightly higher than the general trend which was derived from elastic  $(\alpha,\alpha)$  scattering of heavy target nuclei. Similar to most nuclei under study in this work, the  $\sigma_{\text{red}}$  data for  $^{50}\text{Cr}$  do not show a peculiar behavior.

### 4.3 $^{51}\text{V}$

Many experimental data are available at EXFOR for the  $^{51}\text{V}(\alpha,n)^{54}\text{Mn}$  reaction which can be measured by activation. Contrary, only one data set is available for the  $^{51}\text{V}(\alpha,p)^{54}\text{Cr}$  reaction which was measured using the same technique as for  $^{50}\text{Cr}(\alpha,p)^{53}\text{Mn}$  (see previous Sec. 4.2).

The  $^{51}\text{V}(\alpha,n)^{54}\text{Mn}$  data are shown in Fig. 6. The precision data by Vonach *et al.* [57] were measured by activation and are in excellent agreement with the activation data and the direct neutron counting data by Hansper *et al.* [58]. Earlier data by Vlietks *et al.* [55] are slightly higher especially at energies above 9 MeV. Recent stacked-foil data by Peng *et al.* [11] and Chowdhury *et al.* [12] are in good agreement with the other data whereas earlier stacked-foil data [59,60,61,62,63,64] deviate significantly at the lowest energies. The agreement of the experimental data with the StM calculation is excellent over the full shown energy range.

The  $^{51}\text{V}(\alpha,p)^{54}\text{Cr}$  data by Hansper *et al.* [58] are not shown in Fig. 6 for several reasons. It is impossible to derive the total  $(\alpha,p)$  cross section from the information in the paper. Proton groups ( $p_0, p_1, p_2, p_{3-4}$ , and  $p_{5-7}$ ) are shown in the spectrum (Fig. 3 of [58]) but in the following cross section plots the strong group  $p_{5-7}$  is missing. In addition, the data at EXFOR are re-digitized from the figures in [58] which makes a point-by-point addition of the proton groups practically impossible. Fortunately, the  $^{51}\text{V}(\alpha,p)^{54}\text{Cr}$  reaction contributes only very minor to the total reaction cross section  $\sigma_{\text{reac}}$  of  $^{51}\text{V}$  which is dominated by the  $^{51}\text{V}(\alpha,n)^{54}\text{Mn}$  reaction (see the shown calculations in Fig. 6). Only at the lowest energies below about 5 MeV the  $(\alpha,p)$  cross section becomes comparable to the  $(\alpha,n)$  cross section whereas at higher energies the  $(\alpha,p)$  reaction contributes by less than 20% [57]. The data points at the lowest energies for the  $(\alpha,p)$  reaction in [58] are about

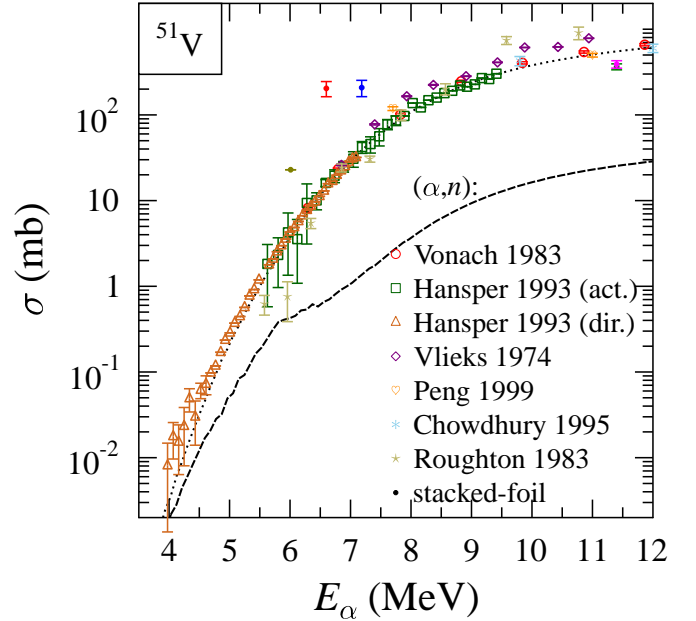


**Fig. 6.** Cross sections of the  $^{51}\text{V}(\alpha,n)^{54}\text{Mn}$  and  $^{51}\text{V}(\alpha,p)^{54}\text{Cr}$  reactions. The experimental data have been taken from [57, 58, 55, 11, 12, 59, 60, 61, 62, 63, 64, 49]. The lowest data points of several stack-foil experiments [59, 60, 61, 62, 63, 64] (shown as small dots in different colors) are in disagreement with the other data. Further discussion see text.

$10^{-2}$  mb at  $\approx 5$  MeV with huge error bars, i.e. close to the theoretically expected values (dashed line in Fig. 6).

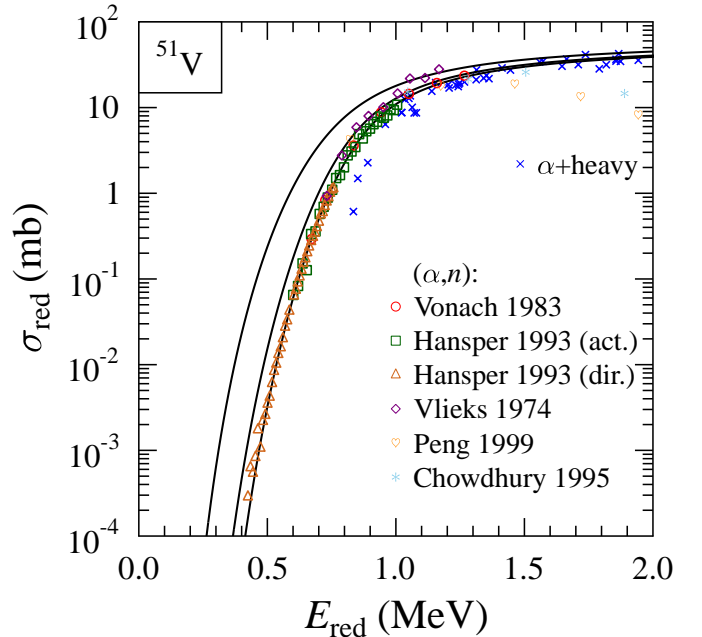


**Fig. 7.** Same as Fig. 5, but for  $\alpha$ -induced reactions on  $^{51}\text{V}$ . The experimental data have been taken from [55, 57, 58, 11, 12]. Further discussion see text.

Fig. 7 shows the reduced cross section  $\sigma_{\text{red}}$  for  $^{51}\text{V}$ . For better readability only the  $(\alpha, n)$  data of [55, 57, 58, 11, 12] are shown. The agreement between the experimental  $(\alpha, n)$  data and the calculated total reaction cross section  $\sigma_{\text{reac}}$  and reduced cross section  $\sigma_{\text{red}}$  is excellent up to  $E_{\text{red}} \approx 1.5$  MeV. At these energies other reaction channels open, and thus the  $(\alpha, n)$  cross section does not represent the total cross section  $\sigma_{\text{reac}}$  anymore. At even higher energies (above the range shown in Fig. 7) the analysis of elastic  $^{51}\text{V}(\alpha, \alpha)^{51}\text{V}$  scattering leads to data points of  $\sigma_{\text{red}} = 55 \pm 2$  mb at  $E_{\text{red}} = 2.90$  MeV [65] and  $\sigma_{\text{red}} = 46 \pm 4$  mb at  $E_{\text{red}} = 2.49$  MeV [33], again in reasonable agreement with the theoretical expectations of 46.4 mb and 43.8 mb. Finally, it is interesting to note that the reduced cross sections  $\sigma_{\text{red}}$  for the semi-magic ( $N = 28$ ) nucleus  $^{51}\text{V}$  are very similar to the non-magic neighboring nuclei  $^{50}\text{Cr}$  (see previous Sec. 4.2) and  $^{48}\text{Ti}$  (see following Sec. 4.5). Similar to most nuclei under study in this work, the  $\sigma_{\text{red}}$  data for  $^{51}\text{V}$  do not show a peculiar behavior.

#### 4.4 $^{50}\text{V}$

The odd-odd ( $Z = 23$ ,  $N = 27$ ) nucleus  $^{50}\text{V}$  has a very low natural abundance. Unfortunately, no data for  $\alpha$ -induced reactions are available below 10 MeV. The only available data set by Peng *et al.* [11] covers the  $^{50}\text{V}(\alpha, 2n)^{52}\text{Mn}$  reaction from close above threshold around  $\approx 13$  MeV to about 26 MeV. The data have been measured using the stacked-foil activation technique. The experimental data are well reproduced by the StM calculation. However, the data do not restrict the total reaction cross section  $\sigma_{\text{reac}}$  of  $\alpha$ -induced reactions on  $^{50}\text{V}$ , and thus no figure for cross sections or reduced cross sections  $\sigma_{\text{red}}$  is shown here. Nevertheless, from the nice agreement between the experimental  $^{50}\text{V}(\alpha, 2n)^{52}\text{Mn}$  data and the StM calculation it can be concluded that there is at least no evidence for a peculiar behavior of the odd-odd nucleus  $^{50}\text{V}$ .

#### 4.5 $^{48}\text{Ti}$

Five data sets for the  $^{48}\text{Ti}(\alpha, n)^{51}\text{Cr}$  reaction are available from EXFOR. All experiments have applied activation techniques. The precision data for the  $^{48}\text{Ti}(\alpha, n)^{51}\text{Cr}$  reaction by Vonach *et al.* [57] have been obtained by measuring the induced activity by  $\gamma$ -spectroscopy. The same technique was used by Morton *et al.* [67] and Baglin *et al.* [68] whereas Chang *et al.* [66] used  $X$ -ray spectroscopy of the 4.95 keV  $X$ -ray which is emitted in  $^{51}\text{V}$  after the electron capture decay of  $^{51}\text{Cr}$ . Iguchi *et al.* [60] used the stacked-foils technique and  $\gamma$ -spectroscopy. It can be seen from Fig. 8 that in general the data are in good agreement. Exceptions are the lowest energy points of the stacked-foil experiment [60] and also the lowest data point of the  $X$ -ray experiment [66]; here the analysis at the lowest energy may be hampered by the relatively thick target ( $485 \mu\text{g}/\text{cm}^2$ ). The agreement with the StM calculation is excellent over the full energy range.

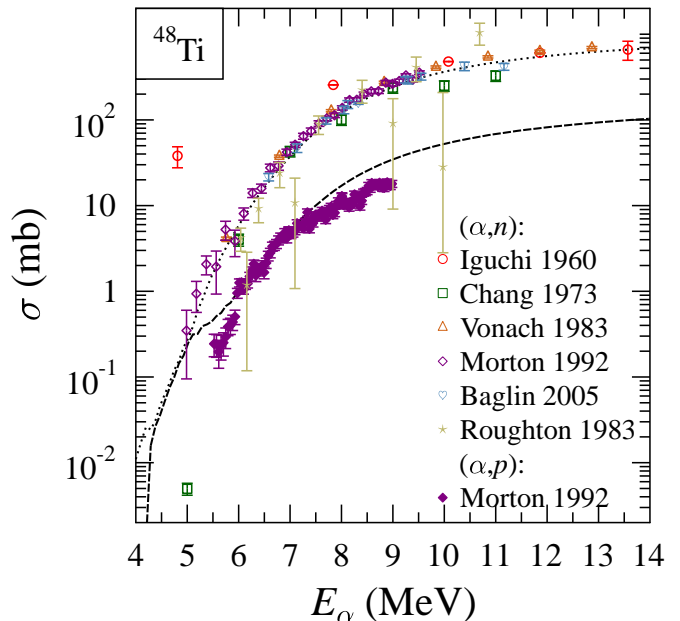


**Fig. 8.** Cross sections of the  $^{48}\text{Ti}(\alpha, n)^{51}\text{Cr}$  and  $^{48}\text{Ti}(\alpha, p)^{51}\text{V}$  reactions. The experimental data have been taken from [60, 66, 57, 67, 68, 49]. Further discussion see text.

The  $^{48}\text{Ti}(\alpha, p)^{51}\text{V}$  reaction has been measured by Morton *et al.* [67]. Cross sections for the proton groups  $p_0$  to  $p_5$  are shown in Fig. 4 of [67]; the sum of these cross sections is shown as  $(\alpha, p)$  cross section in Fig. 8. The proton groups  $p_{6-8}$  could not be resolved from background reactions, but should have only a minor contribution to the

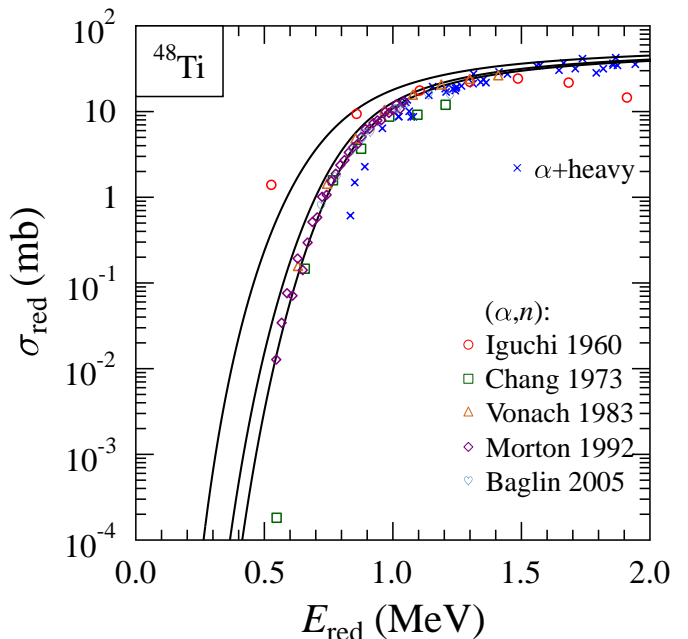


**Fig. 9.** Same as Fig. 5, but for  $\alpha$ -induced reactions on  $^{48}\text{Ti}$ . The experimental data have been taken from [60, 66, 57, 67, 68]. Further discussion see text.

total  $(\alpha,p)$  cross section (see the spectrum in Fig. 3 of [67]). The agreement with the StM calculation is good for the  $^{48}\text{Ti}(\alpha,p)^{51}\text{V}$  reaction although the experimental results are slightly overestimated at the upper and lower end of the measured energy interval. It is interesting to note that the NON-SMOKER calculation for the  $^{48}\text{Ti}(\alpha,p)^{51}\text{Cr}$  reaction deviates from the TALYS calculation, leading to better agreement at higher and lower energies, but underestimation in the middle.

Because the  $(\alpha,n)$  cross section for  $^{48}\text{Ti}$  is much larger than the  $(\alpha,p)$  cross section, the total reaction cross section  $\sigma_{\text{reac}}$  and the reduced cross section  $\sigma_{\text{red}}$  are taken from the  $(\alpha,n)$  data. A contribution of less than 20% was estimated in [57] for the  $(\alpha,p)$  reaction. At higher energies the low  $\sigma_{\text{red}}$  values from [60] can be explained by additional open channels. At even higher energies the analysis of elastic scattering angular distributions in [65] leads to  $\sigma_{\text{red}} = 54.6 \text{ mb}$  at  $E_{\text{red}} = 2.98 \text{ MeV}$  (not shown in Fig. 9). Similar to most nuclei under study in this work, the  $\sigma_{\text{red}}$  data for  $^{48}\text{Ti}$  do not show a peculiar behavior.

#### 4.6 $^{46}\text{Ti}$

Only few data sets are available for  $^{46}\text{Ti}$ . The cross section of the  $^{46}\text{Ti}(\alpha,n)^{49}\text{Cr}$  reaction has been measured by activation and annihilation spectroscopy by Vlieks *et al.* [55] and by Howard *et al.* [69]. The data by Vlieks *et al.* are significantly lower than the data by Howard *et al.* (see Fig. 10). The Vlieks *et al.* data are confirmed by the thick-target yield measured by Roughton *et al.* [49]. As the experimental data from Vlieks *et al.* [55] for  $^{50}\text{Cr}$  (see Sec. 4.2),  $^{51}\text{V}$  (see Sec. 4.3), and  $^{45}\text{Sc}$  (see Sec. 4.8) agree with other experimental data, the data of Vlieks *et al.* should be adopted. In addition, the data by Vlieks *et al.* are available from a table in [55] whereas the data by Howard *et al.* had to be re-digitized from Fig. 3 of [69] (see also comment in Sec. 3.7). Furthermore, also for  $^{40}\text{Ca}$  and  $^{35}\text{Cl}$  the data by Howard *et al.* [69] are slightly higher than other available data (see Sec. 4.11 and 4.18).

The agreement between the data of Vlieks *et al.* [55] and the StM calculation (dotted line in Fig. 10) is again excellent. However, the total reaction cross section  $\sigma_{\text{reac}}$  and the reduced cross section  $\sigma_{\text{red}}$  are dominated by the  $^{46}\text{Ti}(\alpha,p)^{49}\text{V}$  reaction (dashed line in Fig. 10) where no data are available from EXFOR. As a consequence, the  $\sigma_{\text{red}}$  data from the  $^{46}\text{Ti}(\alpha,n)^{49}\text{Cr}$  reaction are significantly lower than the expectation for the total reaction cross section (see Fig. 11).

#### 4.7 $^{44}\text{Ti}$

It is not surprising that only very few data are available for the radioactive nucleus  $^{44}\text{Ti}$ . Nevertheless, a determination of the total reaction cross section at low energies is possible from the dominating  $^{44}\text{Ti}(\alpha,p)^{47}\text{V}$  reaction. The  $^{44}\text{Ti}(\alpha,n)^{47}\text{Cr}$  reaction has a strongly negative  $Q$ -value and does not contribute to  $\sigma_{\text{reac}}$  at low energies.

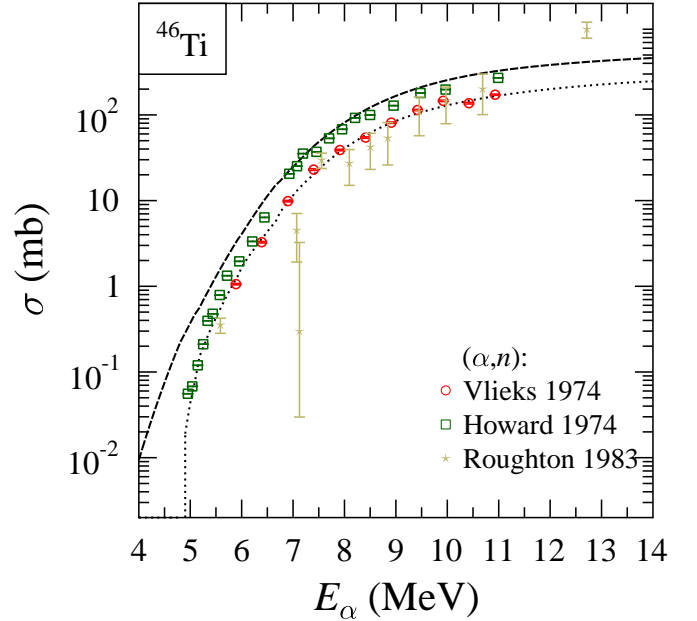


**Fig. 10.** Cross section of the  $^{46}\text{Ti}(\alpha,n)^{49}\text{Cr}$  reaction. The experimental data have been taken from [55,69,49]. Further discussion see text.

The cross section of the  $^{44}\text{Ti}(\alpha,p)^{47}\text{V}$  reaction has been determined by Sonzogni *et al.* [70] using a radioactive  $^{44}\text{Ti}$

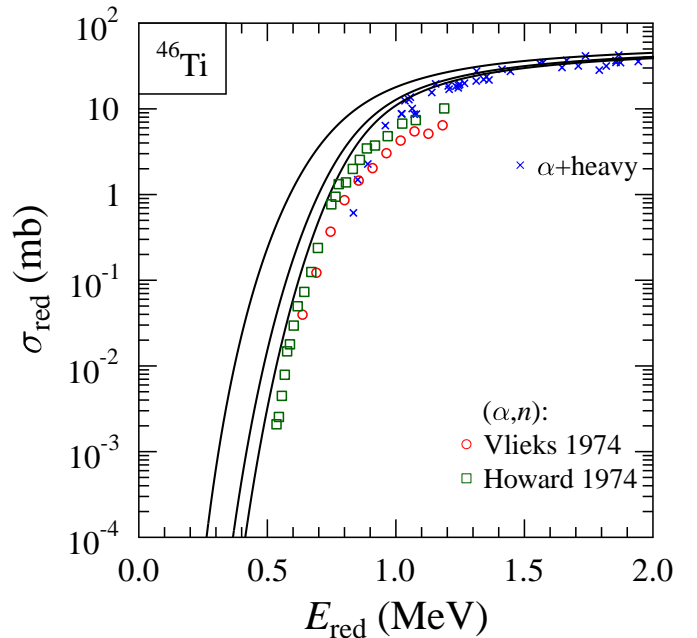


**Fig. 11.** Same as Fig. 5, but for  $\alpha$ -induced reactions on  $^{46}\text{Ti}$ . The experimental data have been taken from [69,55]. According to StM calculations, the shown  $^{46}\text{Ti}(\alpha,n)^{49}\text{Cr}$  cross section is about a factor of two smaller than the dominating  $^{46}\text{Ti}(\alpha,p)^{49}\text{V}$  cross section. Consequently, the total reaction cross section  $\sigma_{\text{reac}}$  should be about a factor of three larger than the shown  $(\alpha,n)$  cross sections. Further discussion see text.

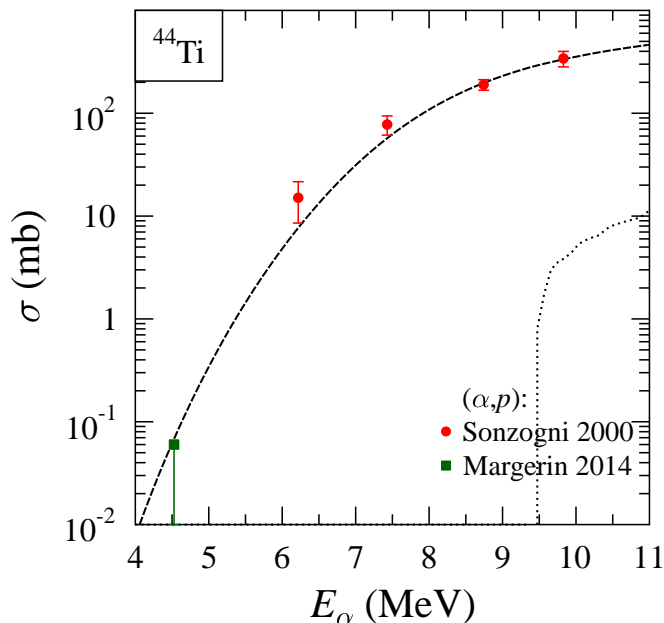


**Fig. 12.** Cross section of the  $^{44}\text{Ti}(\alpha,p)^{47}\text{V}$  reaction. The experimental data have been taken from [70,71]. Further discussion see text.

beam in combination with a  $^4\text{He}$  gas cell and the Argonne fragment mass analyzer. Very recently, at lower energies an upper limit was obtained by Margerin *et al.* [71] at CERN using also a  $^{44}\text{Ti}$  beam. Further suggestions for experiments have been made in [72] very recently. The two data sets [70,71] are shown in Fig. 12 and are compared to a StM calculation. Again very good agreement between experiment and theory is found.

As the total reaction cross section  $\sigma_{\text{reac}}$  is essentially defined by the  $^{44}\text{Ti}(\alpha,p)^{47}\text{V}$  cross section, reduced cross sections  $\sigma_{\text{red}}$  can be determined from the available  $(\alpha,p)$  data [70,71]. The result is shown in Fig. 13. An additional data point from  $^{44}\text{Ti}(\alpha,\alpha)^{44}\text{Ti}$  elastic scattering ( $\sigma_{\text{red}} = 55.8$  mb at  $E_{\text{red}} = 2.53$  MeV; not shown in Fig. 13) has already been presented above in Sec. 2.1. Similar to most nuclei under study in this work, the  $\sigma_{\text{red}}$  data for  $^{44}\text{Ti}$  do not show a peculiar behavior.

#### 4.8 $^{45}\text{Sc}$

$\alpha$ -induced reactions on  $^{45}\text{Sc}$  have been studied by Chen *et al.* [73], Vlieks *et al.* [55], and Hansper *et al.* [74]. Chen *et al.* have used the stacked-foil activation technique in combination with  $\beta$ -proportional counters, Vlieks *et al.* used activation and annihilation spectroscopy, and Hansper *et al.* applied both direct neutron counting and activation in combination with  $\gamma$ -ray spectroscopy. The different techniques provide results which are in excellent agreement with each other (see Fig. 14). The StM calculation reproduces the experimental cross sections of the  $^{45}\text{Sc}(\alpha,n)^{48}\text{V}$  reaction very nicely.

The  $^{45}\text{Sc}(\alpha,p)^{48}\text{Ti}$  reaction cannot be measured by activation because the residual  $^{48}\text{Ti}$  is stable. Only one

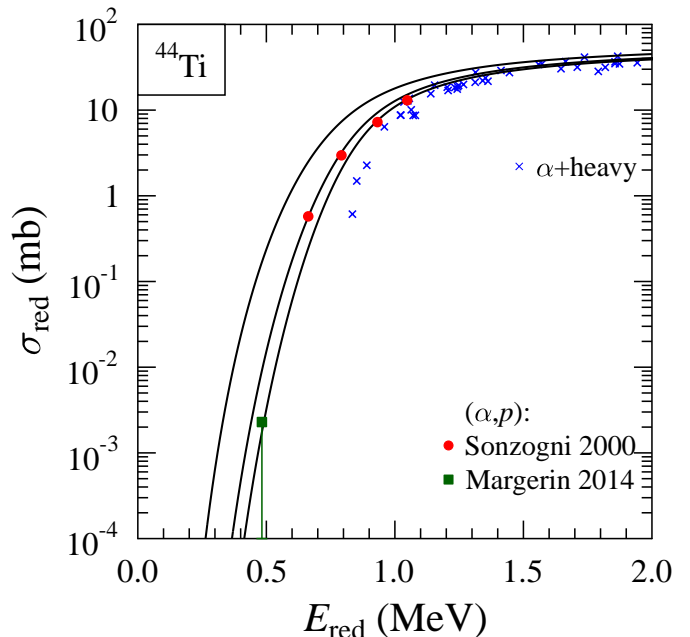


**Fig. 13.** Same as Fig. 5, but for  $\alpha$ -induced reactions on  $^{44}\text{Ti}$ . The experimental data have been taken from [70,71]. Further discussion see text.

data set is available by Hansper *et al.* [74]. However, the shown data cover only the  $p_0$ ,  $p_1$ , and  $p_{2-3}$  groups whereas the spectrum in Fig. 2 of [74] shows additional proton groups at higher excitation energies which cannot be fully resolved from background. A rough estimate from that Fig. 2 shows that about twice the strength of the shown

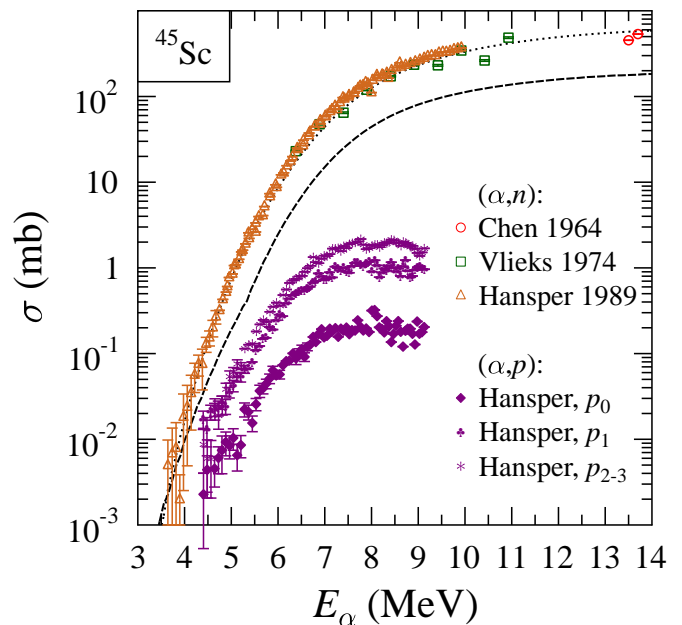


**Fig. 14.** Cross sections of the  $^{45}\text{Sc}(\alpha,n)^{48}\text{V}$  and  $^{45}\text{Sc}(\alpha,p)^{48}\text{Ti}$  reactions. The experimental data have been taken from [73,55,74]. Further discussion see text.

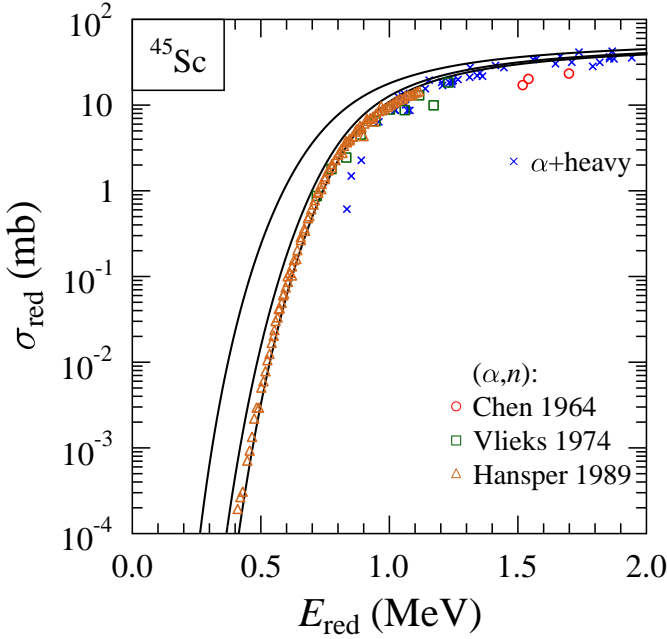


**Fig. 15.** Same as Fig. 5, but for  $\alpha$ -induced reactions on  $^{45}\text{Sc}$ . The experimental data have been taken from [73,55,74]. Further discussion see text.

$p_{0-3}$  groups is found in higher-lying proton groups up to  $p_{48}$  at  $E_\alpha = 6.8$  MeV. As expected, the StM calculation for the total  $(\alpha,p)$  cross section is far above the experimental partial  $p_0$ ,  $p_1$ , and  $p_{2-3}$  cross sections. This is consistent with the finding from the spectrum shown in Fig. 2 of [74]. The determination of the total  $(\alpha,p)$  cross section is further hampered by the fact that only re-digitized data are available for the  $(\alpha,p)$  cross sections.

The calculated total  $(\alpha,n)$  and  $(\alpha,p)$  cross sections for  $^{45}\text{Sc}$  in Fig. 14 show that the total reaction cross section  $\sigma_{\text{reac}}$  and the reduced cross section  $\sigma_{\text{red}}$  are dominated by the  $(\alpha,n)$  contribution at energies above  $\approx 7$  MeV. However, at the lowest energies the  $(\alpha,n)$  and  $(\alpha,p)$  cross sections are of comparable strength. The reduced cross sections  $\sigma_{\text{red}}$  in Fig. 15 are thus well-defined around  $E_{\text{red}} \approx 1$  MeV by the  $(\alpha,n)$  cross section whereas at the lowest energies in Fig. 15 around  $E_{\text{red}} \approx 0.5$  MeV  $\sigma_{\text{red}}$  will be underestimated by about a factor of two. At higher energies one further data point is obtained from elastic  $^{45}\text{Sc}(\alpha,\alpha)^{45}\text{Sc}$  scattering:  $\sigma_{\text{red}} = 52.1$  mb at  $E_{\text{red}} = 3.06$  MeV [65]. Similar to most nuclei under study in this work, the  $\sigma_{\text{red}}$  data for  $^{45}\text{Sc}$  do not show a peculiar behavior.

#### 4.9 $^{48}\text{Ca}$

$^{48}\text{Ca}$  is a doubly-magic ( $Z = 20$ ,  $N = 28$ ) nucleus with a significant neutron excess ( $N/Z = 1.4$ ). As a consequence, the  $^{48}\text{Ca}(\alpha,p)^{51}\text{Sc}$  reaction is strongly suppressed, and the total reaction cross section  $\sigma_{\text{reac}}$  at low energies is well-defined by its dominant  $^{48}\text{Ca}(\alpha,n)^{51}\text{Ti}$  contribution. Unfortunately, no data for this reaction are available a EXFOR. The thick-target yield curve of Roughton *et al.* [49]

has been differentiated to extract the  $^{48}\text{Ca}(\alpha,n)^{51}\text{Ti}$  cross section (see Sect. 3.4). The result is shown in Fig. 16.

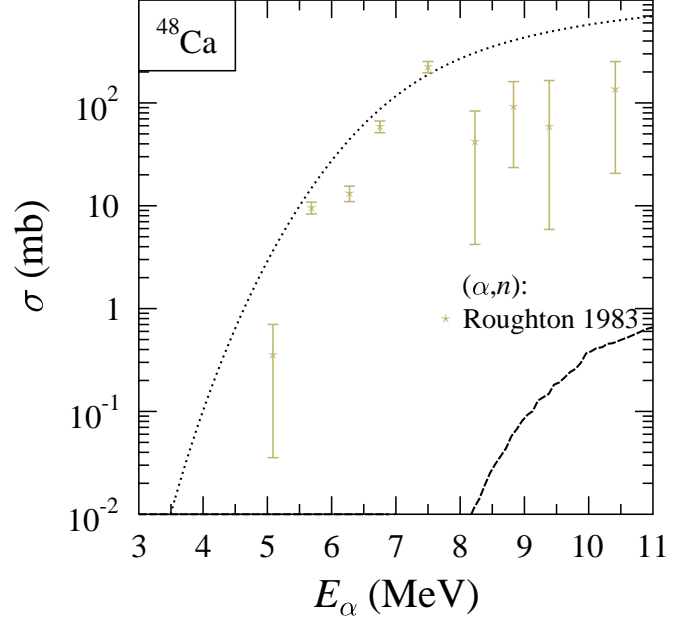


**Fig. 16.** Cross sections of the  $^{48}\text{Ca}(\alpha,n)^{51}\text{Ti}$  and  $^{48}\text{Ca}(\alpha,p)^{51}\text{Sc}$  reactions. The experimental data have been taken from [49]. Further discussion see text.

Because of the few available reaction data for  $^{48}\text{Ca}$ , in addition the elastic  $^{48}\text{Ca}(\alpha,\alpha)^{48}\text{Ca}$  scattering data of

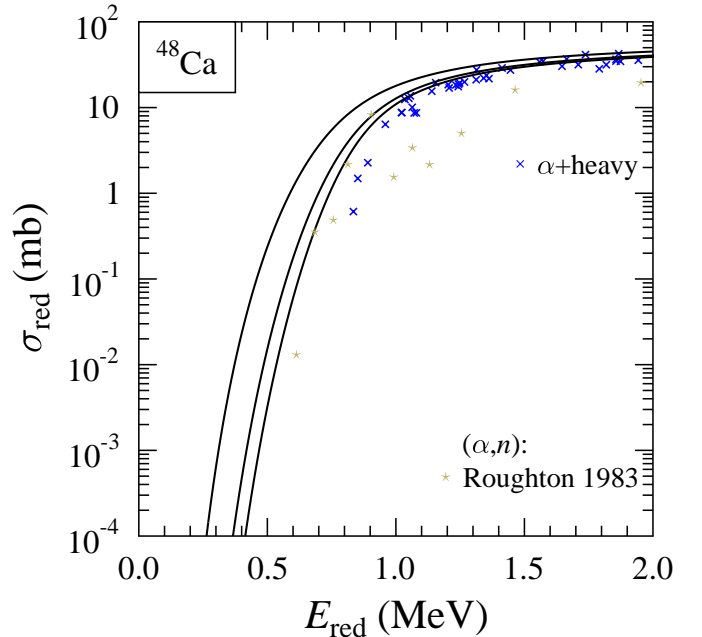


**Fig. 17.** Same as Fig. 5, but for  $\alpha$ -induced reactions on  $^{48}\text{Ca}$ . The experimental data have been taken from [49]. Further discussion see text.

Gaul *et al.* [75] at 18 to 29 MeV were analyzed. Total cross sections  $\sigma_{\text{reac}}$  between 1365 and 1771 mb were obtained for the four angular distributions at 18.0, 22.0, 24.1, and 29.0 MeV, corresponding to reduced cross sections  $\sigma_{\text{red}}$  of 50.0, 58.5, 64.9, and 59.3 mb at  $E_{\text{red}} = 2.17, 2.65, 2.90,$  and 3.49 MeV (above the shown range in Fig. 17). Although the experimental data are quite limited, it can be concluded that there is no evidence for a peculiar behavior of the reduced cross sections  $\sigma_{\text{red}}$  for the doubly-magic nucleus  $^{48}\text{Ca}$ .

#### 4.10 $^{42}\text{Ca}$

The semi-magic  $^{42}\text{Ca}$  nucleus is characterized by relatively large negative  $Q$ -values for the  $(\alpha, n)$  ( $-5.18$  MeV) and  $(\alpha, p)$  ( $-2.34$  MeV) reactions. Therefore, at very low energies the  $^{42}\text{Ca}(\alpha, \gamma)^{46}\text{Ti}$  reaction plays also an important role in the determination of the total reaction cross section.

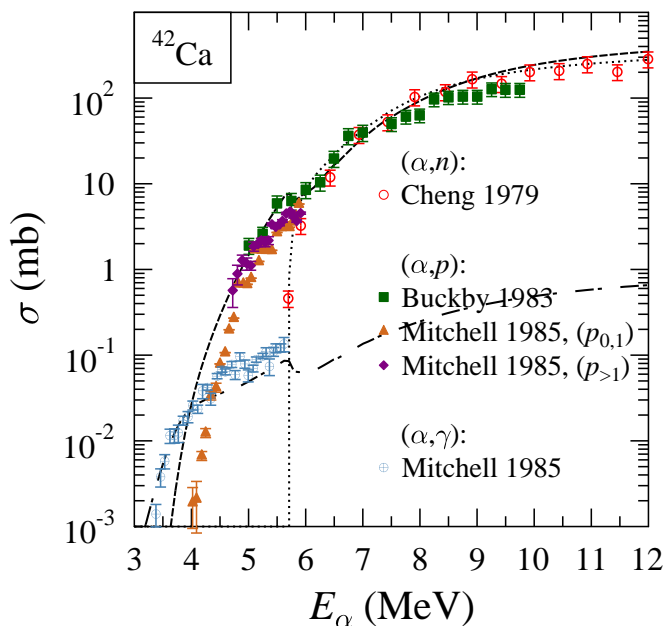


**Fig. 18.** Cross sections of the  $^{42}\text{Ca}(\alpha, n)^{45}\text{Ti}$ ,  $^{42}\text{Ca}(\alpha, p)^{45}\text{Sc}$ , and  $^{42}\text{Ca}(\alpha, \gamma)^{46}\text{Ti}$  reactions. The experimental data have been taken from [76, 77, 78]. The additional dash-dotted line shows the StM calculation for the  $(\alpha, \gamma)$  reaction. Further discussion see text.

The  $^{42}\text{Ca}(\alpha, n)^{45}\text{Ti}$  cross section has been determined by Cheng *et al.* [76] using activation in combination with annihilation spectroscopy. The energy range starts close above the  $(\alpha, n)$  threshold. A comparison with a StM calculation shows excellent agreement (see Fig. 18).

Buckby *et al.* [77] have measured excitation functions for the  $^{42}\text{Ca}(\alpha, p)^{45}\text{Sc}$  reaction at five different angles. Unfortunately, no spectrum is shown in [77], but total cross sections for the  $(\alpha, p)$  reaction are reported, and it is stated

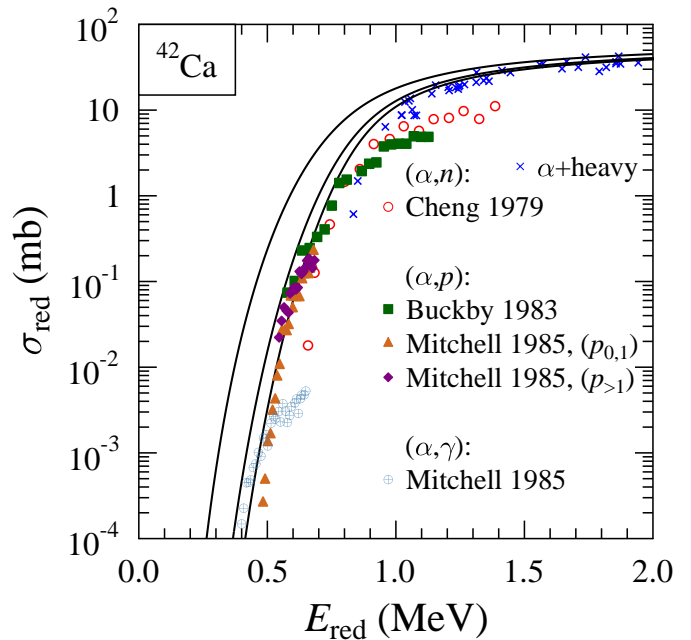


**Fig. 19.** Same as Fig. 5, but for  $\alpha$ -induced reactions on  $^{42}\text{Ca}$ . The experimental data have been taken from [76, 77, 78]. At energies above the  $(\alpha, n)$  threshold, the cross sections of the  $^{42}\text{Ca}(\alpha, n)^{45}\text{Ti}$  and  $^{42}\text{Ca}(\alpha, p)^{45}\text{Sc}$  reactions are very similar. Below the  $(\alpha, p)$  threshold, the total cross section  $\sigma_{\text{reac}}$  is dominated by the  $^{42}\text{Ca}(\alpha, \gamma)^{46}\text{Ti}$  reaction. Further discussion see text.

that “sufficient counts were obtained for the smallest proton peaks in the spectrum” and “The contribution of any remaining missed proton groups was then estimated by reference to their percentage contribution to the total yield at higher energies.” At energies above the  $(\alpha, n)$  threshold the  $(\alpha, p)$  and  $(\alpha, n)$  cross sections are of comparable strength whereas at energies below the  $(\alpha, n)$  threshold (and obviously above the  $(\alpha, p)$  threshold) the total reaction cross section is dominated by the  $(\alpha, p)$  cross section.

The  $(\alpha, p)$  data by Buckby *et al.* are extended towards lower energy by Mitchell *et al.* [78]. Here two techniques were applied. The  $^{42}\text{Ca}(\alpha, p_{0,1})^{45}\text{Sc}$  cross section was measured by a proton detector at  $\vartheta = 145^\circ$ , and isotropy of the angular distributions was checked at few energies with a five-detector array. The  $^{42}\text{Ca}(\alpha, p_{>1})^{45}\text{Sc}$  reaction was measured by the  $\gamma$ -ray yield of de-exciting  $^{45}\text{Sc}$  residual nuclei. The total  $^{42}\text{Ca}(\alpha, p)^{45}\text{Sc}$  cross section is then obtained from the sum of the measured  $(\alpha, p_{0,1})$  and  $(\alpha, p_{>1})$  cross sections. Figs. 18 and 19 show the individual  $(\alpha, p_{0,1})$  and  $(\alpha, p_{>1})$  cross sections. As both contributions are almost equal, the total  $(\alpha, p)$  cross section should be about a factor of 2 higher than the two individual cross sections. However, this sum is slightly higher than the result of Buckby *et al.* [77].

At energies below about  $E_\alpha \approx 4$  MeV, the  $(\alpha, p)$  cross section approaches its threshold ( $Q = -2.34$  MeV), and thus the cross section is further suppressed by the Coulomb barrier in the exit channel. As a consequence, the  $(\alpha, \gamma)$  cross section exceeds the  $(\alpha, p)$  cross section. Experimen-

tal data for the  $^{42}\text{Ca}(\alpha,\gamma)^{46}\text{Ti}$  cross section have also been measured by Mitchell *et al.* [78] by summing the intensities of the  $\gamma$ -rays to the ground state and the  $\gamma$ -ray from the first excited  $2^+$  state to the  $0^+$  ground state in  $^{46}\text{Ti}$ .

The total reaction cross section  $\sigma_{\text{reac}}$  and the reduced cross section  $\sigma_{\text{red}}$  for  $^{42}\text{Ca}$  are essentially given by the  $(\alpha,\gamma)$  cross section at very low energies, by the  $(\alpha,p)$  cross section between about 5 and 6.5 MeV, and the sum of  $(\alpha,p)$  and  $(\alpha,n)$  cross sections at energies above the neutron threshold. The individual  $(\alpha,n)$ ,  $(\alpha,p)$ , and  $(\alpha,\gamma)$  cross sections are shown as reduced cross sections  $\sigma_{\text{red}}$  in Fig. 19. Similar to most nuclei under study in this work, the  $\sigma_{\text{red}}$  data for  $^{42}\text{Ca}$  do not show a peculiar behavior.

#### 4.11 $^{40}\text{Ca}$

Similar to the semi-magic  $^{42}\text{Ca}$ , the doubly-magic  $^{40}\text{Ca}$  nucleus is also characterized by strongly negative  $Q$ -values for the  $(\alpha,p)$  ( $-3.52$  MeV) and the  $(\alpha,n)$  ( $-11.17$  MeV) reactions. As both residual nuclei of the  $(\alpha,p)$  and  $(\alpha,n)$  reaction are unstable, and  $^{43}\text{Ti}$  has a very short half-life of less than 1 second, the activation technique can be applied to measure the sum of the  $(\alpha,p)$  and  $(\alpha,n)$  cross sections by detection of the induced  $^{43}\text{Sc}$  activity. Annihilation spectroscopy was used by Howard *et al.* [69] for this purpose. The result is shown in Fig. 20. The agreement with the StM calculation is excellent for lower energies. At higher energies the experimental data are slightly underestimated. As the StM calculation shows, the  $(\alpha,n)$  cross section is practically negligible for  $^{40}\text{Ca}$ .

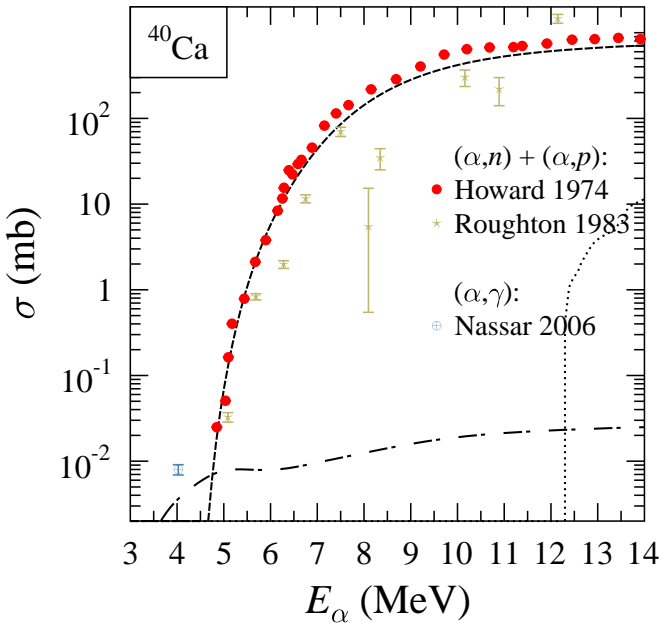


**Fig. 20.** Cross sections of the  $^{40}\text{Ca}(\alpha,n)^{43}\text{Ti}$ ,  $^{40}\text{Ca}(\alpha,p)^{43}\text{Sc}$ , and  $^{40}\text{Ca}(\alpha,\gamma)^{44}\text{Ti}$  reactions. The experimental data have been taken from [69,81,49]. The additional dash-dotted line shows the StM calculation for the  $(\alpha,\gamma)$  reaction. Further discussion see text.

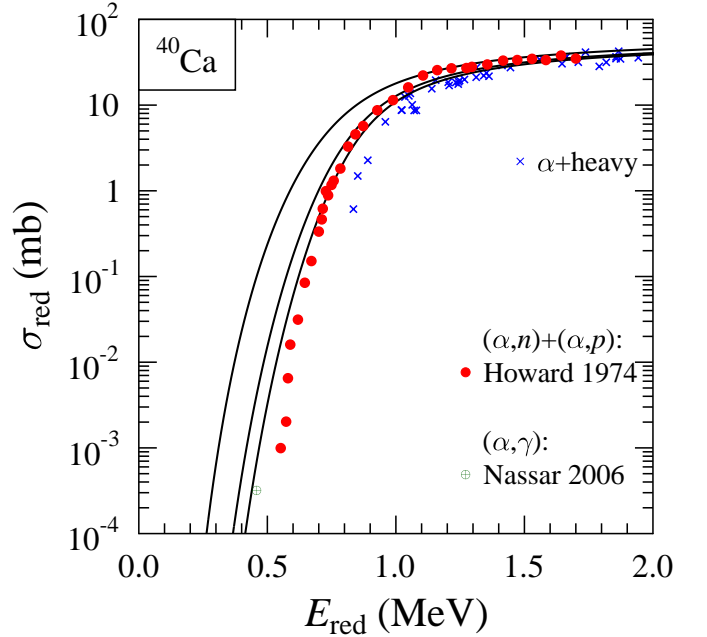


**Fig. 21.** Same as Fig. 5, but for  $\alpha$ -induced reactions on  $^{40}\text{Ca}$ . The experimental data have been taken from [69,81]. Further discussion see text.

Again similar to  $^{42}\text{Ca}$ , at very low energies close above the  $(\alpha,p)$  threshold, the  $(\alpha,p)$  reaction is further suppressed by the Coulomb barrier in the exit channel, and consequently the total reaction cross section is significantly affected by the  $(\alpha,\gamma)$  cross section. However, average cross sections for the  $^{40}\text{Ca}(\alpha,\gamma)^{44}\text{Ti}$  reaction are very rare in literature, and the focus of recent  $(\alpha,\gamma)$  experiments was the astrophysically very important resonance triplet around 4.5 MeV and the properties of resonances [79,80,81,82,83,84,85]. The thick-target data point of Nassar *et al.* [81] leads to an average cross section of  $8.0 \pm 1.1 \mu\text{b}$  for the broad energy range from about 2.1 to 4.2 MeV in the center-of-mass system. Using the calculated average energy dependence of the  $(\alpha,\gamma)$  cross section, the effective energy is  $E_{\text{c.m.}} \approx 3.45$  MeV. This data point is shown in Figs. 20 and 21.

As pointed out above, the total reaction cross section  $\sigma_{\text{reac}}$  and the reduced cross section  $\sigma_{\text{red}}$  are well-defined by the  $(\alpha,p)$  cross section over a wide energy range. The reduced cross section for  $^{40}\text{Ca}$  is shown in Fig. 21. At higher energies above  $E_{\text{red}} \approx 1$  MeV, the obtained  $\sigma_{\text{red}}$  is close to the other nuclei in the  $A \approx 20 - 50$  mass range. However, at lower energies below  $E_{\text{red}} \approx 1$  MeV, the reduced cross section  $\sigma_{\text{red}}$  for  $^{40}\text{Ca}$  is slightly lower than for neighboring nuclei. This reflects the doubly-magic nature of  $^{40}\text{Ca}$ .

#### 4.12 $^{41}\text{K}$

Whereas the previously studied nuclei are located completely in the  $fp$ -shell,  $^{41}\text{K}$  with  $Z = 19$  and  $N = 22$  enters the transition region between the  $sd$ -shell and the  $fp$ -shell. Several experimental data sets are available for

the  $^{41}\text{K}(\alpha,n)^{44}\text{Sc}$  reaction. Scott *et al.* [88] have measured the  $(\alpha,n)$  cross section by neutron counting and by activation in combination with  $\gamma$ -ray detection of the 1157 keV  $\gamma$ -ray in the decay  $^{44}\text{Sc} \rightarrow ^{44}\text{Ca}$ . Both experimental techniques provide consistent results in the energy range under study by Scott *et al.*; a small correction of a few per cent was applied to the activation data to take into account a long-living  $J^\pi = 6^+$  isomer with  $T_{1/2} = 2.44$  days.

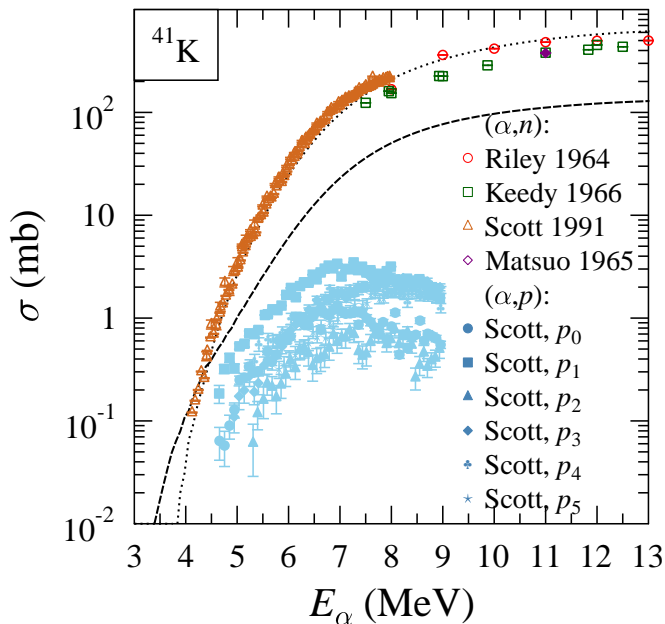


**Fig. 22.** Cross sections of the  $^{41}\text{K}(\alpha,n)^{44}\text{Sc}$  and  $^{41}\text{K}(\alpha,p)^{44}\text{Ca}$  reactions. The experimental data have been taken from [86,87,88,89] and are the sum of the ground state and isomer cross sections in the  $(\alpha,n)$  channel. Further discussion see text.

At higher energies yields for the ground state and isomeric state have been measured separately. Keedy *et al.* [87] used activation in combination with annihilation spectroscopy whereas Riley *et al.* [86] and Matsuo *et al.* [89] used also activation, but in combination with  $\gamma$ -ray spectroscopy. All experimental data sets are in reasonable agreement within the experimental uncertainties, with about 10 – 25% lower cross sections in [87] and [89]. The results are shown in Fig. 22; the ground state cross section and the isomeric cross section have been added to provide the total  $(\alpha,n)$  cross section. The agreement between the experimental data and a StM calculation is again excellent.

Scott *et al.* [88] also provide cross sections for the  $^{41}\text{K}(\alpha,p)^{44}\text{Ca}$  reaction from an excitation function measurement at one angle  $\vartheta = 125^\circ$ . Fig. 4 of [88] shows only the cross sections of the lowest  $p_0, p_1, p_2, p_3, p_4,$  and  $p_5$  proton groups. However, the spectrum in Fig. 3 of [88] shows a dominating peak for  $p_{6-9}$ , another strong peak for  $p_{10-14}$ , and further peaks for  $p_{15-35}$ . The results for the low-lying proton groups are shown in Fig. 22; as expected, they are significantly lower than the StM calculation for the total  $(\alpha,p)$  cross section. A point-by-point summing

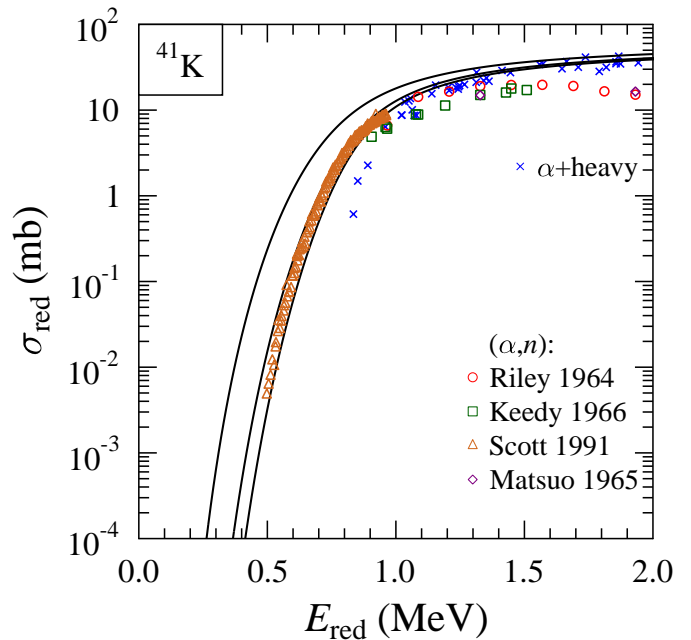


**Fig. 23.** Same as Fig. 5, but for  $\alpha$ -induced reactions on  $^{41}\text{K}$ . The experimental data have been taken from [86,87,88,89] and include the ground state and isomer contributions of the  $^{41}\text{K}(\alpha,n)^{44}\text{Sc}$  reaction. Further discussion see text.

of the  $p_i$  channels is again hampered by the fact that the EXFOR data had to be re-digitized from Fig. 4 of [88].

The total reaction cross section  $\sigma_{\text{reac}}$  and the reduced cross section  $\sigma_{\text{red}}$  are dominated by the  $^{41}\text{K}(\alpha,n)^{44}\text{Sc}$  reaction for energies above 5 MeV, i.e., over almost the entire energy range under study. The results for  $\sigma_{\text{red}}$  from the  $(\alpha,n)$  channel are shown in Fig. 23. Only at the lowest energies a significant contribution of the  $(\alpha,p)$  channel is found. Similar to most nuclei under study in this work, the  $\sigma_{\text{red}}$  data for  $^{41}\text{K}$  do not show a peculiar behavior.

#### 4.13 $^{40}\text{K}$

The odd-odd ( $Z = 19, N = 21$ ) nucleus  $^{40}\text{K}$  has a very low natural abundance, and in addition it is unstable. The 1461 keV  $\gamma$ -ray of the  $^{40}\text{K} \rightarrow ^{40}\text{Ar}$  decay is a prominent background line in almost any  $\gamma$ -ray spectrum. Therefore, only very few experimental data are available for  $^{40}\text{K}$ . Elastic  $^{40}\text{K}(\alpha,\alpha)^{40}\text{K}$  scattering has been measured by Oeschler *et al.* [90] at 24 MeV. Unfortunately, the experimental data are only presented as a line in Fig. 1 of [90] which had to be re-digitized for EXFOR. As this is the only data set for  $^{40}\text{K}$ , a phase shift fit was made to the angular distribution (as provided by EXFOR). The result of  $\sigma_{\text{red}} = 67.5$  mb at  $E_{\text{red}} = 2.88$  MeV is within the expected range. Because of the lack of experimental data, no figure is shown for  $\sigma_{\text{red}}$  of  $^{40}\text{K}$ . But from the only available data set it can be concluded that there is at least no evidence for a peculiar behavior of  $\sigma_{\text{red}}$  for the odd-odd  $^{40}\text{K}$ .

#### 4.14 $^{39}\text{K}$

Contrary to  $^{41}\text{K}$  with the dominating  $(\alpha, n)$  cross section, the semi-magic ( $N = 20$ )  $^{39}\text{K}$  has a much larger  $(\alpha, p)$  cross section. The  $^{39}\text{K}(\alpha, n)^{42}\text{Sc}$  reaction has a strongly negative  $Q$ -value ( $Q = -7.33$  MeV). Only two data points are available by Nelson *et al.* [91], one for the ground state and one for the  $(7)^+$  isomer in  $^{42}\text{Sc}$  which decays to a  $6^+$  state in  $^{42}\text{Ca}$ . The two data points are shown in Fig. 24; both experimental  $(\alpha, n)$  data are far below the theoretical expectation from the StM model. As the  $(\alpha, n)$  cross section is by far more than one order of magnitude below the  $(\alpha, p)$  cross section, this deviation does fortunately not affect the determination of the total reaction cross section  $\sigma_{\text{reac}}$  which is close to the  $(\alpha, p)$  cross section.

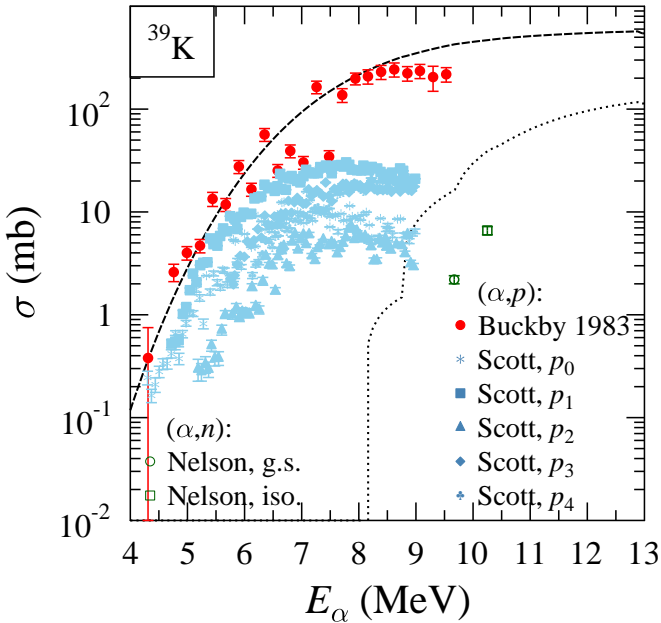


**Fig. 24.** Cross sections of the  $^{39}\text{K}(\alpha, n)^{42}\text{Sc}$  and  $^{39}\text{K}(\alpha, p)^{42}\text{Ca}$  reactions. The experimental data have been taken from [77, 92, 91]; the  $(\alpha, n)$  of [91] data are separated for the ground state and the isomer in  $^{42}\text{Sc}$ . Further discussion see text.

The  $^{39}\text{K}(\alpha, p)^{42}\text{Ca}$  reaction has been studied by Buckby *et al.* [77] and Scott *et al.* [92]. Buckby *et al.* have measured five-point angular distributions (for a discussion of the experimental procedure, see Sec. 4.10). Scott *et al.* have measured excitation functions at one angle  $\vartheta = 125^\circ$ , and results are reported for the proton groups  $p_0$ ,  $p_1$ ,  $p_2$ ,  $p_3$ , and  $p_4$ . However, it can be seen from the spectrum in Fig. 1 of [92], that significant contributions to the total  $(\alpha, p)$  cross section come also from the  $p_{5-9}$  and  $p_{10}$  proton groups, and it is stated in the text that additional proton groups  $p_{11-18}$ ,  $p_{19-28}$ , and  $p_{29-32}$  have been observed at higher energies. In addition, the EXFOR data of Scott *et al.* had to be re-digitized. Thus, it is impossible to determine the total  $(\alpha, p)$  cross section from these data. But it can be seen in Fig. 24 that the Scott *et al.* data for each proton group are – as expected – below the total  $(\alpha, p)$

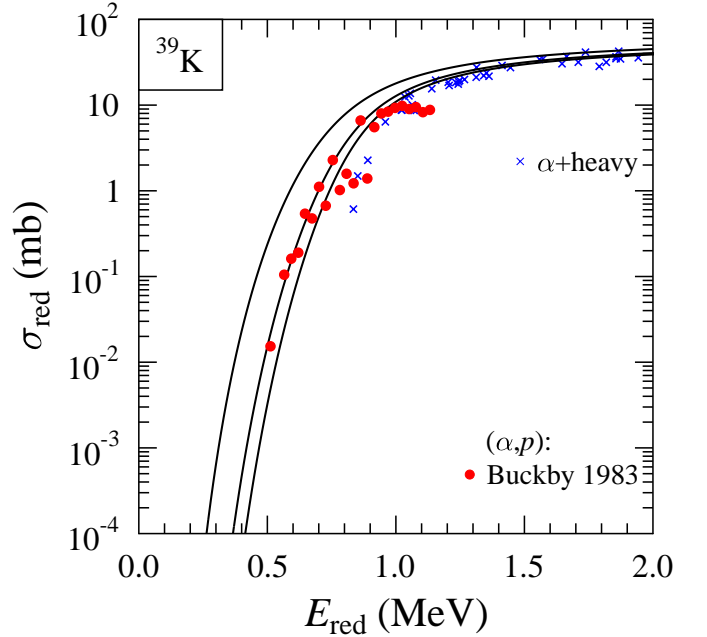


**Fig. 25.** Same as Fig. 5, but for  $\alpha$ -induced reactions on  $^{39}\text{K}$ . The experimental data have been taken from [77]. Further discussion see text.

cross section reported by Buckby *et al.* in their Table 1 of [77].

For the determination of the total reaction cross section  $\sigma_{\text{reac}}$  and the reduced cross section  $\sigma_{\text{red}}$  only the data by Buckby *et al.* [77] are used. The results are shown in Fig. 25. Similar to most nuclei under study in this work, the  $\sigma_{\text{red}}$  data for  $^{39}\text{K}$  do not show a peculiar behavior.

#### 4.15 $^{40}\text{Ar}$

For the neutron-rich  $^{40}\text{Ar}$  it is obvious that the  $(\alpha, n)$  cross section dominates whereas the  $(\alpha, p)$  cross section is much smaller. Unfortunately, only few experimental data for  $^{40}\text{Ar}$  are available at EXFOR. The  $^{40}\text{Ar}(\alpha, n)^{43}\text{Ca}$  cross section was determined by Schwartz *et al.* [93] at  $E_\alpha = 7.4$  MeV using a argon-filled gas target. The emitted particles were detected by nuclear track counting at one angle ( $\vartheta = 90^\circ$ ), and isotropy was assumed. The result of 33 mb has an uncertainty of a factor of two and is much lower than the prediction from the StM (see Fig. 26). It should be noted that the energy loss of the beam in the entrance window of the gas target and in the gas cell was not taken into account in [93]. This energy loss should be of the order of 500 keV for the entrance window. The target thickness in [93] is given with 130 keV leading to an effective energy which is about 65 keV lower. These corrections of more than 500 keV bring the data point closer to the StM prediction.

In addition to the Schwartz *et al.* [93] experiment at 7.4 MeV, the  $^{40}\text{Ar}(\alpha, p)^{43}\text{K}$  reaction was also measured at higher energies by Tanaka *et al.* [94] and Fenyvesi *et al.* [14]. Both experiments used a stacked-target technique

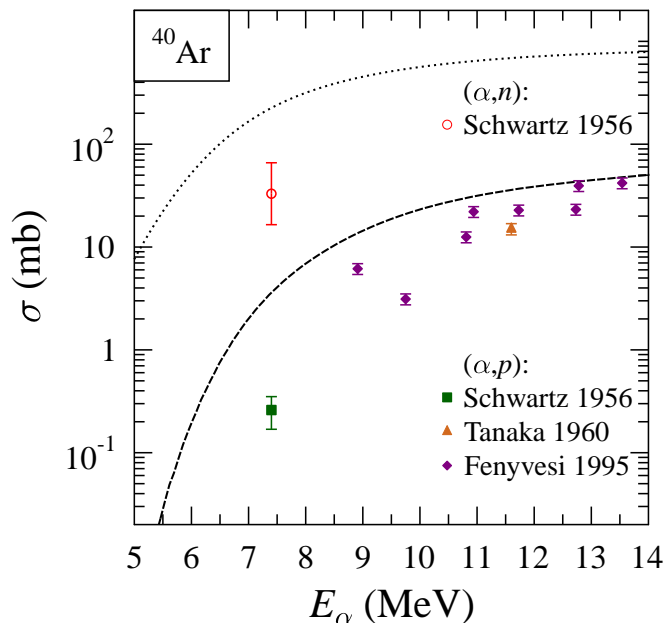


**Fig. 26.** Cross sections of the  $^{40}\text{Ar}(\alpha, n)^{43}\text{Ca}$  and  $^{40}\text{Ar}(\alpha, p)^{43}\text{K}$  reactions. The experimental data have been taken from [93,94,14]. The energy of the data points by Schwartz *et al.* [93] at  $E_\alpha = 7.4$  MeV should be corrected by about 500 keV because of the energy loss of the beam in the entrance window of the gas target and in the gas cell. Further discussion see text.

and  $4\pi$ - $\beta$ -counting in [94] and  $\gamma$ -spectroscopy in [14] for the detection of the decay of the residual  $^{43}\text{K}$  nucleus. The results of the experiments of [94,14] are in good agreement, and also the 7.4 MeV data point of Schwartz *et al.* [93] seems roughly to follow the expected energy dependence (in particular, if the energy of this data point is corrected by about 500 keV as discussed above). Similar to the  $^{40}\text{Ar}(\alpha, n)^{43}\text{Ca}$  cross section, also the  $^{40}\text{Ar}(\alpha, p)^{43}\text{K}$  cross section is overestimated by the StM calculation at low energies. For completeness it should be noted that the StM calculations using either TALYS or NON-SMOKER are almost identical for  $^{40}\text{Ar}$ .

The total reaction cross section  $\sigma_{\text{reac}}$  and the reduced cross section  $\sigma_{\text{red}}$  can be derived from the  $^{40}\text{Ar}(\alpha, n)^{43}\text{Ca}$  cross section. However, there is only one data point with large uncertainties [93] which may need a correction of the energy. The results for  $\sigma_{\text{red}}$  are shown in Fig. 27. Based on the one data point by Schwartz *et al.* [93] with its large error bars, the reduced cross section of  $^{40}\text{Ar}$  seems to be smaller than for most neighboring nuclei in the  $A \approx 20-50$  mass region. Improved data for  $^{40}\text{Ar}$  are highly desirable.

Because of the noticeable behavior of  $\sigma_{\text{red}}$  of  $^{40}\text{Ar}$  at low energies,  $\sigma_{\text{red}}$  of  $^{40}\text{Ar}$  was additionally studied at higher energies using  $^{40}\text{Ar}(\alpha, \alpha)^{40}\text{Ar}$  elastic scattering. Data at relatively low energies are available in [95,96], and data above 20 MeV have also been measured in [75,90]. Only the 18 MeV data by Seidlitz *et al.* [96] are available numerically from Table I of [96]; the other data had to be redigitized from small figures with logarithmic scale in [95,

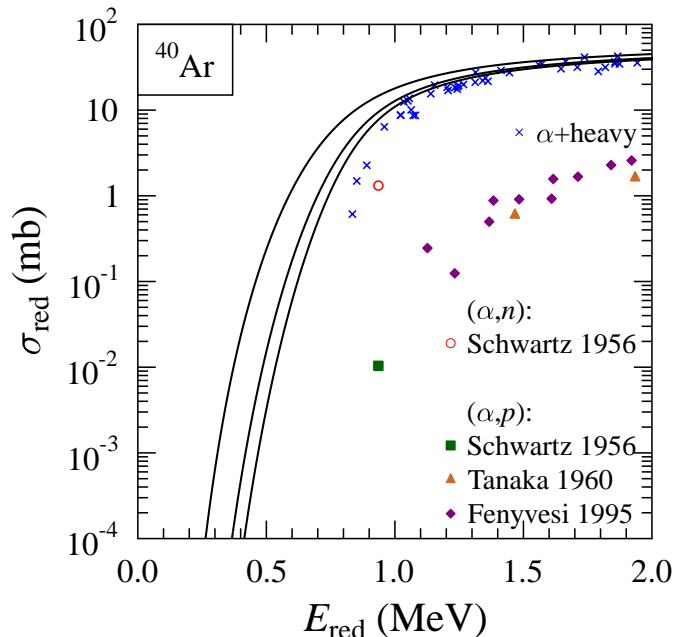


**Fig. 27.** Same as Fig. 5, but for  $\alpha$ -induced reactions on  $^{40}\text{Ar}$ . The experimental data have been taken from [93,94,14]. The energy of the data points by Schwartz *et al.* [93] at  $E_\alpha = 7.4$  MeV should be corrected by about 500 keV because of the energy loss of the beam in the entrance window of the gas target and in the gas cell. Only one data point is available for the dominating  $^{40}\text{Ar}(\alpha, n)^{43}\text{Ca}$  reaction. The  $^{40}\text{Ar}(\alpha, p)^{43}\text{K}$  reaction contributes only minor to the total reaction cross section  $\sigma_{\text{reac}}$ . Further discussion see text.

75,90], and no error bars are available in the EXFOR data. Therefore the following study is restricted to the data by Seidlitz *et al.* [96] and the data at the lowest energies by Bucurescu *et al.* [95]. It turns out that the limited angular range of the angular distributions by Bucurescu *et al.* [95] is not sufficient to derive the total reaction cross section  $\sigma_{\text{reac}}$  from these data. The angular distribution of Seidlitz *et al.* [96] covers the full angular range; however, at forward angles the measured cross section is almost twice the Rutherford cross section of pointlike charges. Therefore, Gaul *et al.* [75] have suggested to scale the angular distribution by Seidlitz *et al.* by a factor of 0.55; a similar scaling factor of 0.57 is suggested from the best fit obtained in this work. The total reaction cross section is  $\sigma_{\text{reac}} = 1468$  mb at  $E_\alpha = 17.98$  MeV, corresponding to a reduced cross section  $\sigma_{\text{red}} = 58.5$  mb at  $E_{\text{red}} = 2.27$  MeV. This value fits nicely into the general systematics of reduced cross sections at higher energies around  $E_{\text{red}} \approx 2$  MeV (see Fig. 1). Thus, the behavior of  $\sigma_{\text{red}}$  for  $^{40}\text{Ar}$  is extraordinary only at low energies.

#### 4.16 $^{36}\text{Ar}$

Contrary to the neutron-rich nucleus  $^{40}\text{Ar}$ , the dominating channel for  $^{36}\text{Ar}$  is the  $^{36}\text{Ar}(\alpha, p)^{39}\text{K}$  reaction. The  $^{36}\text{Ar}(\alpha, n)^{39}\text{Ca}$  reaction has a strongly negative  $Q$ -value

( $Q = -8.60$  MeV) and thus cannot contribute to the total cross section  $\sigma_{\text{reac}}$  for  $^{36}\text{Ar}$  at low energies. There is only one data point for the  $^{36}\text{Ar}(\alpha,p)^{39}\text{K}$  reaction at 7.4 MeV by Schwartz *et al.* [93] with large uncertainties. The energy of this data point should be corrected by about 500 keV because of the energy loss of the beam in the entrance window of the gas target and in the gas cell (see discussion in the previous Sec. 4.15). Even with the correction of the energy, the experimental data point of [93] is significantly below the StM calculation (see Fig. 28).

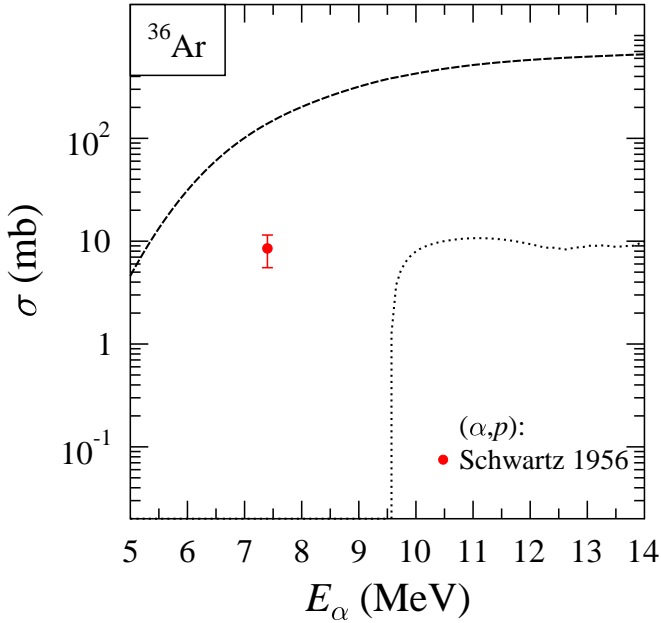


**Fig. 28.** Cross sections of the  $^{36}\text{Ar}(\alpha,n)^{39}\text{Ca}$  and  $^{36}\text{Ar}(\alpha,p)^{39}\text{K}$  reactions. The experimental data point has been taken from [93]. The energy of the data point by Schwartz *et al.* [93] at  $E_\alpha = 7.4$  MeV should be corrected by about 500 keV because of the energy loss of the beam in the entrance window of the gas target and in the gas cell. Further discussion see text.

The determination of the total reaction cross section  $\sigma_{\text{reac}}$  and reduced cross section  $\sigma_{\text{red}}$  for  $^{36}\text{Ar}$  is possible from the dominating  $^{36}\text{Ar}(\alpha,p)^{39}\text{K}$  cross section. However, this determination is obviously hampered by the availability of experimental data, and improved data for the  $^{36}\text{Ar}(\alpha,p)^{39}\text{K}$  reaction are highly desirable.

Similar to  $^{40}\text{Ar}$ , the noticeable behavior of  $\sigma_{\text{red}}$  for  $^{36}\text{Ar}$  at low energies requires further studies. Elastic scattering data are available by Gaul *et al.* [75], Oeschler *et al.* [90], and at higher energies by Kocher *et al.* [97]. A reasonable description of the 18 MeV data by Gaul *et al.* [75] was only obtained in the later analysis by Kocher *et al.* [97]. Therefore, the total reaction cross section  $\sigma_{\text{reac}}$  at 18 MeV was obtained by repeating the optical model calculation in [97]. This leads to  $\sigma_{\text{reac}} = 1241$  mb or  $\sigma_{\text{red}} = 51.9$  mb at  $E_{\text{red}} = 2.20$  MeV. Also this value fits nicely into the general systematics of reduced cross sections at higher energies around  $E_{\text{red}} \approx 2$  MeV (see Fig. 1). Thus,

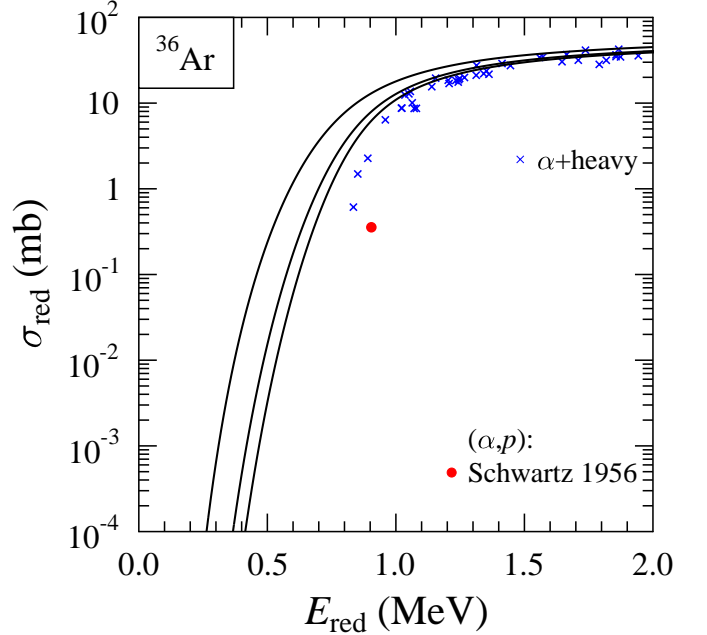


**Fig. 29.** Same as Fig. 5, but for  $\alpha$ -induced reactions on  $^{36}\text{Ar}$ . The experimental data have been taken from [93]. The energy of the data point by Schwartz *et al.* [93] at  $E_\alpha = 7.4$  MeV should be corrected by about 500 keV because of the energy loss of the beam in the entrance window of the gas target and in the gas cell. Further discussion see text.

also the behavior of  $\sigma_{\text{red}}$  for  $^{36}\text{Ar}$  is extraordinary only at low energies.

#### 4.17 $^{37}\text{Cl}$

Surprisingly, no experimental data are available in EXFOR for the  $^{37}\text{Cl}(\alpha,n)^{40}\text{K}$  and  $^{37}\text{Cl}(\alpha,p)^{40}\text{Ar}$  reactions. This may be related to the fact that both experiments cannot be done by activation because  $^{40}\text{K}$  is quasi-stable with its half-life of more than 1 billion years and  $^{40}\text{Ar}$  is stable. An excitation function for the  $^{37}\text{Cl}(\alpha,\gamma)^{41}\text{K}$  reaction is available by Zyskind *et al.* [98]; therefore, the presentation of results for  $^{37}\text{Cl}$  deviates from the usual restriction of this work on  $(\alpha,p)$  and  $(\alpha,n)$  cross sections.

Zyskind *et al.* [98] used a Ge(Li) detector to measure excitation functions for five strong  $\gamma$ -transitions at the angle of  $\vartheta = 55^\circ$ , i.e. at a zero of the  $P_2(\cos \vartheta)$  Legendre polynomial. The total cross section of the  $^{37}\text{Cl}(\alpha,\gamma)^{41}\text{K}$  reaction was derived from the sum of the five strong transitions. Additionally, careful corrections were made for weak transitions which were measured in special very long runs; these corrections were of the order of about 25%. The data are compared to a StM calculation in Fig. 30. At low energies below the  $(\alpha,n)$  threshold, good agreement is found. It has to be noted that the shown data by Zyskind *et al.* from the EXFOR database are taken from a table in the underlying Ph.D. thesis; the three data points at the highest energies which deviate from the expected energy dependence are not shown in the paper [98].

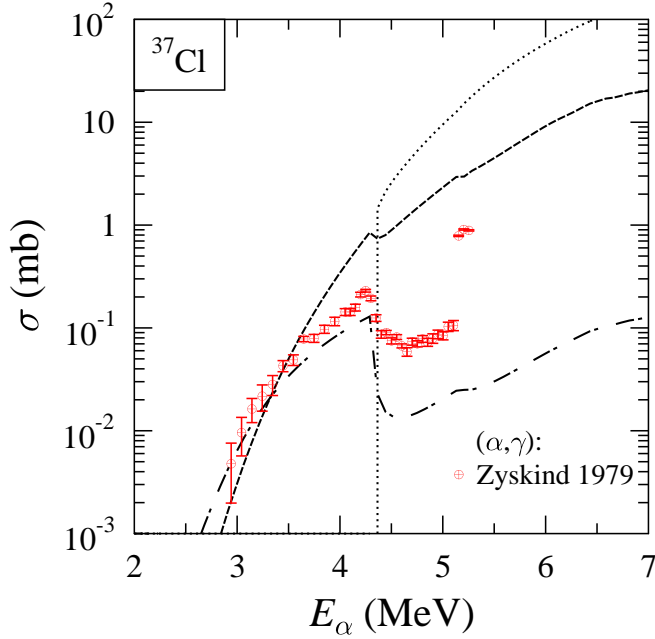


**Fig. 30.** Cross sections of the  $^{37}\text{Cl}(\alpha, n)^{40}\text{K}$ ,  $^{37}\text{Cl}(\alpha, p)^{40}\text{Ar}$ , and  $^{37}\text{Cl}(\alpha, \gamma)^{41}\text{K}$  reactions. The experimental data for the  $^{37}\text{Cl}(\alpha, \gamma)^{41}\text{K}$  reaction have been taken from [98]. No data are available in EXFOR for the  $^{37}\text{Cl}(\alpha, n)^{40}\text{K}$  and  $^{37}\text{Cl}(\alpha, p)^{40}\text{Ar}$  reactions. The additional dash-dotted line shows the StM calculation for the  $(\alpha, \gamma)$  reaction. Further discussion see text.

According to the StM calculations, at very low energies below about 3 MeV the  $(\alpha, \gamma)$  reaction is dominating. However, above 3 MeV up to the  $(\alpha, n)$  threshold, the  $(\alpha, p)$  cross section is comparable or even larger than the  $(\alpha, \gamma)$  cross section, and above the  $(\alpha, n)$  threshold the  $(\alpha, n)$  reaction becomes dominant. Due to the lack of other experimental data, the reduced cross section  $\sigma_{\text{red}}$  is taken from the  $^{37}\text{Cl}(\alpha, \gamma)^{41}\text{K}$  cross section (see Fig. 31). At the lowest energies the real  $\sigma_{\text{red}}$  should be only slightly larger than the shown data points from the  $(\alpha, \gamma)$  reaction. Around  $E_{\text{red}} \approx 0.5$  MeV one can see a weak kink in the excitation function, indicating that a contribution of the  $(\alpha, p)$  cross section is missing here. At energies above  $E_{\text{red}} \approx 0.6$  MeV there is a strong cusp indicating the  $(\alpha, n)$  threshold. Although the limited availability of experimental data somewhat hampers the analysis for  $^{37}\text{Cl}$ , it can nevertheless be stated that similar to most nuclei under study in this work, the  $\sigma_{\text{red}}$  data for  $^{37}\text{Cl}$  do not show a peculiar behavior.

#### 4.18 $^{35}\text{Cl}$

Three data sets are available for  $\alpha$ -induced reactions on  $^{35}\text{Cl}$ , but the experimental data cover the  $^{35}\text{Cl}(\alpha, n)^{38}\text{K}$  reaction only. Because of the negative  $Q$ -value of the  $(\alpha, n)$  reaction ( $Q = -5.86$  MeV), the  $(\alpha, n)$  data cannot restrict the total reaction cross section  $\sigma_{\text{reac}}$  and the reduced cross section  $\sigma_{\text{red}}$  at low energies.

Howard *et al.* [69] used the activation technique in combination with annihilation spectroscopy to measure

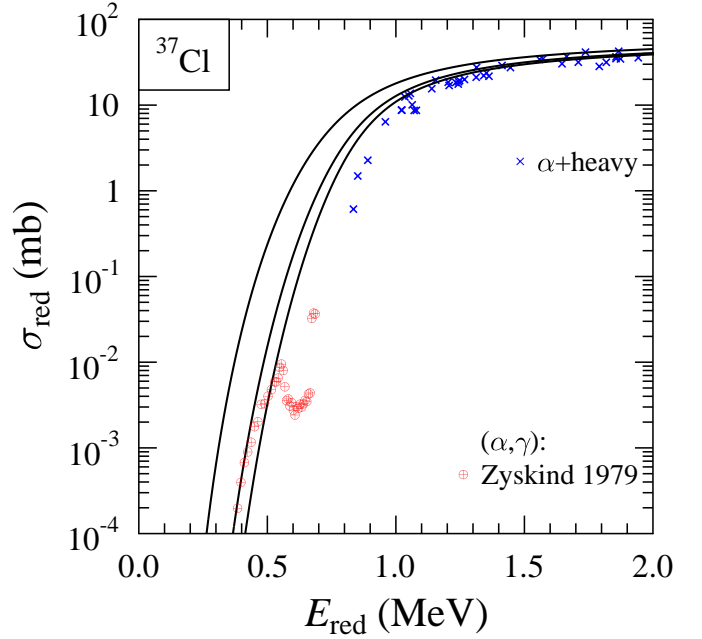


**Fig. 31.** Same as Fig. 5, but for  $\alpha$ -induced reactions on  $^{37}\text{Cl}$ . The experimental data have been taken from [98] for the  $^{37}\text{Cl}(\alpha, \gamma)^{41}\text{K}$  reaction. No data are available at EXFOR for the  $^{37}\text{Cl}(\alpha, n)^{40}\text{K}$  and  $^{37}\text{Cl}(\alpha, p)^{40}\text{Ar}$  reactions. Further discussion see text.

the  $^{35}\text{Cl}(\alpha, n)^{38}\text{K}$  cross section from about 7 to 11 MeV. At higher energies the stacked-foil activation technique has been used by Qaim *et al.* [99] and by Tárkányi *et al.* [100]; the activity of the residual  $^{38}\text{K}$  nucleus was observed

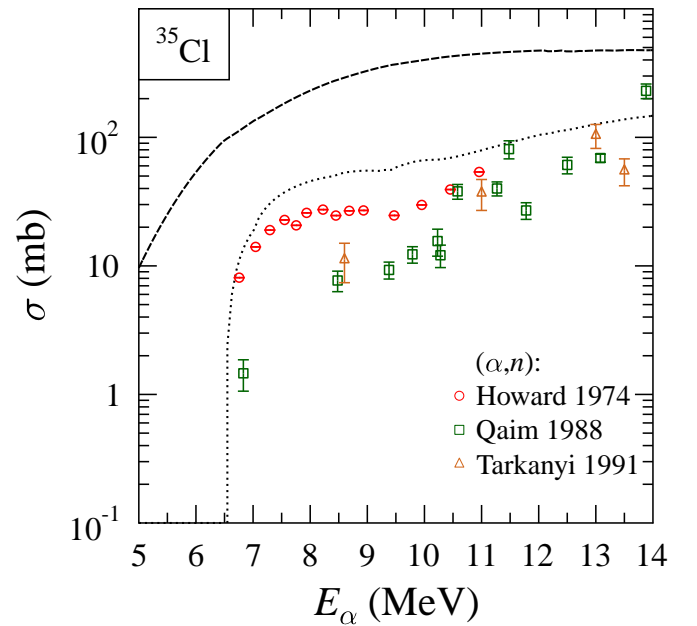


**Fig. 32.** Cross sections of the  $^{35}\text{Cl}(\alpha, n)^{38}\text{K}$  and  $^{35}\text{Cl}(\alpha, p)^{38}\text{Ar}$  reactions. The experimental data have been taken from [69, 99, 100]. Further discussion see text.

in both cases by  $\gamma$ -spectroscopy. The agreement between the different data sets is not very good; deviations are of the order of at least a factor of two (see Fig. 32).

As already stated above, a determination of the total reaction cross section  $\sigma_{\text{reac}}$  and reduced cross section  $\sigma_{\text{red}}$  is not possible from the available  $^{35}\text{Cl}(\alpha,n)^{38}\text{K}$  data because the  $^{35}\text{Cl}(\alpha,p)^{38}\text{Ar}$  reaction is dominating. Taking into account the factor of about 5–7 from the StM calculation in Fig. 32, the estimated reduced cross section  $\sigma_{\text{red}}$  is close to the expected values. The  $^{35}\text{Cl}(\alpha,n)^{38}\text{K}$  data thus do not show evidence for a peculiar behavior of  $\sigma_{\text{red}}$  for  $^{35}\text{Cl}$ .

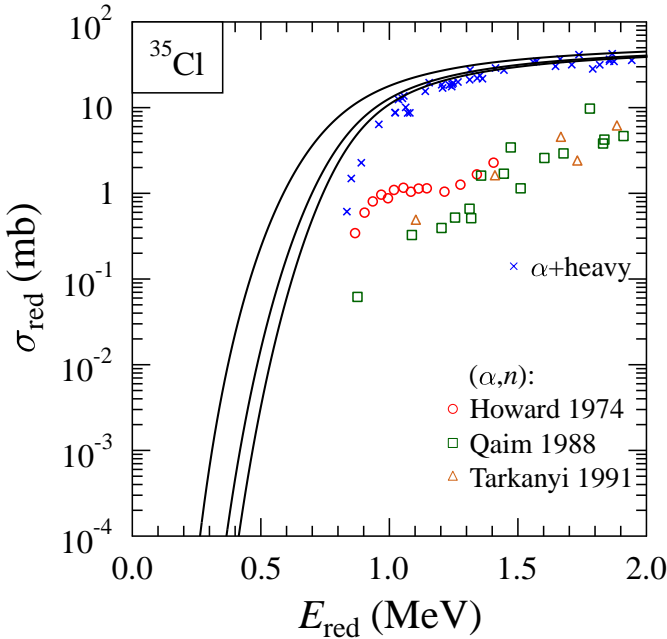


**Fig. 33.** Same as Fig. 5, but for  $\alpha$ -induced reactions on  $^{35}\text{Cl}$ . The experimental data have been taken from [69,99,100] for the  $^{35}\text{Cl}(\alpha,n)^{38}\text{K}$  reaction. The  $^{35}\text{Cl}(\alpha,n)^{38}\text{K}$  reaction is only a small ( $\approx 10 - 15\%$ ) contribution to the total reaction cross section  $\sigma_{\text{reac}}$  which is dominated by the  $^{35}\text{Cl}(\alpha,p)^{38}\text{Ar}$  reaction. Further discussion see text.

#### 4.19 $^{34}\text{S}$

The  $^{34}\text{S}(\alpha,n)^{37}\text{Ar}$ ,  $^{34}\text{S}(\alpha,p)^{37}\text{Cl}$ , and  $^{34}\text{S}(\alpha,\gamma)^{38}\text{Ar}$  reactions have been measured simultaneously by Scott *et al.* [101]. These data should allow to determine the total reaction cross section  $\sigma_{\text{reac}}$  and the reduced cross section  $\sigma_{\text{red}}$  with small uncertainties.

The  $^{34}\text{S}(\alpha,n)^{37}\text{Ar}$  reaction has been measured in [101] by direct neutron counting from the  $(\alpha,n)$  threshold ( $Q = -4.63$  MeV) up to about 10 MeV. Although minor problems with background from the  $^{13}\text{C}(\alpha,n)^{16}\text{O}$  reaction are reported in [101], an overall uncertainty of about 16% is estimated in [101]. The data are shown in Fig. 34. The comparison with the StM calculation shows that the energy dependence is nicely reproduced; however, the abso-

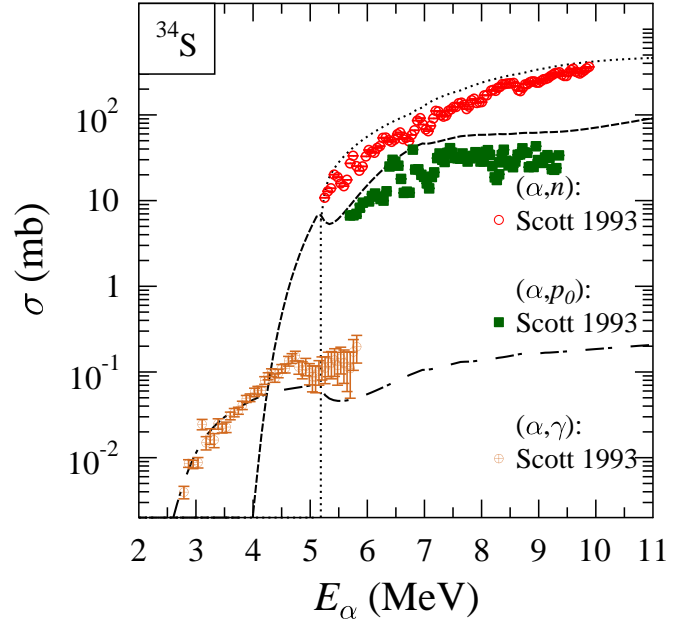


**Fig. 34.** Cross sections of the  $^{34}\text{S}(\alpha,n)^{37}\text{Ar}$ ,  $^{34}\text{S}(\alpha,p)^{37}\text{Cl}$ , and  $^{34}\text{S}(\alpha,\gamma)^{38}\text{Ar}$  reactions. The experimental data have been taken from [101]. The additional dash-dotted line shows the StM calculation for the  $(\alpha,\gamma)$  reaction. Further discussion see text.

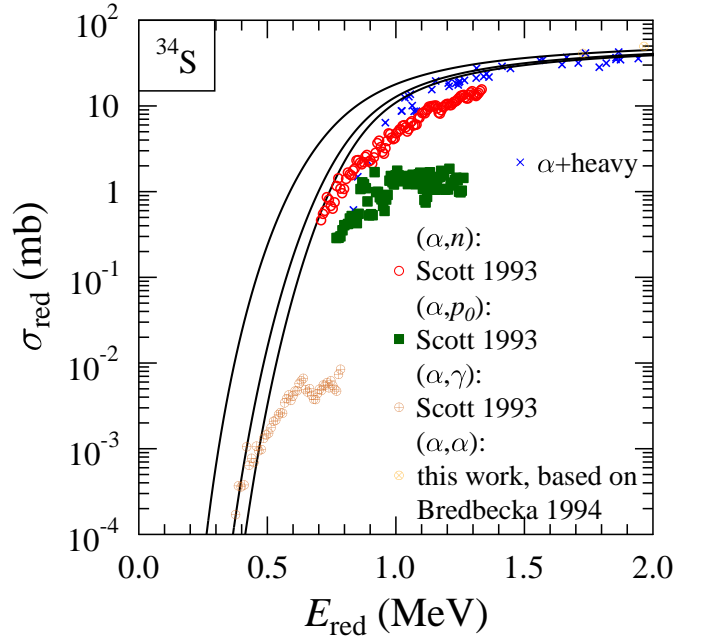


**Fig. 35.** Same as Fig. 5, but for  $\alpha$ -induced reactions on  $^{34}\text{S}$ . The experimental data have been taken from [101,34]. Above the  $(\alpha,n)$  threshold, the total reaction cross section is dominated by the  $^{34}\text{S}(\alpha,n)^{37}\text{Ar}$  reaction. For completeness, the  $^{34}\text{S}(\alpha,p)^{37}\text{Cl}$  and  $^{34}\text{S}(\alpha,\gamma)^{38}\text{Ar}$  cross sections and data points from  $^{34}\text{S}(\alpha,\alpha)^{34}\text{S}$  elastic scattering (see also Figs. 1 and 2) are also shown. Further discussion see text.

lute values of the cross section are slightly overestimated by the StM. It is obvious that the total reaction cross section  $\sigma_{\text{reac}}$  is dominated by the  $(\alpha, n)$  cross section as soon as the energy is a few hundred keV above the threshold. It is interesting to note that the scatter in the experimental data points is probably related to the appearance of individual resonances. The target in the experiment of Scott *et al.* [101] is not thick enough to average over a sufficient number of resonances because of the relatively low level density in the semi-magic ( $N = 20$ )  $^{38}\text{Ar}$  compound nucleus.

Below the  $(\alpha, n)$  threshold, the  $^{34}\text{S}(\alpha, p)^{37}\text{Cl}$  reaction dominates. The total  $(\alpha, p)$  cross section was derived from the excitation function of the  $^{34}\text{S}(\alpha, p_0)^{37}\text{Cl}_{\text{g.s.}}$  reaction which was measured at one particular angle ( $\vartheta = 125^\circ$ ). Corrections for the angular distribution of the emitted protons and for proton groups  $p_{i>0}$  were estimated to be small in [101]. The shown data in Fig. 34 represent the  $p_0$  channel only which contributes to about 90% to the total  $(\alpha, p)$  cross section [101]. Similar to the  $^{34}\text{S}(\alpha, n)^{37}\text{Ar}$  cross section, also the  $^{34}\text{S}(\alpha, p)^{37}\text{Cl}$  cross section is slightly overestimated by the StM.

At energies below about 4 MeV the  $^{34}\text{S}(\alpha, p)^{37}\text{Cl}$  cross section approaches its threshold ( $Q = -3.03$  MeV), and consequently the total reaction cross section  $\sigma_{\text{reac}}$  is essentially given by the  $^{34}\text{S}(\alpha, \gamma)^{38}\text{Ar}$  reaction. The experimental data in [101] are restricted to the analysis of the 2168 keV  $\gamma$ -ray from the decay of the first excited state in  $^{38}\text{Ar}$  to the ground state. Corrections for capture events which bypass the first  $2^+$  in  $^{38}\text{Ar}$  were estimated to be of the order of about 20%. Excellent agreement with the StM calculation is found for the low-energy region below the  $(\alpha, n)$  and  $(\alpha, p)$  thresholds.

The reduced cross section of  $^{34}\text{S}$  has been extracted from the available data of Scott *et al.* [101]. Additional data points have been obtained from the analysis of the  $^{34}\text{S}(\alpha, \alpha)^{34}\text{S}$  elastic scattering data (see also Figs. 1 and 2). Whereas the elastic scattering data are in the expected range, the data of Scott *et al.* [101] are somewhat lower than expected. This holds in particular at the highest energies of the Scott *et al.* experiment where unobserved contributions of higher proton groups  $p_{>0}$  in the  $^{34}\text{S}(\alpha, p)^{37}\text{Ar}$  reaction may be relevant. Similar to most nuclei under study in this work, the  $\sigma_{\text{red}}$  data for  $^{34}\text{S}$  do not show a peculiar behavior.

#### 4.20 $^{33}\text{S}$

Recently, the cross section of the  $^{33}\text{S}(\alpha, p)^{36}\text{Cl}$  reaction was measured by Bowers *et al.* [102]. A  $^4\text{He}$  gas target was irradiated with a  $^{33}\text{S}$  beam in inverse kinematics, and the residual  $^{36}\text{Cl}$  nuclei were captured in an aluminum catcher foil. The number of produced  $^{36}\text{Cl}$  nuclei was determined using accelerator mass spectrometry. The result is shown in Fig. 36; here the cross section is presented as a function of  $E_\alpha$  (i.e., in forward kinematics). The observed cross section shows a smooth energy dependence; no individual resonances are visible. Compared to  $^{34}\text{S}$  in the previous

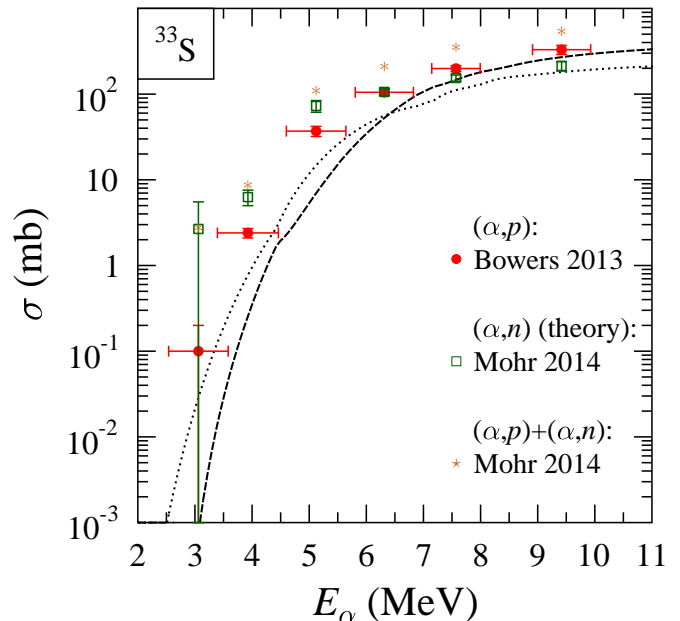


**Fig. 36.** Cross section of the  $^{33}\text{S}(\alpha, n)^{36}\text{Ar}$  and  $^{33}\text{S}(\alpha, p)^{36}\text{Cl}$  reactions. The experimental data for the  $(\alpha, p)$  reaction have been taken from [102]; the  $(\alpha, n)$  cross section was calculated from the experimental  $(\alpha, p)$  cross section and theoretical ratios between the  $(\alpha, n)$  and  $(\alpha, p)$  cross section [20]. Further discussion see text.

Sec. 4.19, the level density in the odd-even compound nucleus  $^{37}\text{Ar}$  is higher, and the target thickness is larger in the  $^{33}\text{S}$  experiment. Thus, the experimental results are average cross sections, averaged over a sufficient number of resonances within the energy spread of the experimental data points, and the StM should provide excellent results.

The experimental data of [102] are compared to a StM calculation in Fig. 36. At the upper end of the energy range of [102] close to 10 MeV, the StM calculation slightly underestimates the experimental data. However, towards lower energies the discrepancy increases significantly.

The  $Q$ -values of the  $(\alpha, p)$  and  $(\alpha, n)$  reactions on  $^{33}\text{S}$  are similar ( $Q = -1.93$  MeV and  $-2.00$  MeV). Thus, at low energies very close above the almost common threshold, the  $(\alpha, n)$  cross section dominates. But at somewhat higher energies around 6 MeV the  $(\alpha, p)$  cross section becomes dominant because of the larger number of states in the exit channel towards the odd-odd nucleus  $^{36}\text{Cl}$ . The  $^{33}\text{S}(\alpha, n)^{36}\text{Ar}$  cross section was estimated in [20] from the experimental  $^{33}\text{S}(\alpha, p)^{36}\text{Cl}$  cross section [102] and the theoretical ratio between the  $(\alpha, n)$  and  $(\alpha, p)$  cross section (for details see [20]). Finally, the total reaction cross section  $\sigma_{\text{reac}}$  is determined from the sum of  $(\alpha, p)$  and  $(\alpha, n)$  cross sections. Because the ratio between the  $(\alpha, n)$  and  $(\alpha, p)$  cross sections is well constrained by theory [20], the uncertainties for the  $(\alpha, n)$  cross section and the total reaction cross section  $\sigma_{\text{reac}}$  remain acceptable.

The reduced cross section  $\sigma_{\text{red}}$  was derived from the total reaction cross section  $\sigma_{\text{reac}}$ . The result is shown in Fig. 37. At the highest energies the results for  $^{33}\text{S}$  lie

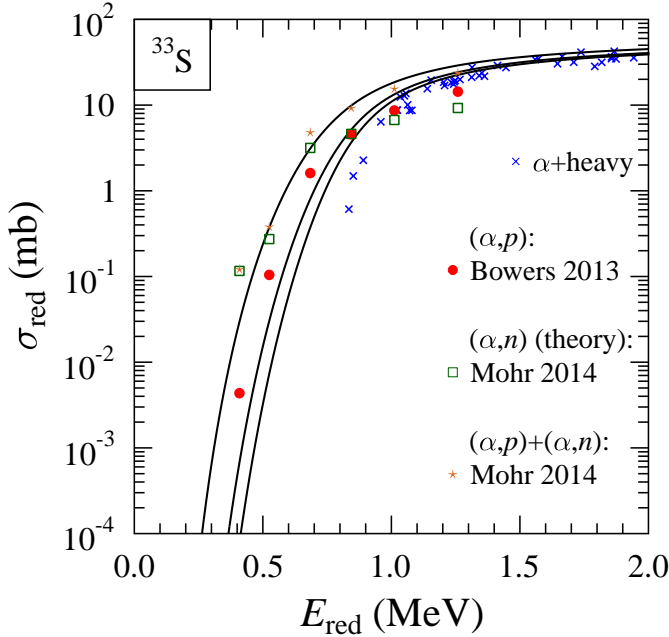


**Fig. 37.** Same as Fig. 5, but for  $\alpha$ -induced reactions on  $^{33}\text{S}$ . The experimental data have been taken from [102] for the  $^{33}\text{S}(\alpha,p)^{36}\text{Cl}$  reaction. In addition, the  $^{33}\text{S}(\alpha,n)^{36}\text{Ar}$  cross section has been estimated using a theoretical branching ratio from the StM [20], and the total reaction cross section is calculated from the sum of the  $(\alpha,p)$  and  $(\alpha,n)$  contributions. Further discussion see text and [20].

within the typical range which is indicated by the reduced cross sections for  $^{21}\text{Ne}$  and  $^{51}\text{V}$  in Fig. 37. However, at lower energies the  $\sigma_{\text{red}}$  values are significantly above the typical range. This means that the reduced cross section  $\sigma_{\text{red}}$  of  $^{33}\text{S}$  behaves significantly different compared to most other nuclei in the  $A \approx 20 - 50$  mass range under study, and also the energy dependence is unusually flat for  $^{33}\text{S}$ . A detailed discussion of this unexpected behavior is given in [20].

#### 4.21 $^{32}\text{S}$

Individual resonances shape the energy dependence of  $\alpha$ -induced cross sections for  $^{32}\text{S}$  at low energies. Because of the strongly negative  $Q$ -value of the  $(\alpha,n)$  reaction ( $Q = -8.61$  MeV), the total reaction cross section  $\sigma_{\text{reac}}$  is governed by the  $^{32}\text{S}(\alpha,p)^{35}\text{Cl}$  reaction which was measured by Soltani-Farshi *et al.* [13]. The proton groups  $p_0$ ,  $p_1$ ,  $p_2$ ,  $p_3$ ,  $p_4$ ,  $p_5$ , and  $p_6$  are nicely resolved in the spectrum at  $E_\alpha = 12$  MeV (Fig. 2 of [13]), and excitation functions have been measured from about 6 to 12 MeV at six angles. Unfortunately, only the  $p_0$  cross section data are shown in Fig. 3 of [13]. The EXFOR database provides this minor part by re-digitization and states that it was impossible to obtain data tables from the authors.

Some estimates can nevertheless be made from available information of Soltani-Farshi *et al.* [13]. The average differential cross section at 12 MeV is about  $(d\sigma/d\Omega) \approx$

2.5 mb/sr. This leads to an angle-integrated cross section of 31.4 mb with an uncertainty below a factor of two. In the shown spectrum (Fig. 2 of [13]) the  $p_0$  group has a about the same intensity as the  $p_3$ ,  $p_4$ ,  $p_5$ , and  $p_6$  groups; the  $p_1$  and  $p_2$  groups are much weaker. This leads to a total  $(\alpha,p)$  cross section of about  $5.5 \times 31.4 \text{ mb} \approx 173 \text{ mb}$  (assuming that higher-lying proton groups do not contribute). In addition, at this energy the  $(\alpha,n)$  channel is already open; i.e., the value at 12 MeV should be considered as a lower limit. This value corresponds to a reduced cross section  $\sigma_{\text{red}} > 7.6 \text{ mb}$  at  $E_{\text{red}} = 1.59 \text{ MeV}$ . At the lowest energy of 6 MeV  $(d\sigma/d\Omega) \approx 1 \text{ mb/sr}$ , leading to  $\sigma(p_0) \approx 12.6 \text{ mb}$ . Higher-lying proton groups should be much weaker, leading to a total  $(\alpha,p)$  cross section of about a factor of two larger than the  $p_0$  cross section:  $\sigma(\alpha,p) \approx 25 \text{ mb}$ . This corresponds to  $\sigma_{\text{red}} \approx 1.1 \text{ mb}$  at  $E_{\text{red}} = 0.79 \text{ MeV}$ . These roughly estimated data points are shown in Fig. 38. The StM calculation is slightly above the estimated experimental data. Although only roughly estimated, it can be seen that the data are at least not far above the expectations.

Because of the few available reaction data for  $^{32}\text{S}$ , in addition  $^{32}\text{S}(\alpha,\alpha)^{32}\text{S}$  elastic scattering data were analyzed. Low-energy angular distributions are available from Coban *et al.* [103] and Aldridge *et al.* [104]. Unfortunately, both data had to be re-digitized from figures in [103,104],

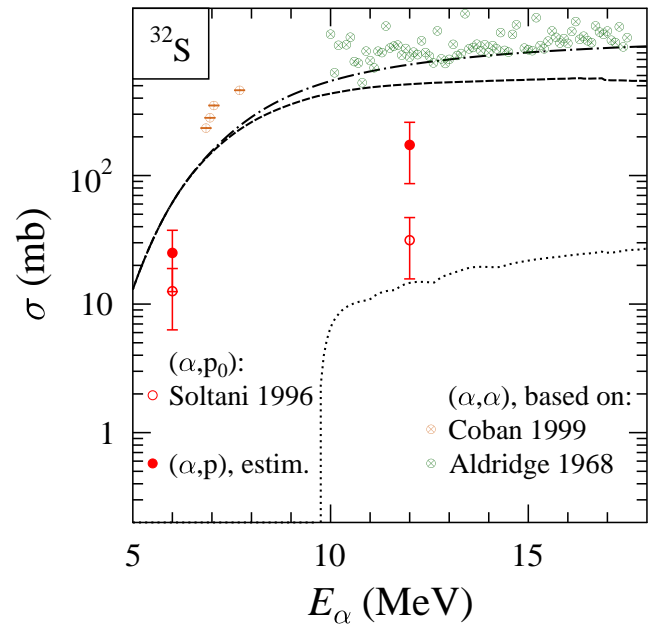


**Fig. 38.** Cross section of the  $^{32}\text{S}(\alpha,p)^{35}\text{Cl}$  reaction and total reaction cross sections from  $^{32}\text{S}(\alpha,\alpha)^{32}\text{S}$  elastic scattering. The experimental data have been taken from [13] for the  $^{32}\text{S}(\alpha,p_0)^{35}\text{Cl}$  reaction with the additional estimates for  $^{32}\text{S}(\alpha,p)^{35}\text{Cl}$  as discussed in the text; the upper data point should be considered as a lower limit only. Elastic  $^{32}\text{S}(\alpha,\alpha)^{32}\text{S}$  data from [103,104] have been re-analyzed in this study to determine the total reaction cross section  $\sigma_{\text{red}}$  and should be compared to the corresponding calculation (dash-dotted line) which is shown in addition to the  $(\alpha,p)$  and  $(\alpha,n)$  cross sections.

and the EXFOR data are provided without the original error bars. Because the angular distributions have to be fitted for the determination of the total reaction cross section  $\sigma_{\text{reac}}$ , the resulting numbers have significant uncertainties from the digitizing error and from the missing original uncertainties (for the fitting procedure a fixed uncertainty of 5% was used for all data points).

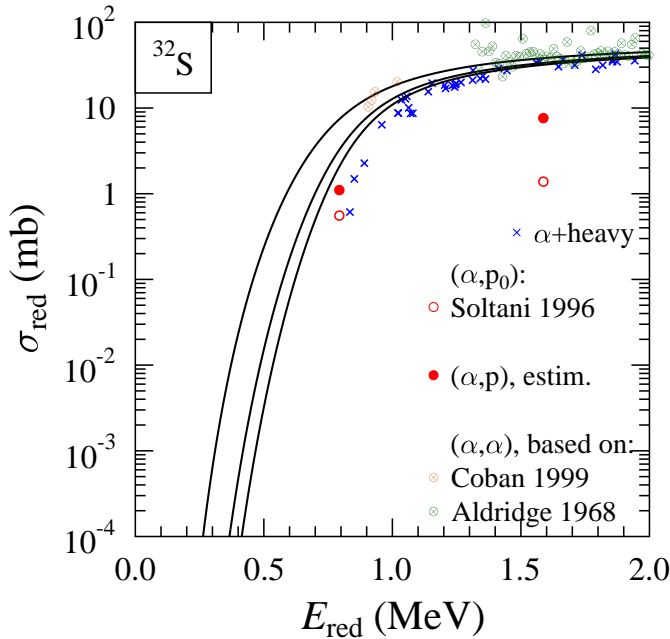


**Fig. 39.** Same as Fig. 5, but for  $\alpha$ -induced reactions on  $^{32}\text{S}$ . The experimental data have been taken from [13, 103, 104]. Further discussion see text.

Resonant structures in the excitation function of the  $^{32}\text{S}(\alpha,\alpha)^{32}\text{S}$  elastic scattering were analyzed in the study of Coban *et al.* [103]. At resonance energies detailed angular distribution measurements were carried out for a  $J^\pi$  assignment. Therefore, the total cross sections  $\sigma_{\text{reac}}$  from these detailed angular distributions around 7 MeV in [103] (corresponding to reduced energies  $E_{\text{red}} \approx 0.9 - 1$  MeV, shown as data points in Fig. 39) should be considered as resonance-based upper limits. At the same energies the resonance properties were confirmed by an enhanced yield in the  $(\alpha,p_0)$  cross section which was observed in [103].

Angular distributions in 100 keV steps were measured by Aldridge *et al.* [104] at about 30 angles. A phase shift fit of these angular distributions is at the limits of numerical stability because the number of adjustable parameters (two parameters per partial wave: reflexion coefficient  $\eta_L$  and phase shift  $\delta_L$ ) is not much lower than the number of experimental data points. Nevertheless, the general trend of the reduced cross sections  $\sigma_{\text{red}}$  is close to the expected values, and at least in the overlap region with [13] the outliers are correlated with maxima in the excitation function of the  $(\alpha,p_0)$  cross section of [13]. The resulting  $\sigma_{\text{red}}$  values for  $^{32}\text{S}$  are shown in Fig. 39.

Concluding the analysis of  $^{32}\text{S}$ , it can be said that the  $\sigma_{\text{red}}$  data for  $^{32}\text{S}$  do not show evidence for unusual behavior. Thus, for the even-even sulfur isotopes  $^{32,34}\text{S}$  the  $\sigma_{\text{red}}$  values behave regularly or even low, whereas  $\sigma_{\text{red}}$  for  $^{33}\text{S}$  is significantly enhanced in particular at low energies.

#### 4.22 $^{31}\text{P}$

The present study focuses on low-energy cross sections of  $\alpha$ -induced energies around  $E_{\text{red}} \approx 0.5 - 1$  MeV. The corresponding energies  $E_\alpha$  decrease towards lighter nuclei. Simultaneously, the level density decreases towards lighter nuclei. Whereas for heavier nuclei a smooth energy dependence of the  $\alpha$ -induced reaction cross sections was found, for lighter nuclei individual resonances become more and more important. Calculations in the StM model cannot reproduce these individual resonances; nevertheless, the general trend of the data should be reproduced.

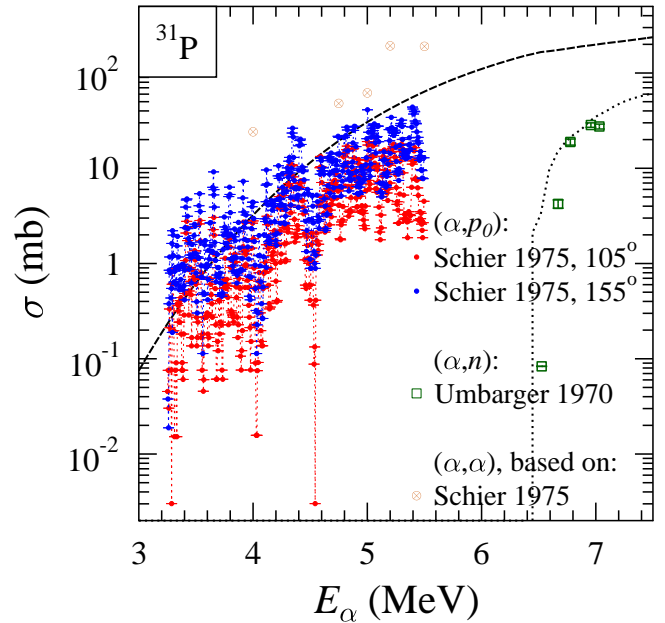


**Fig. 40.** Cross section of the  $^{31}\text{P}(\alpha,n)^{34}\text{Cl}$  and  $^{31}\text{P}(\alpha,p)^{34}\text{S}$  reactions. The experimental data have been taken from the  $(\alpha,n)$  data of [107] and from the  $(\alpha,p_0)$  and  $(\alpha,\alpha)$  data of [105]. Further discussion see text.

Experimental data for the  $^{31}\text{P}(\alpha,p_0)^{34}\text{S}$  reaction have been measured by Schier *et al.* [105]. Two excitation functions at  $\vartheta = 105^\circ$  and  $155^\circ$  are shown in their Fig. 2. As no spectrum is shown in [105], it is not possible to determine the contributions of higher-lying proton groups from this experiment. However, at low energies close above the threshold the  $p_0$  channel should be dominating. The experimental data are shown in Fig. 40 together with a StM calculation. As expected, at higher energies the  $(\alpha,p_0)$  data of [105] are below the theoretical estimate whereas at low energies there is – on average – reasonable agreement between theory and experiment. At lower energies resonance

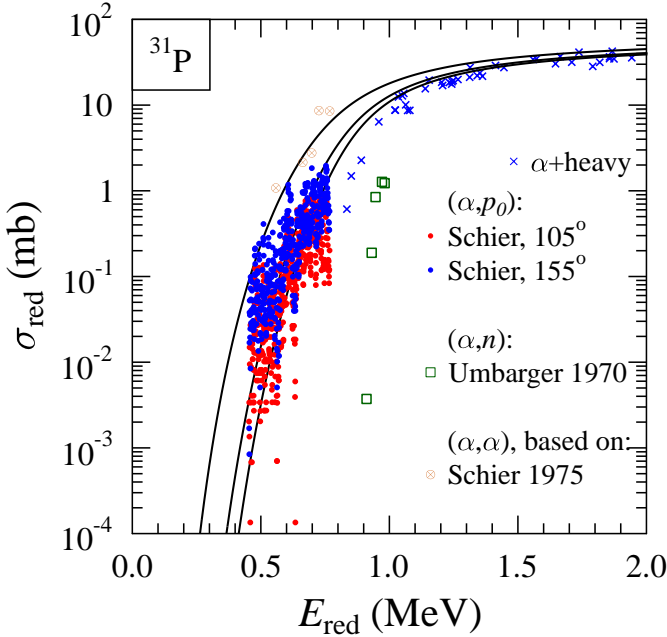


**Fig. 41.** Same as Fig. 5, but for  $\alpha$ -induced reactions on  $^{31}\text{P}$ . The experimental data have been taken from [105,107]: the differential cross sections ( $d\sigma/d\Omega$ ) at  $\vartheta = 105^\circ$  and  $155^\circ$  of the dominating  $^{31}\text{P}(\alpha,p_0)^{34}\text{S}$  reaction has been converted to the total cross section assuming isotropy. Further discussion see text.

parameters of the  $^{31}\text{P}(\alpha,p)^{34}\text{S}$  reaction were determined by McMurray *et al.* [106].

Because of the relatively high  $(\alpha,n)$  threshold ( $Q = -5.65$  MeV), the  $^{31}\text{P}(\alpha,n)^{34}\text{Cl}$  reaction does practically not contribute to the total reaction cross section  $\sigma_{\text{reac}}$  and the reduced cross section  $\sigma_{\text{red}}$ . The  $(\alpha,n)$  data by Umbarger *et al.* [107] are also shown in Figs. 40 and 41. In addition, five data points from a re-analysis of the elastic scattering data of Schier *et al.* [105] are shown which have been measured simultaneously with the  $(\alpha,p_0)$  cross section. However, this re-analysis is hampered by the limited number of data points in the angular distributions which had to be re-digitized from Fig. 1 of [105]. As four of the five angular distributions in Fig. 1 of [105] are measured in resonances (see the corresponding yield maxima in the  $(\alpha,p_0)$  excitation functions in Fig. 2 of [105]), the resulting  $\sigma_{\text{reac}}$  and  $\sigma_{\text{red}}$  should again be considered as resonance-based upper limits. The off-resonance point at  $E_\alpha = 4.75$  MeV corresponds to  $E_{\text{red}} = 0.70$  MeV and  $\sigma_{\text{red}} = 2.77$  mb. Although the eye may be misled by the many resonant data points of the  $(\alpha,p_0)$  cross section in Fig. 41, the  $\sigma_{\text{red}}$  data for  $^{31}\text{P}$  behave on average similar to most nuclei under study in the  $A \approx 20 - 50$  mass region.

#### 4.23 $^{30}\text{Si}$

The  $^{30}\text{Si}(\alpha,n)^{33}\text{S}$  cross section was measured by Flynn *et al.* [108] by direct neutron counting. Because a very thin target was used in this experiment, the measured

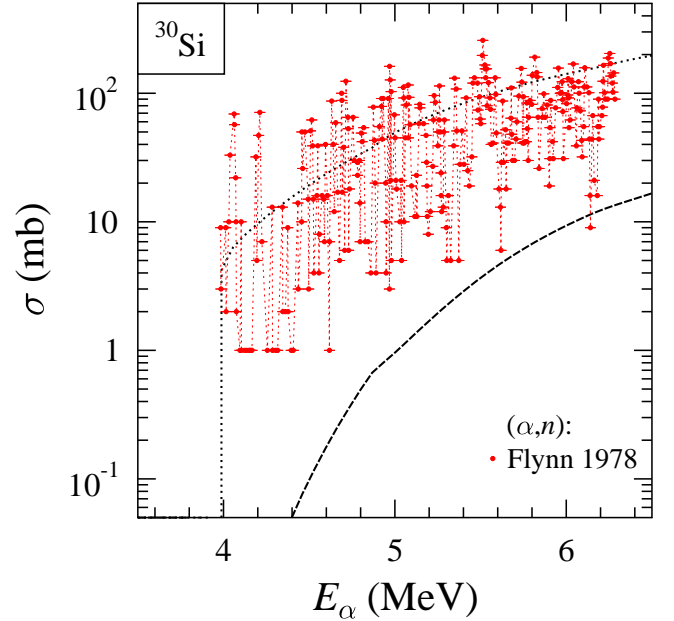


**Fig. 42.** Cross section of the  $^{30}\text{Si}(\alpha,n)^{33}\text{S}$  and  $^{30}\text{Si}(\alpha,p)^{33}\text{P}$  reactions. The experimental data have been taken from [108]. Further discussion see text.

cross section is governed by many resonances. It has been shown already in [108] that the average cross section is well reproduced by a StM calculation, and a similar result is obtained in this study. The experimental data of [108] and the present StM calculation are shown in Fig. 42.

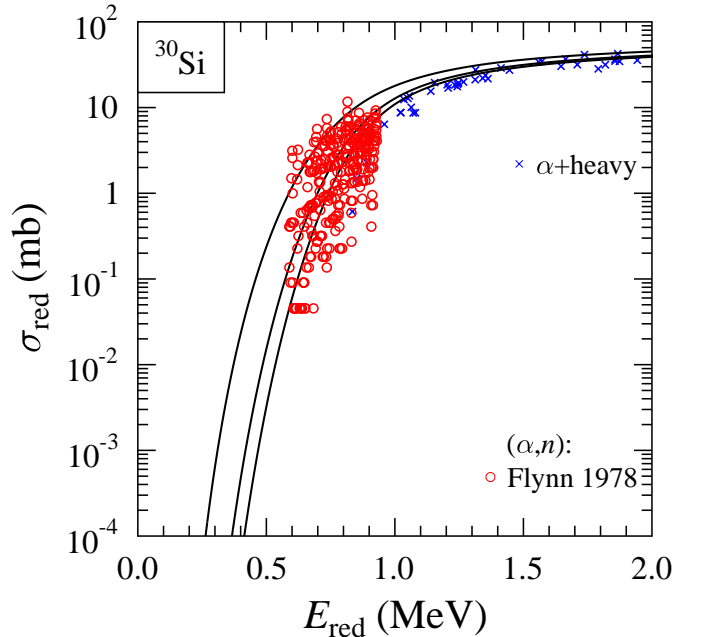


**Fig. 43.** Same as Fig. 5, but for  $\alpha$ -induced reactions on  $^{30}\text{Si}$ . The experimental data have been taken from [108]. Further discussion see text.

It is obvious from Fig. 42 that the  $^{30}\text{Si}(\alpha,n)^{33}\text{S}$  reaction dominates the total reaction cross section  $\sigma_{\text{reac}}$  and the reduced cross section  $\sigma_{\text{red}}$ . The  $^{30}\text{Si}(\alpha,p)^{33}\text{P}$  reaction has a cross section which is about one order of magnitude smaller over the entire measured energy range of the experiment in [108]. Hence, the reduced cross section  $\sigma_{\text{red}}$  of  $^{30}\text{Si}$  is well-defined by the experimental data of [108].

Similar to most nuclei under study in this work, the  $\sigma_{\text{red}}$  data for  $^{30}\text{Si}$  – on average – do not show a peculiar behavior. This is also confirmed by the analysis of  $^{30}\text{Si}(\alpha,\alpha)^{30}\text{Si}$  elastic scattering at 15.7 MeV [109]. The analysis of the EXFOR data leads to a relatively high  $\sigma_{\text{red}} = 68.7\text{mb}$  at  $E_{\text{red}} = 2.32\text{MeV}$ . However, the  $\chi^2/F$  of the phase shift fit can be reduced by about a factor of three if the experimental data of [109] are scaled by a factor of  $\approx 0.6$ , leading to a lower value of  $\sigma_{\text{red}} = 61.2\text{mb}$ .

#### 4.24 $^{29}\text{Si}$

Three experimental data sets are available at EXFOR for the  $^{29}\text{Si}(\alpha,n)^{32}\text{S}$  reaction. The main focus of these experiments was the determination of resonance properties from the measured neutron yield, and thus relatively thin targets were used. Gibbons and Macklin [110] provide data from about 2 to 4.5 MeV, obtained with a  $43\ \mu\text{g}/\text{cm}^2$  target. Balakrishnan *et al.* [111] identify 134 resonances for  $E_\alpha = 2.15 - 5.25\text{MeV}$  using a very thin target ( $\Delta E \approx 5\text{keV}$ , corresponding to less than  $5\ \mu\text{g}/\text{cm}^2$ ), and Flynn *et al.* [108] show data for  $E_\alpha \approx 2.75 - 7\text{MeV}$  using a  $9\ \mu\text{g}/\text{cm}^2$  target. In addition, for the measurements close above the threshold, a thicker target with  $113\ \mu\text{g}/\text{cm}^2$  was used in [108]. At energies around 4 MeV the newer data

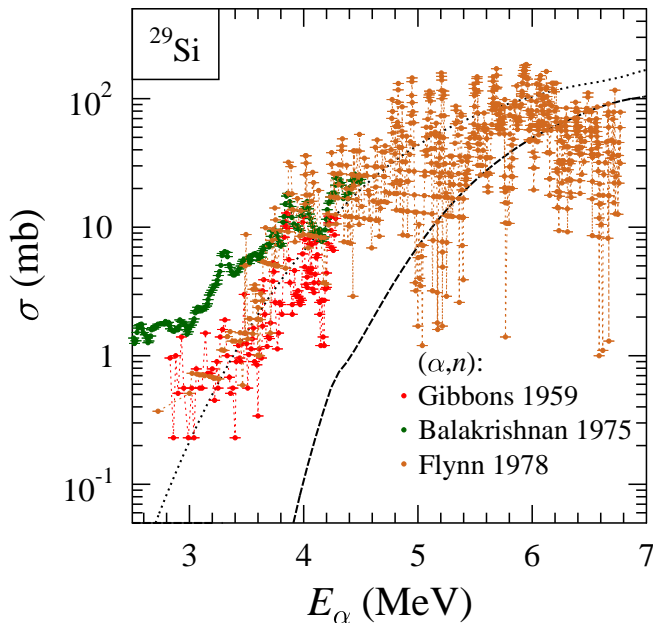


**Fig. 44.** Cross section of the  $^{29}\text{Si}(\alpha,n)^{32}\text{S}$  and  $^{29}\text{Si}(\alpha,p)^{32}\text{P}$  reactions. The experimental data have been taken from [110, 111, 108]. Further discussion see text.

by Flynn *et al.* and Balakrishnan *et al.* are in good agreement. However, at lower energies the data by Balakrishnan *et al.* are much higher. Flynn *et al.* [108] state in their discussion that the data by Balakrishnan *et al.* show structures which are also visible in the  $^{13}\text{C}(\alpha,n)^{16}\text{O}$  reaction, and thus the Balakrishnan *et al.* data are contaminated by background. The early data by Gibbons *et al.* [110] are about a factor of two below the later Flynn *et al.* data around 4 MeV where the cross section of the  $^{13}\text{C}(\alpha,n)^{16}\text{O}$  reaction is small. At lower energies the agreement between the Flynn *et al.* data and the Gibbons and Macklin data may be considered as accidental because also the Gibbons and Macklin experiment seems to suffer from  $^{13}\text{C}$  background at lower energies (as discussed in [108]). In a further experiment McMurray *et al.* [106] have determined resonance properties of the  $^{29}\text{Si}(\alpha,n)^{32}\text{S}$  reaction.

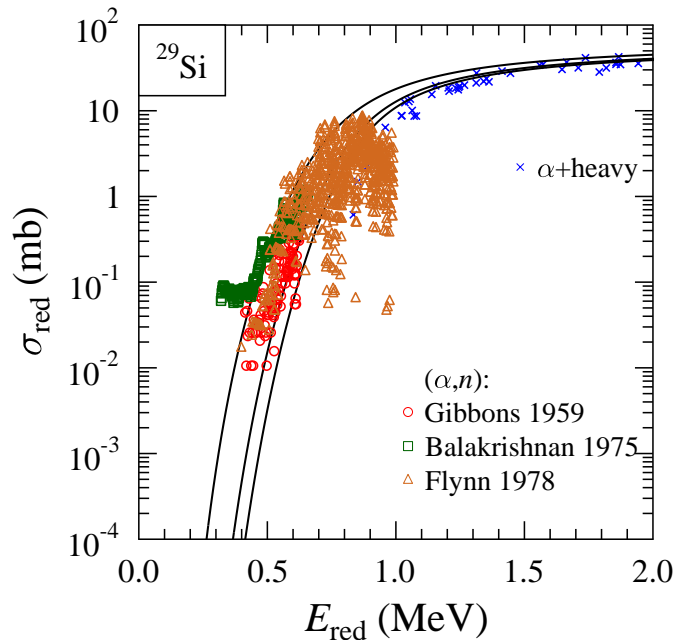


**Fig. 45.** Same as Fig. 5, but for  $\alpha$ -induced reactions on  $^{29}\text{Si}$ . The experimental data have been taken from [110, 111, 108]. Further discussion see text.

The experimental data of [110, 111, 108] are shown in Fig. 44. The data are – on average – in reasonable agreement with the StM calculation. According to the StM calculation, the cross section of the  $^{29}\text{Si}(\alpha,p)^{32}\text{P}$  reaction is much lower in the entire energy range under study. Unfortunately, no data for the  $^{29}\text{Si}(\alpha,p)^{32}\text{P}$  reaction are available at EXFOR.

The  $^{29}\text{Si}(\alpha,n)^{32}\text{S}$  data are shown as reduced cross sections  $\sigma_{\text{red}}$  in Fig. 45. An additional data point can be taken from the analysis of  $^{29}\text{Si}(\alpha,\alpha)^{29}\text{Si}$  elastic scattering. The fit to the angular distribution at  $E_\alpha = 26.6\text{MeV}$  in [112] leads to  $\sigma_{\text{red}} \approx 55\text{mb}$  at the relatively high reduced energy  $E_{\text{red}} \approx 3.89\text{MeV}$ . Similar to most nuclei under study in this work, the  $\sigma_{\text{red}}$  data for  $^{29}\text{Si}$  do not show a peculiar behavior.

#### 4.25 $^{28}\text{Si}$

Data for the  $^{28}\text{Si}(\alpha,p)^{31}\text{P}$  and  $^{28}\text{Si}(\alpha,n)^{31}\text{S}$  reactions are available at EXFOR. Because of the relatively high negative  $Q$ -value of the  $(\alpha,n)$  reaction ( $Q = -9.10$  MeV), at low energies the  $(\alpha,p)$  reaction is dominating. At very low energies also the  $(\alpha,p)$  channel is closed, and the only open reaction channel is  $^{28}\text{Si}(\alpha,\gamma)^{32}\text{S}$ . However, only resonance strengths are available for the  $(\alpha,\gamma)$  reaction [113, 114, 115, 116].

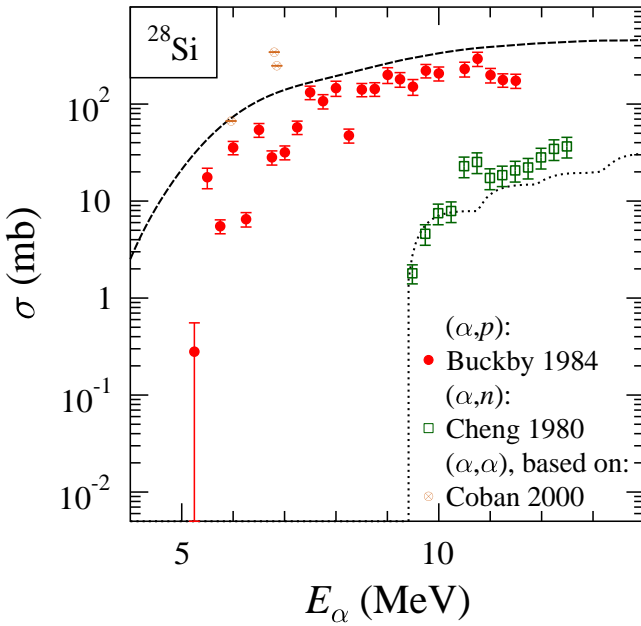


**Fig. 46.** Cross section of the  $^{28}\text{Si}(\alpha,n)^{31}\text{S}$  and  $^{28}\text{Si}(\alpha,p)^{31}\text{P}$  reactions. Three additional data points have been derived from a phase shift analysis of  $^{28}\text{Si}(\alpha,\alpha)^{28}\text{Si}$  elastic scattering. The experimental data have been taken from [117, 118, 119]. Further discussion see text.

The  $^{28}\text{Si}(\alpha,p)^{31}\text{P}$  reaction was measured by Buckby *et al.* [117]. The total  $(\alpha,p)$  cross section was derived from proton angular distributions (further discussion see also Sec. 4.10, 4.14, and [77]). The results are shown in Fig. 46. The StM calculation slightly overestimates the experimental data, in particular at the lowest energies.

Contrary to the finding for the  $(\alpha,p)$  reaction, the  $^{28}\text{Si}(\alpha,n)^{31}\text{S}$  data by Cheng *et al.* [118] are nicely reproduced by the StM. Here the  $(\alpha,n)$  cross section was determined by activation in combination with annihilation spectroscopy.

Because of the deviation between the experimental  $(\alpha,p)$  data and the StM model calculation, additionally  $^{28}\text{Si}(\alpha,\alpha)^{28}\text{Si}$  elastic scattering data are studied. The angular distributions measured by Coban *et al.* [119] around  $E_\alpha \approx 6 - 7$  MeV can be nicely fitted by a phase shift analysis. The result at 5.96 MeV is in almost perfect agreement with the StM calculation; at this energy the excitation functions in [119] do not show strong resonances. At the higher energies (6.80 and 6.85 MeV) a broad resonance

(perhaps a doublet of resonances) can be seen in the excitation functions; the existence of this resonance is confirmed by the excitation function at backward angles measured by Källman *et al.* [120]. Therefore it is not surprising that the total reaction cross sections  $\sigma_{\text{reac}}$  from elastic scattering at resonant energies are significantly above the StM prediction.

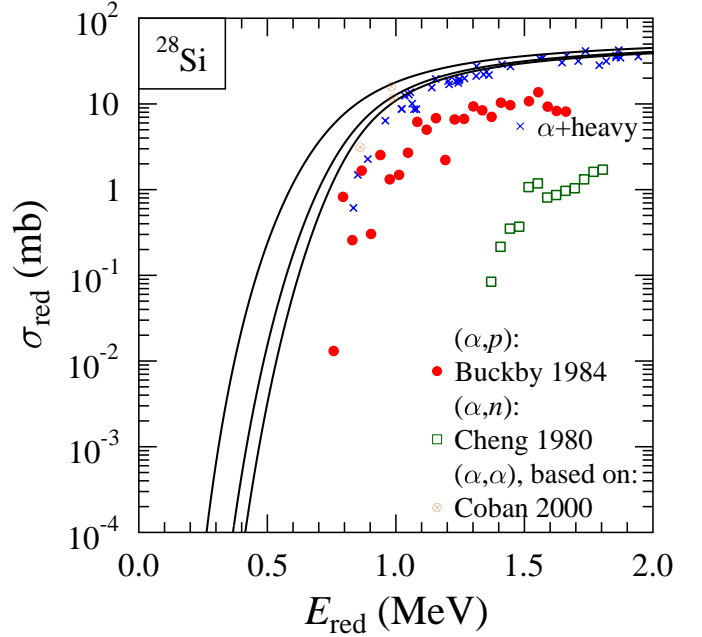


**Fig. 47.** Same as Fig. 5, but for  $\alpha$ -induced reactions on  $^{28}\text{Si}$ . The experimental data have been taken from [117, 118, 119]. Further discussion see text.

Around 6 MeV a discrepancy of about a factor of two is found between the  $(\alpha,p)$  cross section by Buckby *et al.* [117] and the total reaction cross section  $\sigma_{\text{reac}}$  from the analysis of elastic scattering data by Coban *et al.* [119]. Unfortunately, there is no simple explanation for this discrepancy.

The available  $\alpha$ -induced cross sections are converted to reduced cross sections. Fig. 47 shows that the  $\sigma_{\text{red}}$  values for  $^{28}\text{Si}$  are smaller than for neighboring nuclei. Obviously, this effect is more pronounced when one considers the lower  $(\alpha,p)$  cross sections of Buckby *et al.* [117] compared to the higher results from the analysis of elastic scattering data by Coban *et al.* [119].

#### 4.26 $^{27}\text{Al}$

Although the EXFOR database contains a lot of data for  $\alpha$ -induced reactions on  $^{27}\text{Al}$ , there are practically no data for the  $^{27}\text{Al}(\alpha,p)^{30}\text{Si}$  reaction which dominates the total reaction cross section  $\sigma_{\text{reac}}$  at low energies. Barros *et al.* [121] have measured angular distributions for a relatively thick ( $70 \mu\text{g}/\text{cm}^2$ )  $^{27}\text{Al}$  target using nuclear track detection. From the measured angular distributions of the resolved  $p_0$ ,  $p_1$ ,  $p_2$ ,  $p_3$ , and  $p_4$  proton groups a total  $(\alpha,p)$

cross section for  $^{27}\text{Al}$  can be roughly estimated to about 54 mb. This result is very close to the StM calculation (see Fig. 48). Unfortunately, only resonance parameters were extracted from the experimental low-energy data by Kuperus [122].

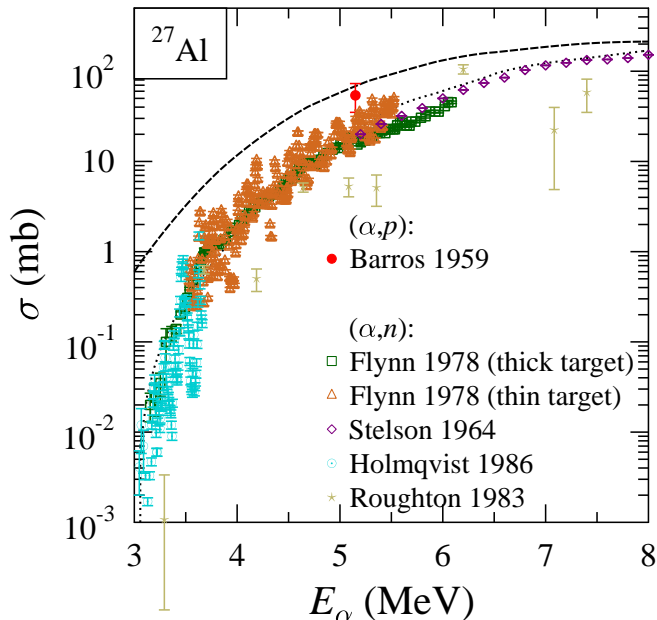


**Fig. 48.** Cross section of the  $^{27}\text{Al}(\alpha,n)^{30}\text{P}$  and  $^{27}\text{Al}(\alpha,p)^{30}\text{Si}$  reactions. The experimental data have been taken from [121, 108, 125, 126, 49]. Further discussion see text.

The  $^{27}\text{Al}(\alpha,n)^{30}\text{P}$  reaction was already reviewed recently in the first NACRE compilation of astrophysical reaction rates [123] (the later NACRE-II compilation [124] is restricted to lower masses up to  $A < 16$ ). The following discussion is thus shortened and focuses on information which is particularly relevant for this study.

The  $^{27}\text{Al}(\alpha,n)^{30}\text{P}$  reaction was measured by Flynn *et al.* [108] by direct neutron counting from about 3.5 to 6 MeV with two different targets. Whereas the thin-target (thickness  $27 \mu\text{g}/\text{cm}^2$ ) measurement shows resonant structures, the thick-target ( $442 \mu\text{g}/\text{cm}^2$ ) measurement averages over the resonances, and the resulting excitation function shows a smooth energy dependence. The smooth thick-target measurement is in good agreement with a StM calculation.

Earlier data by Stelson *et al.* [125] extend the data by Flynn *et al.* [108] towards higher energies. Stelson *et al.* have used a similar experimental technique and also thick targets. In the overlap region, the Flynn *et al.* data are slightly lower but roughly compatible within the experimental uncertainties.

At even higher energies (only shown in Fig. 49) Sahakandu *et al.* [15] have used activation and the stacked-foil technique. As often, the lowest data points of the stacked-foil experiment deviate significantly from the other

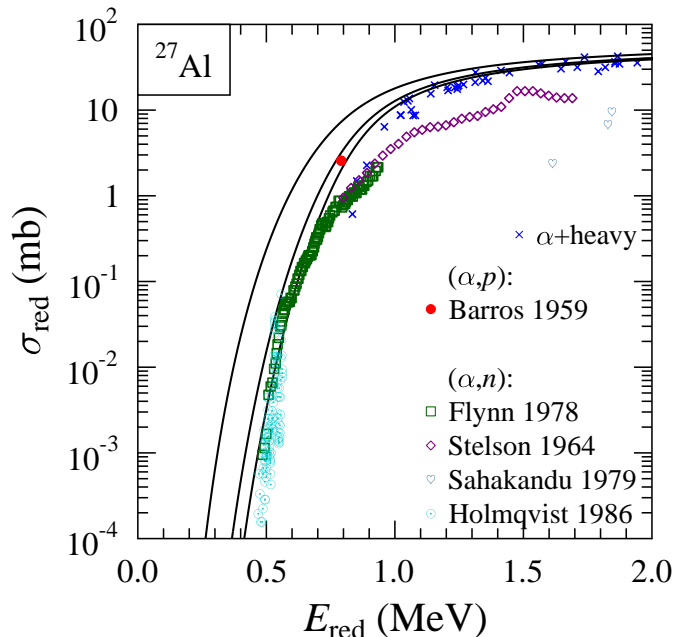


**Fig. 49.** Same as Fig. 5, but for  $\alpha$ -induced reactions on  $^{27}\text{Al}$ . The experimental data have been taken from [121] for the dominating  $^{27}\text{Al}(\alpha,p)^{30}\text{Si}$  reaction and from [108, 125, 15, 126] for the  $^{27}\text{Al}(\alpha,n)^{30}\text{P}$  reaction. Further discussion see text.

available data whereas at higher energies the agreement becomes much better.

A similar energy range as in Flynn *et al.* [108] and in Stelson *et al.* [125] was investigated by Howard *et al.* [69]. The data are in good agreement with the other experiments but show larger uncertainties. Following the NACRE recommendations, these data are disregarded because of their larger uncertainties [123].

The above data are extended towards lower energies by Holmqvist and Ramström [126]. An infinitely thick  $^{27}\text{Al}$  target was irradiated in small energy steps, and the observed neutron yield as a function of energy was differentiated to obtain the cross section of the  $^{27}\text{Al}(\alpha,n)^{30}\text{P}$  reaction. The experimental data by Holmqvist and Ramström agree nicely with the other available data sets.

An attempt was made to add further data points at low energies from the analysis of  $^{27}\text{Al}(\alpha,\alpha)^{27}\text{Al}$  elastic scattering data. Unfortunately, the available low-energy angular distribution by Dyachkov *et al.* [127] does not provide a sufficient number of experimental data points for a stable phase shift fit or optical model analysis. The phase shift analysis of the angular distribution by Gailar *et al.* [128] at  $E_\alpha = 18.82$  MeV leads to  $\sigma_{\text{reac}} = 1278$  mb, corresponding to  $E_{\text{red}} = 2.89$  MeV and  $\sigma_{\text{red}} = 60.7$  mb, i.e. a result in the expected range.

The reduced cross section  $\sigma_{\text{red}}$  from the  $^{27}\text{Al}(\alpha,n)^{30}\text{P}$  data (see Fig. 49) is obviously below the typical range of  $\sigma_{\text{red}}$  values for  $A \approx 20-50$  nuclei because the  $^{27}\text{Al}(\alpha,p)^{30}\text{Si}$  reaction is the dominating channel. But from the ratio of the  $(\alpha,n)$  and  $(\alpha,p)$  cross sections in the StM calculation it can be concluded that the  $\sigma_{\text{red}}$  values for  $^{27}\text{Al}$  do not show an unusual behavior.

#### 4.27 $^{26}\text{Mg}$

Because  $^{26}\text{Mg}$  is a relatively neutron-rich nucleus, the low-energy cross section is dominated by the  $^{26}\text{Mg}(\alpha,n)^{29}\text{Si}$  reaction. Data for the  $^{26}\text{Mg}(\alpha,p)^{29}\text{Al}$  reaction are available at higher energies. Minai *et al.* [16] cover the energy range between 6 and 34 MeV, and the data of Probst *et al.* [129] are restricted to energies above 10 MeV (i.e., above the range shown in Fig. 50). Both experiments used the stacked-foil activation technique in combination with  $\gamma$ -ray spectroscopy for the detection of the residual  $^{29}\text{Al}$  nuclei. Surprisingly, the experimental  $(\alpha,p)$  data are almost one order of magnitude lower than the StM calculation. This holds for both TALYS and NON-SMOKER. However, the  $(\alpha,p)$  cross sections from the thick-target yield of Roughton *et al.* [49] are in reasonable agreement with the StM calculation. Fortunately, this discrepancy does not affect the conclusions on the total reaction cross section  $\sigma_{\text{reac}}$  which is dominated by the  $(\alpha,n)$  channel.

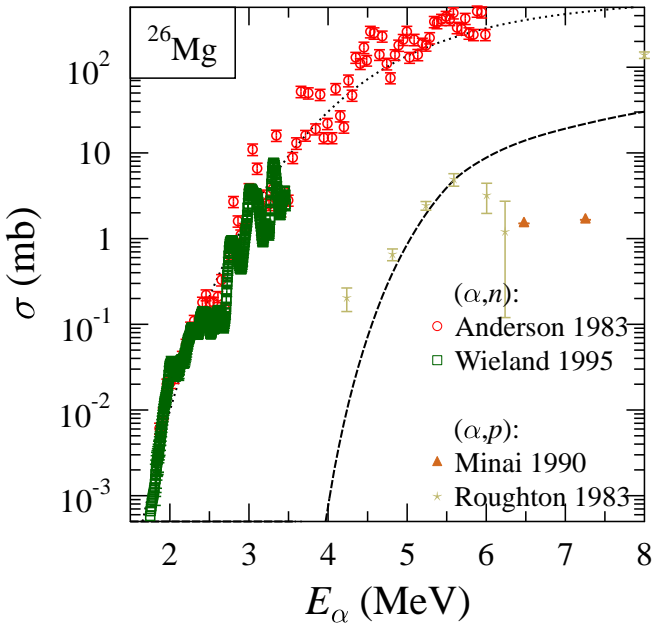


**Fig. 50.** Cross section of the  $^{26}\text{Mg}(\alpha,n)^{29}\text{Si}$  and  $^{26}\text{Mg}(\alpha,p)^{29}\text{Al}$  reactions. The experimental data have been taken from [130,131,16,49]. Further discussion see text.

The  $^{26}\text{Mg}(\alpha,n)^{29}\text{Si}$  reaction is included in the NACRE compilation [123]. At low energies the data by Anderson *et al.* [130] and the unpublished data by Wieland [131] are recommended. Both experiments used direct neutron counting. According to NACRE, at very low energies the Wieland data should be preferred because special care was taken to minimize background from the  $^{13}\text{C}(\alpha,n)^{16}\text{O}$  reaction. In the overlap region there is reasonable agreement between both data sets. As the  $(\alpha,n)$  cross section at low energies is dominated by resonances, the StM calculation is only able to reproduce the average trend of the data (see Fig. 50). For completeness it has to be noted that recently

much lower data for the  $^{26}\text{Mg}(\alpha,n)^{29}\text{Si}$  reaction have been reported in an unpublished PhD thesis by Falahat [132].

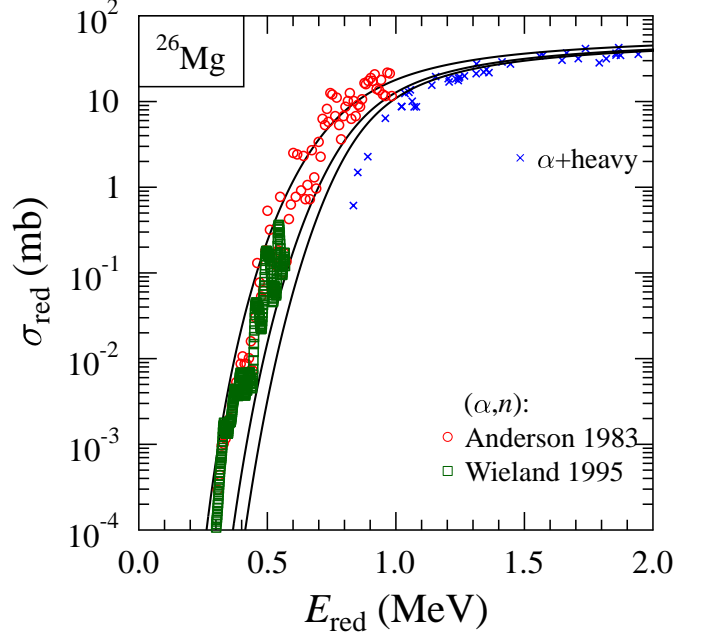


**Fig. 51.** Same as Fig. 5, but for  $\alpha$ -induced reactions on  $^{26}\text{Mg}$ . The experimental data have been taken from [130,131]. Further discussion see text.

The total reaction cross section  $\sigma_{\text{reac}}$  for  $^{26}\text{Mg}$  is well-defined from the available  $^{26}\text{Mg}(\alpha,n)^{29}\text{Si}$  data. The derived reduced cross sections  $\sigma_{\text{red}}$  are shown in Fig. 51. Similar to most nuclei under study in this work, the  $\sigma_{\text{red}}$  data for  $^{26}\text{Mg}$  do not show a peculiar behavior.

#### 4.28 $^{25}\text{Mg}$

Similar to  $^{26}\text{Mg}$  in the previous section 4.27, at low energies the  $^{25}\text{Mg}(\alpha,n)^{28}\text{Si}$  cross section is much larger than the  $^{25}\text{Mg}(\alpha,p)^{28}\text{Al}$  cross section. The NACRE compilation [123] recommends the experimental data by Anderson *et al.* [130], Wieland [131], and an additional data set which is available from van der Zwan *et al.* [133]. The present status of the  $^{25}\text{Mg}(\alpha,n)^{28}\text{Si}$  reaction is also reviewed in [6]. It is concluded in [6] that all data sets agree well, in particular if the  $(\alpha,n\gamma)$  data of [130] are considered which are less sensitive to background than the  $(\alpha,n)$  data. The average trend of the data is nicely reproduced by the StM calculation (see Fig. 52). Similar to  $^{26}\text{Mg}$ , the recent PhD thesis by Falahat [132] reports lower results, and because of these discrepancies new experimental efforts have been started by Caciulli *et al.* [134].

The determination of the total reaction cross section  $\sigma_{\text{reac}}$  for  $^{25}\text{Mg}$  is well defined by the above  $(\alpha,n)$  data. But because of the huge deviation between the StM calculation and experimental data for the  $^{26}\text{Mg}(\alpha,p)^{29}\text{Al}$  reaction in the previous section, the  $^{25}\text{Mg}(\alpha,p)^{28}\text{Al}$  reaction is

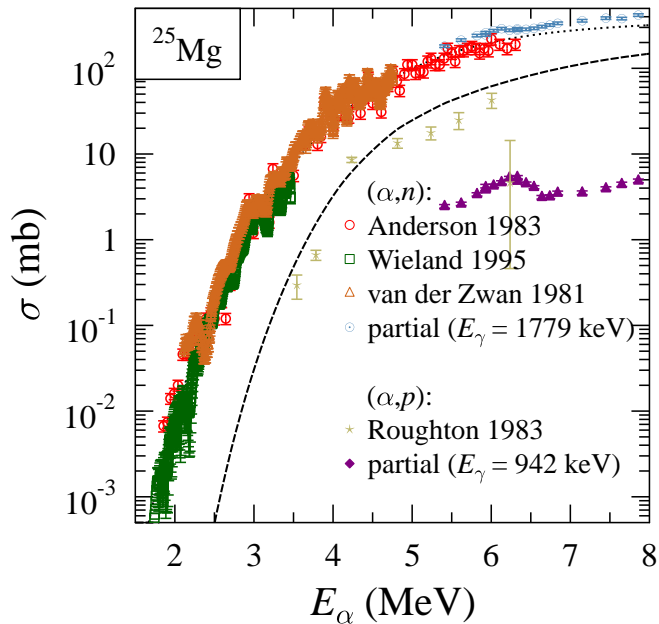


**Fig. 52.** Cross section of the  $^{25}\text{Mg}(\alpha,n)^{28}\text{Si}$  and  $^{25}\text{Mg}(\alpha,p)^{28}\text{Al}$  reactions. The experimental data have been taken from [130,131,133,135,49]. Further discussion see text.

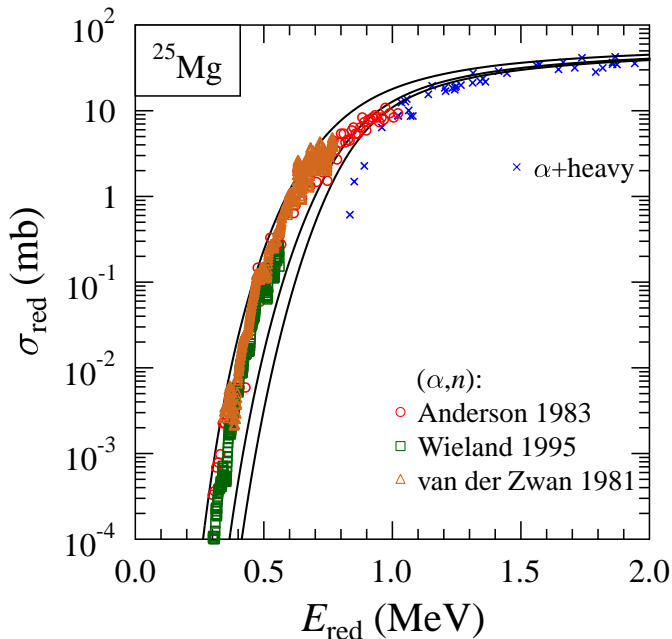


**Fig. 53.** Same as Fig. 5, but for  $\alpha$ -induced reactions on  $^{25}\text{Mg}$ . The experimental data have been taken from [130,131,133]. Further discussion see text.

also analyzed here. Unfortunately, data are available only for a partial  $(\alpha,p)$  cross section. Recently, Negret *et al.* [135] have measured the  $\gamma$ -ray yields after bombardment of  $^{25}\text{Mg}$  by  $\alpha$ -particles. The yield of the 1779 keV  $\gamma$ -ray from the first excited  $2^+$  state in  $^{28}\text{Si}$  to the  $0^+$  ground state corresponds to almost the total  $^{25}\text{Mg}(\alpha,n)^{28}\text{Si}$  cross section because practically all excited states in  $^{28}\text{Si}$  decay through

the first  $2^+$  state. Fig. 52 shows that the partial  $(\alpha,n)$  cross section from the 1779 keV  $\gamma$ -ray yield is even slightly above the  $(\alpha,n)$  cross sections from direct neutron counting. In a similar way, a partial  $(\alpha,p)$  cross section can be derived from the yield of the 942 keV  $\gamma$ -ray in the  $^{25}\text{Mg}(\alpha,p)^{28}\text{Al}$  reaction. This  $\gamma$ -ray corresponds to the transition from the second excited state ( $J^\pi = 0^+$ ,  $E^* = 972.4$  keV) to the first excited state ( $J^\pi = 2^+$ ,  $E^* = 30.6$  keV); the ground state of  $^{28}\text{Al}$  has  $J^\pi = 3^+$ . This  $\gamma$ -ray transition should also represent a considerable amount of the total  $(\alpha,p)$  cross section at energies sufficiently far above the  $(\alpha,p)$  threshold. Surprisingly, similar to the  $^{26}\text{Mg}$  case, the experimental  $^{25}\text{Mg}(\alpha,p)^{28}\text{Al}$  data are overestimated by the StM by about one order of magnitude. Again, this statement holds for TALYS and NON-SMOKER calculations. However, again similar to  $^{26}\text{Mg}$ , the estimated  $(\alpha,p)$  cross sections from the thick-target yield of Roughton *et al.* [49] show reasonable agreement with the StM calculation.

The total reaction cross section  $\sigma_{\text{reac}}$  of  $^{25}\text{Mg}$  is well defined by the dominating  $^{25}\text{Mg}(\alpha,n)^{28}\text{Si}$  data, leading to the reduced cross sections  $\sigma_{\text{red}}$  shown in Fig. 53. Similar to most nuclei under study in this work, the  $\sigma_{\text{red}}$  data for  $^{25}\text{Mg}$  do not show a peculiar behavior.

#### 4.29 $^{24}\text{Mg}$

It is difficult to determine the total reaction cross section  $\sigma_{\text{reac}}$  of  $^{24}\text{Mg}$  at low energies. The  $^{24}\text{Mg}(\alpha,n)^{27}\text{Si}$  reaction has a strongly negative  $Q$ -value ( $Q = -7.20$  MeV) and thus does not contribute at low energies. Also the  $^{24}\text{Mg}(\alpha,p)^{27}\text{Al}$  reaction has a slightly negative  $Q$ -value ( $Q = -1.60$  MeV), and practically no experimental data

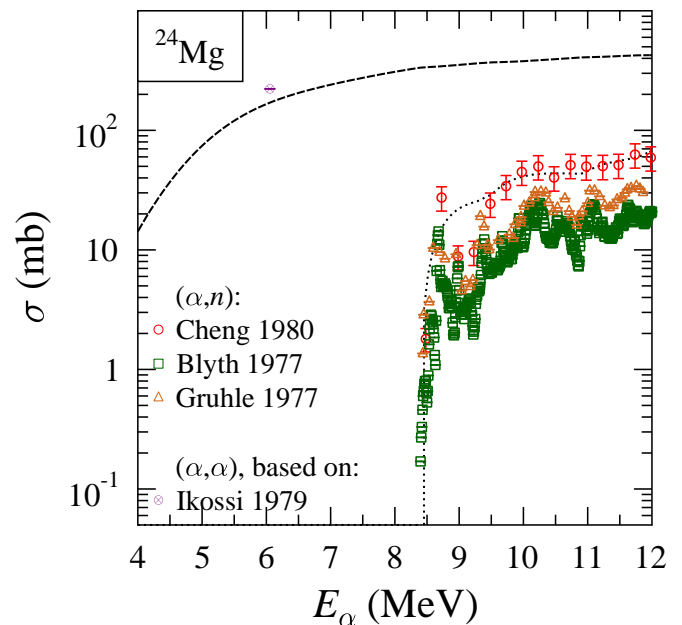


**Fig. 54.** Cross section of the  $^{24}\text{Mg}(\alpha,n)^{27}\text{Si}$  and  $^{24}\text{Mg}(\alpha,p)^{27}\text{Al}$  reactions. The experimental data have been taken from [118,136,137,138]. Further discussion see text.

can be found in EXFOR at low energies. At very low energies individual resonances of the  $^{24}\text{Mg}(\alpha,\gamma)^{28}\text{Si}$  reaction dominate.

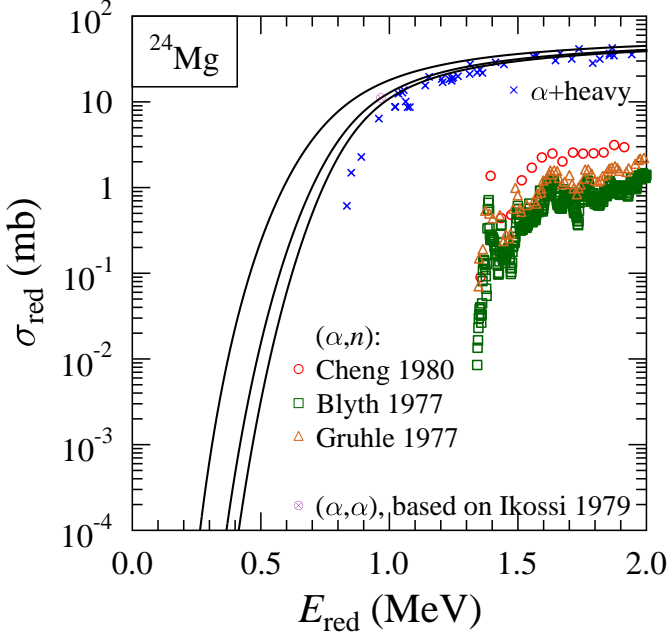


**Fig. 55.** Same as Fig. 5, but for  $\alpha$ -induced reactions on  $^{24}\text{Mg}$ . The experimental data have been taken from [118,136,137,138]. Further discussion see text.

The  $^{24}\text{Mg}(\alpha,n)^{27}\text{Si}$  reaction has been studied by Cheng *et al.* [118], by Blyth *et al.* [136], and by Gruhle *et al.* [137]. The data are shown in Fig. 54. All experiments used the activation technique in combination with annihilation spectroscopy. Unfortunately, there is a disagreement of about a factor of two between the three data sets. Note that the EXFOR data are based on a numerical table ([118]) and have been provided by the authors in numerical form ([136]), and only the data set of [137] had to be re-digitized from a figure; thus, the above discrepancy cannot be explained by simple digitization errors. Excellent agreement is found between the StM calculation and the data by Cheng *et al.* whereas the data by Blyth *et al.* and Gruhle *et al.* are overestimated.

Angular distributions of  $^{24}\text{Mg}(\alpha,\alpha)^{24}\text{Mg}$  elastic scattering have been measured by Ikossi *et al.* [138] at low energies. For one particular angular distribution at  $E_\alpha = 6.055\text{ MeV}$  a relatively thick target ( $33\ \mu\text{g}/\text{cm}^2$ ) was used; this angular distribution is appropriate for the determination of an average cross section because in addition the excitation function shows a smooth behavior around this energy. A phase shift fit leads to  $\sigma_{\text{reac}} = 222\text{ mb}$ , corresponding to  $\sigma_{\text{red}} = 11.1\text{ mb}$  at  $E_{\text{red}} = 0.97\text{ MeV}$ .

As the  $(\alpha,n)$  cross section contributes only minor to the total reaction cross section  $\sigma_{\text{reac}}$  of  $^{24}\text{Mg}$ , the experimental  $(\alpha,n)$  data are far below the expectations for  $\sigma_{\text{red}}$  as shown in Fig. 55. However, the data point from  $^{24}\text{Mg}(\alpha,\alpha)^{24}\text{Mg}$  elastic scattering is close to the general

expectation. Therefore, there is no evidence that the  $\sigma_{\text{red}}$  values for  $^{24}\text{Mg}$  behave extraordinary.

#### 4.30 $^{23}\text{Na}$

The  $^{23}\text{Na}(\alpha,n)^{26}\text{Al}$  reaction has significant astrophysical relevance because it affects the production of the long-lived  $^{26}\text{Al}$  nucleus. The observation of  $\gamma$ -rays from the  $^{26}\text{Al}$  decay in our galaxy confirms ongoing nucleosynthesis [139]. Very recently, an updated galactic emission map was derived from the SPI spectrometer data aboard the INTEGRAL mission [140]. Because of a low-lying  $0^+$  isomer in  $^{26}\text{Al}$  which decays directly to  $^{26}\text{Mg}$  and bypasses the  $5^+$  ground state of  $^{26}\text{Al}$ , much efforts have been made to distinguish the  $^{23}\text{Na}(\alpha,n)^{26}\text{Al}_{\text{g.s.}}$  and  $^{23}\text{Na}(\alpha,n)^{26\text{m}}\text{Al}$  reactions.

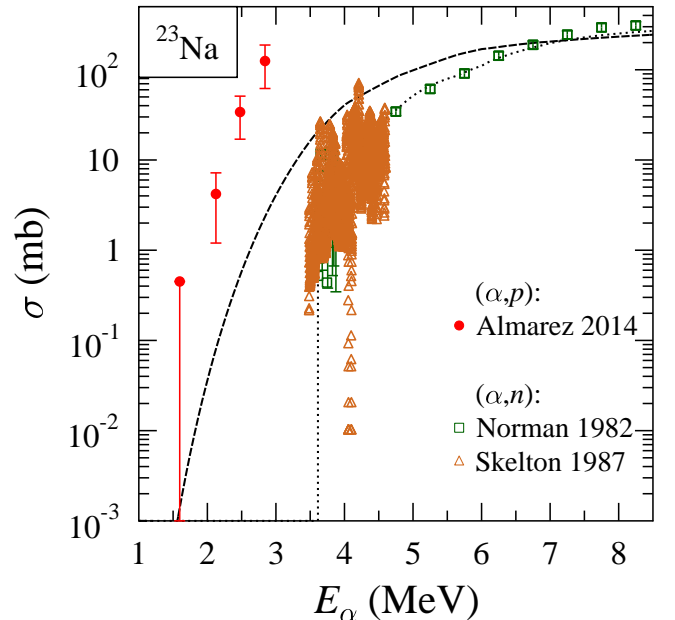


**Fig. 56.** Cross section of the  $^{23}\text{Na}(\alpha,n)^{26}\text{Al}$  and  $^{23}\text{Na}(\alpha,p)^{26}\text{Mg}$  reactions. The experimental data have been taken from [142,143,146]. Further discussion see text.

The  $^{23}\text{Na}(\alpha,n)^{26}\text{Al}$  reaction has been reviewed in the NACRE compilation [123], and the role of the isomer is discussed e.g. in [141]. Because of its negative  $Q$ -value ( $Q = -2.97\text{ MeV}$ ), this reaction does not affect the total reaction cross section  $\sigma_{\text{reac}}$  of  $^{23}\text{Na}$  at low energies. Therefore, only the total cross section of the  $^{23}\text{Na}(\alpha,n)^{26}\text{Al}$  is studied here.

The NACRE compilation [123] recommends three data sets for the  $^{23}\text{Na}(\alpha,n)^{26}\text{Al}$  reaction: Skelton *et al.* [142] and Norman *et al.* [143] have measured the total yield which can be directly converted to the total  $(\alpha,n)$  cross section. Doukellis and Rapaport [144] used the time-of-flight technique to resolve the  $n_0$ ,  $n_1$ , and  $n_2$  neutron groups at six laboratory angles. The data by Doukellis and

Rapaport are not available at EXFOR, and the numerical data at the NACRE web site seem to be re-digitized because the given energies are discrepant for the  $n_0$ ,  $n_1$ , and  $n_2$  groups. Consequently, it is practically impossible to derive the total  $(\alpha, n)$  cross section from the data by Doukellis and Rapaport. Such a determination is further hampered at higher energies by contributions of higher neutron groups  $n_{>2}$ . The recommendation of NACRE that “The DO87 time of flight experiment is indeed considered to be more reliable than the NO82 thick target measurements” is not well traceable, and the resulting recommendation to scale the Norman *et al.* data by a factor of 1/3 to adjust to the Doukellis and Rapaport data is not taken into account in this work. Here the original data of Norman *et al.* [143] and the data by Skelton *et al.* [142] are shown in Fig. 56. As thin-target measurements of [142] show many resonances, the StM calculation is only able to reproduce the average behavior of the excitation function. Furthermore, it can be seen from the StM calculations in Fig. 56 that the cross section of the  $^{23}\text{Na}(\alpha, p)^{26}\text{Mg}$  reaction exceeds the  $^{23}\text{Na}(\alpha, n)^{26}\text{Al}$  cross section significantly for energies below about 6 MeV.

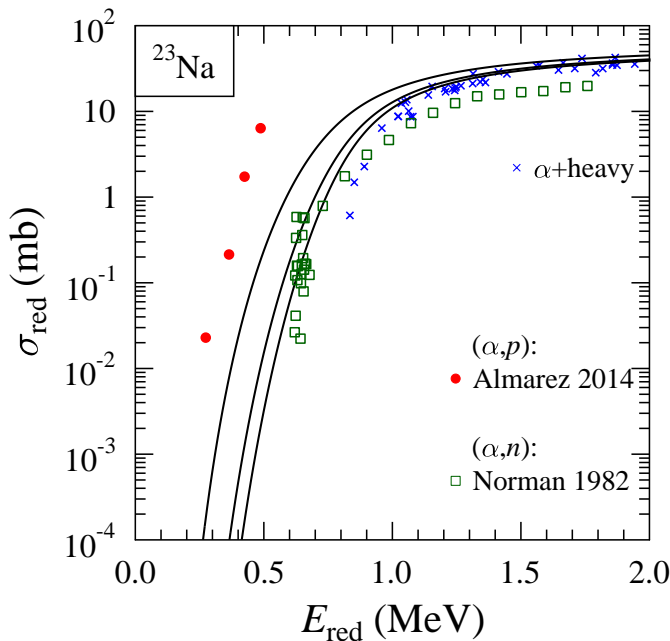


**Fig. 57.** Same as Fig. 5, but for  $\alpha$ -induced reactions on  $^{23}\text{Na}$ . The experimental data have been taken from [143, 146]. The lowest data point of Almarez-Calderon *et al.* [146] represents an upper limit only. For better visibility the data of Skelton *et al.* [142] are omitted. Further discussion see text.

In a detailed sensitivity study of the production of  $^{26}\text{Al}$  [6] it has been shown that the  $^{23}\text{Na}(\alpha, p)^{26}\text{Mg}$  reaction also plays an essential role in the production of  $^{26}\text{Al}$ . Low-energy data for the  $^{23}\text{Na}(\alpha, p)^{26}\text{Mg}$  reaction are available from Whitmire and Davids [145]. However, only resonance strengths have been determined in [145]. Some criticisms to this work have been reported in [6], and it was con-

cluded in [6] that StM calculations should be preferred and that the  $^{23}\text{Na}(\alpha, p)^{26}\text{Mg}$  reaction is a prime target for future measurements.

In a very recent study new experimental data for the  $^{23}\text{Na}(\alpha, p)^{26}\text{Mg}$  reaction at low energies became available. Almarez-Calderon *et al.* [146] used a  $^{23}\text{Na}$  beam in inverse kinematics to irradiate a cryogenic  $^4\text{He}$  gas target, and a silicon strip detector was placed 20 cm downstream from the target to detect protons in an angular range from  $\vartheta_{\text{lab}} = 6.8^\circ - 13.5^\circ$ . From the observed proton groups  $p_0$  and  $p_1$  average cross sections (averaged over the energy distribution of the beam which is caused by energy loss and straggling in the entrance window and in the target gas cell itself) were determined. However, the measured differential  $(\alpha, p)$  cross sections constrain the angular distribution of the  $(\alpha, p)$  cross section only in a very limited angular range. The determination of angle-integrated cross sections in [146] had to use angular distributions of the  $^{27}\text{Al}(\alpha, p)^{30}\text{Si}$  reaction where similar  $J^\pi$  of the nuclei under study are found. The resulting cross section of the  $p_0$  and  $p_1$  groups are finally summed to provide the total  $^{23}\text{Na}(\alpha, p)^{26}\text{Mg}$  cross sections. It can be seen from Fig. 56 that the experimental results are dramatically underestimated by the StM calculation. The total reaction cross section of  $^{23}\text{Na}$  is well defined by the  $^{23}\text{Na}(\alpha, p)^{26}\text{Mg}$  reaction already below about 6 MeV, and below the  $(\alpha, n)$  threshold the total reaction cross section  $\sigma_{\text{reac}}$  is almost entirely given by the only open particle channel. The results for the reduced cross section  $\sigma_{\text{red}}$  are shown in Fig. 57. It is obvious from Fig. 57 that the recent data by Almarez-Calderon *et al.* [146] deviate dramatically from the general behavior which is otherwise found for nuclei in the  $A \approx 20 - 50$  mass region. The new data lead not only to significantly higher  $\sigma_{\text{red}}$  values, but also to a steeper energy dependence than for other nuclei in the  $A \approx 20 - 50$  mass range.

#### 4.31 $^{22}\text{Ne}$

Because of the negative  $Q$ -value of the  $^{22}\text{Ne}(\alpha, p)^{25}\text{Na}$  reaction ( $Q = -3.53$  MeV), at astrophysically relevant energies the  $^{22}\text{Ne}(\alpha, n)^{25}\text{Mg}$  reaction dominates the total reaction cross section of  $^{22}\text{Ne}$ . This reaction plays a major role as neutron source for the astrophysical  $s$ -process. It is included in the NACRE compilation [123] where the data of Haas *et al.* [147] and Drotleff *et al.* [148, 149] are recommended. These data are shown in Fig. 58 and compared to a StM calculation. As the cross section is dominated by resonances at low energies, the StM calculation is only able to reproduce the average properties of the excitation function. Later data by Jaeger *et al.* [150] extend the measurements of Drotleff *et al.* towards lower energies. The cross section at these very low energies is essentially given by resonant contributions, and only an experimental yield (but not the cross section) is presented in [150]. Therefore, the data by Jaeger *et al.* [150] are not shown in Fig. 58 because there is no straightforward conversion from the experimental yield to the  $(\alpha, n)$  reaction cross section for extended gas target measurements (see e.g. [151]).

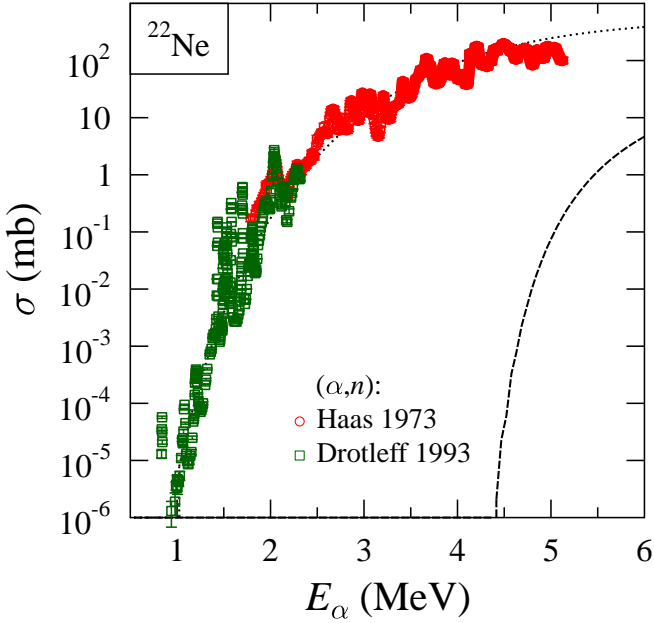


**Fig. 58.** Cross section of the  $^{22}\text{Ne}(\alpha,n)^{25}\text{Mg}$  and  $^{22}\text{Ne}(\alpha,p)^{25}\text{Na}$  reactions. The experimental data have been taken from [147,149]. Further discussion see text.

A full discussion of this reaction and the derived astrophysical reaction rate  $N_A\langle\sigma v\rangle$  has to include further indirect information (e.g., properties of levels in the compound  $^{26}\text{Mg}$  nucleus). This is beyond the scope of the present paper. New results for the  $^{22}\text{Ne}(\alpha,n)^{25}\text{Mg}$  reaction after publication of the first NACRE compilation [123] are

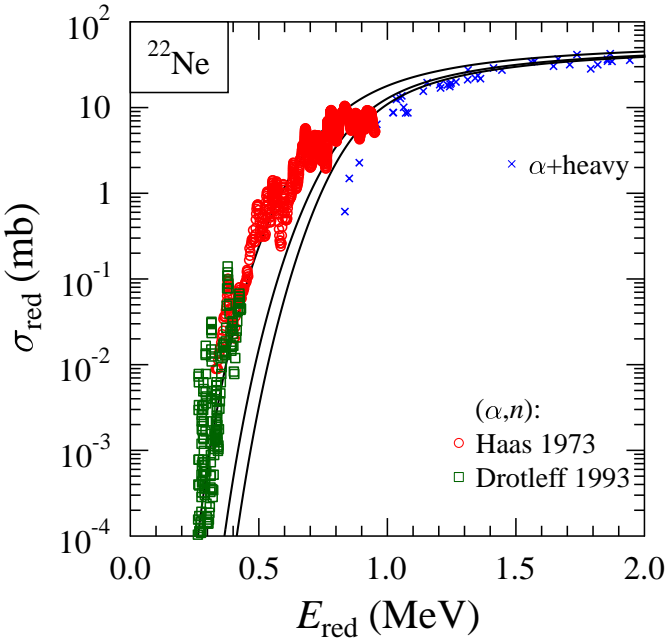


**Fig. 59.** Same as Fig. 5, but for  $\alpha$ -induced reactions on  $^{22}\text{Ne}$ . The experimental data have been taken from [147,149]. Further discussion see text.

e.g. summarized in [152], and further information is given in [153,154,155].

No data for the  $^{22}\text{Ne}(\alpha,p)^{25}\text{Na}$  reaction are listed in the EXFOR database. Fortunately, this does not affect the determination of the total reaction cross section  $\sigma_{\text{reac}}$  of  $^{22}\text{Ne}$  because of the dominating  $^{22}\text{Ne}(\alpha,n)^{25}\text{Mg}$  reaction. The  $(\alpha,n)$  cross section is presented as reduced cross section  $\sigma_{\text{red}}$  in Fig. 59. Similar to most nuclei under study in this work, the  $\sigma_{\text{red}}$  data for  $^{22}\text{Ne}$  do not show a peculiar behavior.

#### 4.32 $^{21}\text{Ne}$

Similar to the results for  $^{22}\text{Ne}$  in the previous section, the  $^{21}\text{Ne}(\alpha,n)^{24}\text{Mg}$  cross section is much larger than the  $^{21}\text{Ne}(\alpha,p)^{24}\text{Na}$  cross section. Because of the low natural abundance of  $^{21}\text{Ne}$ , only very few data exist for this nucleus. The NACRE compilation [123] recommends the data by Haas *et al.* [147] and Denker [156]. Surprisingly, the data of Mak *et al.* [157] are not taken into account in NACRE. Mak *et al.* report average cross sections (averaged over a about 100 keV thick neon gas target) which are in good agreement with the other data which are recommended in NACRE. In Fig. 60 the experimental data are compared to a StM calculation which is able to reproduce the average properties of the  $^{21}\text{Ne}(\alpha,n)^{24}\text{Mg}$  cross section. No data are available at EXFOR for the  $^{21}\text{Ne}(\alpha,p)^{24}\text{Na}$  reaction which has a negative  $Q$ -value of  $Q = -2.18$  MeV.

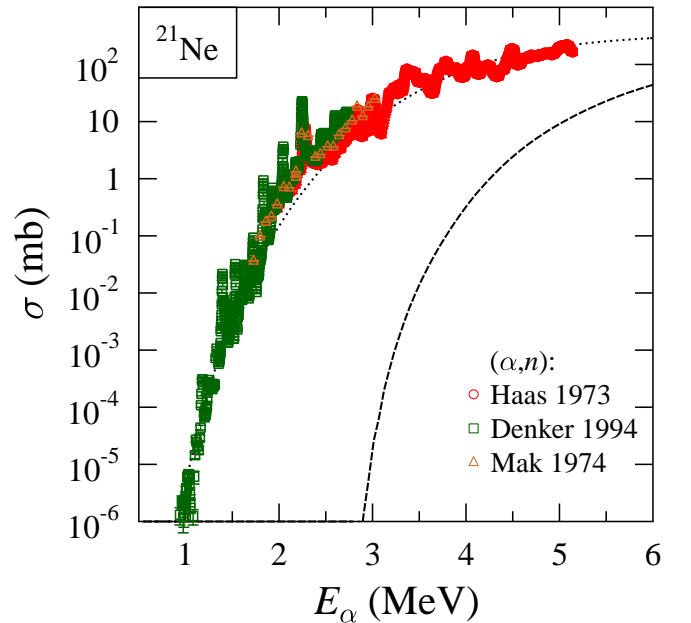


**Fig. 60.** Cross section of the  $^{21}\text{Ne}(\alpha,n)^{24}\text{Mg}$  and  $^{21}\text{Ne}(\alpha,p)^{24}\text{Na}$  reactions. The experimental data have been taken from [147,156,157]. Further discussion see text.

The reduced cross sections  $\sigma_{\text{red}}$  for  $^{21}\text{Ne}$  from the experimental  $^{21}\text{Ne}(\alpha,n)^{24}\text{Mg}$  data of [147,156,157] are shown

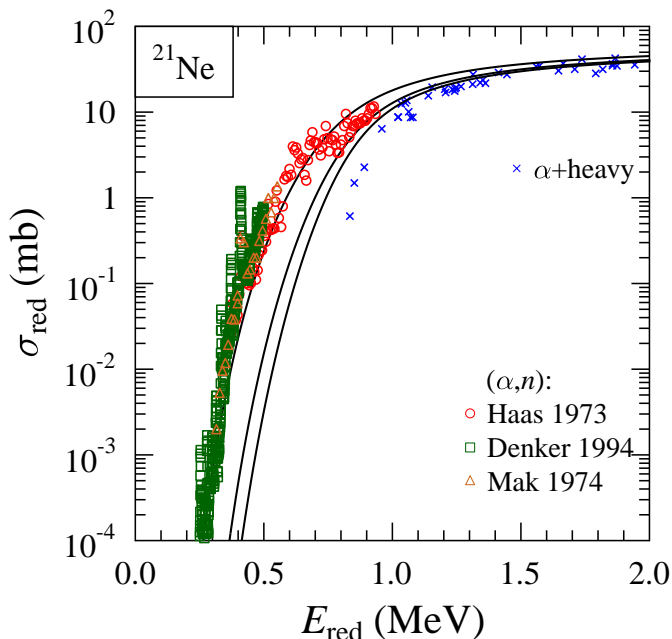


**Fig. 61.** Same as Fig. 5, but for  $\alpha$ -induced reactions on  $^{21}\text{Ne}$ . The experimental data have been taken from [147,156,157]. Further discussion see text.

in Fig. 61. Similar to most nuclei under study in this work, the  $\sigma_{\text{red}}$  data for  $^{21}\text{Ne}$  do not show a peculiar behavior.

#### 4.33 $^{20}\text{Ne}$

Because of the negative  $Q$ -values of the  $^{20}\text{Ne}(\alpha, n)^{23}\text{Mg}$  ( $Q = -7.22$  MeV) and  $^{20}\text{Ne}(\alpha, p)^{23}\text{Na}$  ( $Q = -2.38$  MeV) reactions, it is not possible to determine the total cross section of  $^{20}\text{Ne}$  at low energies from  $(\alpha, p)$  and  $(\alpha, n)$  data. The  $^{20}\text{Ne}(\alpha, \gamma)^{24}\text{Mg}$  reaction at low energies is dominated by isolated resonances (e.g., [159,151]), and the experimental yield in these gas target measurements is dominated over broad energy ranges by the tails of strong resonances.

Fig. 62 shows the available  $^{20}\text{Ne}(\alpha, n)^{23}\text{Mg}$  data at higher energies, i.e. above the  $(\alpha, n)$  threshold, in comparison to a StM calculation. As the cross section of the  $^{20}\text{Ne}(\alpha, n)^{23}\text{Mg}$  reaction is much smaller than the cross section of the  $^{20}\text{Ne}(\alpha, p)^{23}\text{Na}$  reaction, an attempt was made to estimate the total reaction cross section  $\sigma_{\text{reac}}$  from  $^{20}\text{Ne}(\alpha, \alpha)^{20}\text{Ne}$  elastic scattering at low energies. However, a phase shift analysis to the data of [95] at 13.1 MeV is only able to constrain  $\sigma_{\text{reac}}$  in a relatively wide range of  $\sigma_{\text{reac}} = 600 \pm 300$  mb because of the limited number of data points in [95]; this corresponds to  $\sigma_{\text{red}} = 32$  mb at  $E_{\text{red}} = 2.35$  MeV. Somewhat higher  $\sigma_{\text{red}}$  values between 58 and 78 mb were found from the analysis of full angular distributions from [160] at slightly higher energies from 15.8 to 17.8 MeV, corresponding to  $E_{\text{red}}$  between 2.83 and 3.19 MeV.

Unfortunately, no data for the  $^{20}\text{Ne}(\alpha, p)^{23}\text{Na}$  reaction can be found in the EXFOR database.  $\gamma$ -ray yields after bombardment of  $^{20}\text{Ne}$  with  $\alpha$ -particles have been reported in [161]. In principle, these yields should allow to

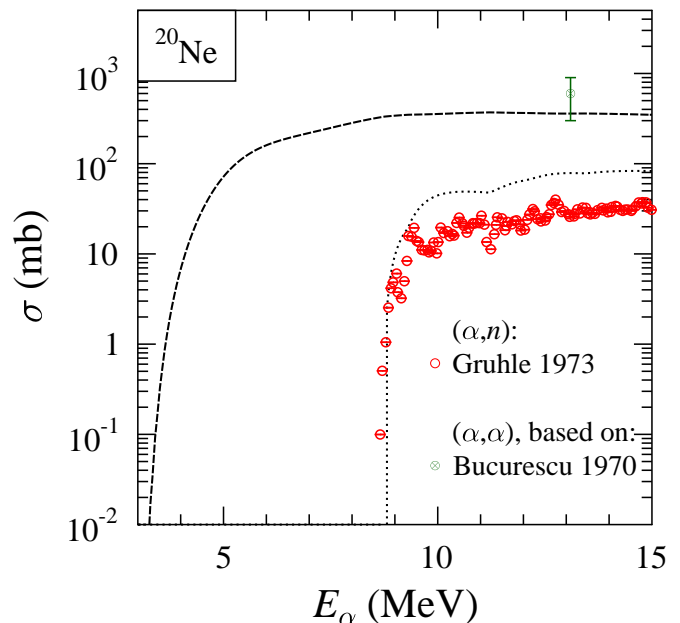


**Fig. 62.** Cross section of the  $^{20}\text{Ne}(\alpha, n)^{23}\text{Mg}$  and  $^{20}\text{Ne}(\alpha, p)^{23}\text{Na}$  reactions. The experimental data have been taken from [158,95]. Further discussion see text.

constrain the  $^{20}\text{Ne}(\alpha, p)^{23}\text{Na}$  cross section. However, the strong  $\gamma$  transition in  $^{23}\text{Na}$  at 1637 keV ( $7/2^+$ ; 2076 keV  $\rightarrow 5/2^+$ ; 440 keV) almost coincides with the first  $2^+$  in  $^{20}\text{Ne}$  at 1634 keV which is excited by inelastic scattering, and therefore it was not possible to distinguish between the  $(\alpha, p)$  reaction and inelastic scattering in [161]. No in-

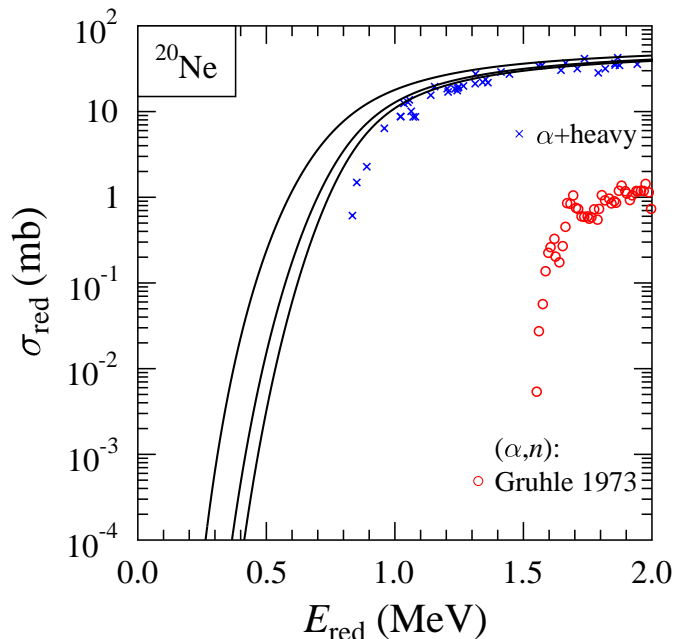


**Fig. 63.** Same as Fig. 5, but for  $\alpha$ -induced reactions on  $^{20}\text{Ne}$ . The experimental data have been taken from [158]. Further discussion see text.

formation is given in [161] on the 440 keV transition from the first excited state in  $^{23}\text{Na}$  to the ground state.

It is clear that the  $^{20}\text{Ne}(\alpha,n)^{23}\text{Mg}$  data are much lower than the expected values for reduced cross sections  $\sigma_{\text{red}}$  (see Fig. 63) because of the dominating  $^{20}\text{Ne}(\alpha,p)^{23}\text{Na}$  reaction. Nevertheless, together with the additional data from  $^{20}\text{Ne}(\alpha,\alpha)^{20}\text{Ne}$  elastic scattering at higher energies (above the shown range in Fig. 63) it can be concluded that there is at least no evidence for an unexpected behavior of  $\sigma_{\text{red}}$  of  $^{20}\text{Ne}$ .

#### 4.34 $^{18}\text{Ne}$

The experimental situation for the unstable  $^{18}\text{Ne}$  nucleus is completely different from all above examples. Only indirect data are available to constrain the  $^{18}\text{Ne}(\alpha,p)^{21}\text{Na}$  cross section, and the  $^{18}\text{Ne}(\alpha,n)^{21}\text{Mg}$  reaction does not contribute to the total reaction cross section  $\sigma_{\text{reac}}$  at low energies because of the strongly negative  $Q$ -value ( $Q = -11.24$  MeV). The available experimental information for the  $^{18}\text{Ne}(\alpha,p)^{21}\text{Na}$  reaction has been summarized recently in [28,162]. Although the  $^{18}\text{Ne}(\alpha,p)^{21}\text{Na}$  cross section is dominated by individual resonances, it has been shown in [28] that a StM calculation is roughly able to reproduce the average properties of the excitation function.

The latest result of [28] for the  $^{18}\text{Ne}(\alpha,p)^{21}\text{Na}$  cross section has been converted to the reduced cross section  $\sigma_{\text{red}}$ ; the result is shown in Fig. 64. Similar to most nuclei under study in this work, the  $\sigma_{\text{red}}$  data for  $^{18}\text{Ne}$  do not show a peculiar behavior.

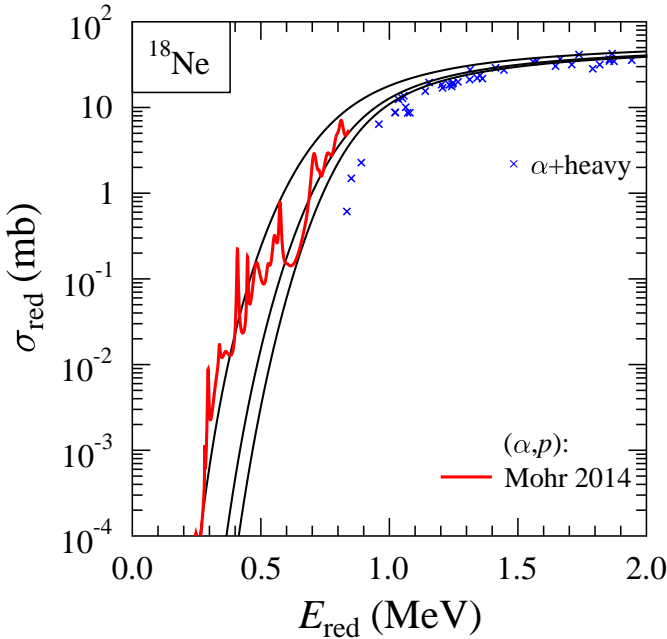


**Fig. 64.** Same as Fig. 5, but for  $\alpha$ -induced reactions on  $^{18}\text{Ne}$ . The estimate for the experimental cross section is taken from [28]. Further discussion see text.

#### 4.35 $^{19}\text{F}$

Because of its positive  $Q$ -value, the  $^{19}\text{F}(\alpha,p)^{22}\text{Ne}$  reaction dominates at low energies. Unfortunately, no total cross section data are available at EXFOR. The differential cross sections measured by Ugalde *et al.* [163] are fitted by an R-matrix calculation, and the R-matrix result is directly converted to the stellar reaction rate in [163]. The adopted rate of [163] is well reproduced by StM calculations using the  $\alpha$ -nucleus potential by McFadden and Satchler [21] (see Fig. 9 of [163]).

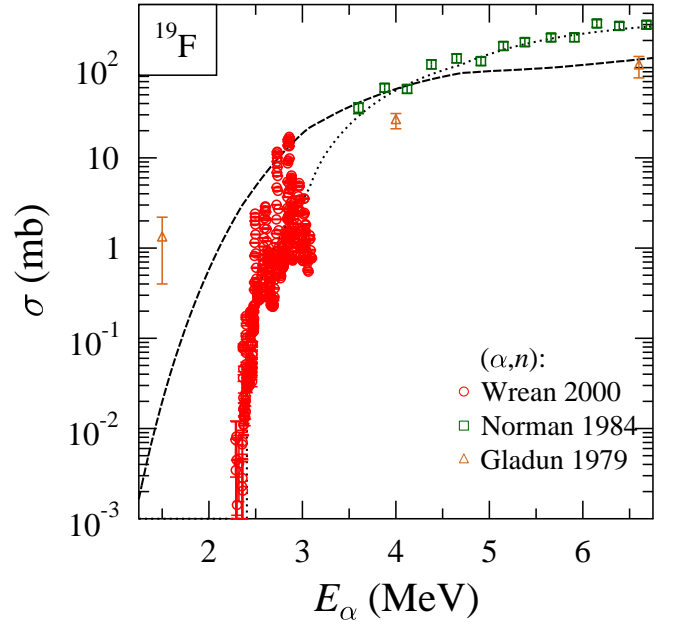


**Fig. 65.** Cross section of the  $^{19}\text{F}(\alpha,n)^{22}\text{Na}$  and  $^{19}\text{F}(\alpha,p)^{22}\text{Ne}$  reactions. The experimental data have been taken from [164, 165, 166]. Further discussion see text.

Several data sets are available for the  $^{19}\text{F}(\alpha,n)^{22}\text{Na}$  reaction. Wrean and Kavanagh [164] have used thin targets and direct neutron detection for their measurement at low energies below about 3.5 MeV. At higher energies Norman *et al.* [165] have measured thick-target neutron yields which were converted to cross sections by differentiation. The earlier data by Gladun and Chursin [166] have huge uncertainties in energy and deviate from the other experimental results [164, 165]. The thick-target data at higher energies [165] are well reproduced by the StM, and as expected, at lower energies the StM is only able to reproduce the average energy dependence of the experimental data of [164]. Earlier data by Balakrishnan *et al.* [167] are omitted because of problems with background from  $^{13}\text{C}$  (see discussion in [164] and similar problems of these authors for  $^{29}\text{Si}$ , see Sec. 4.24).

As the  $^{19}\text{F}(\alpha,p)^{22}\text{Ne}$  reaction dominates at low energies, it is not surprising that the reduced cross sections  $\sigma_{\text{red}}$  from the  $^{19}\text{F}(\alpha,n)^{22}\text{Na}$  data [164, 165, 166] are somewhat lower than the general trend of reduced cross

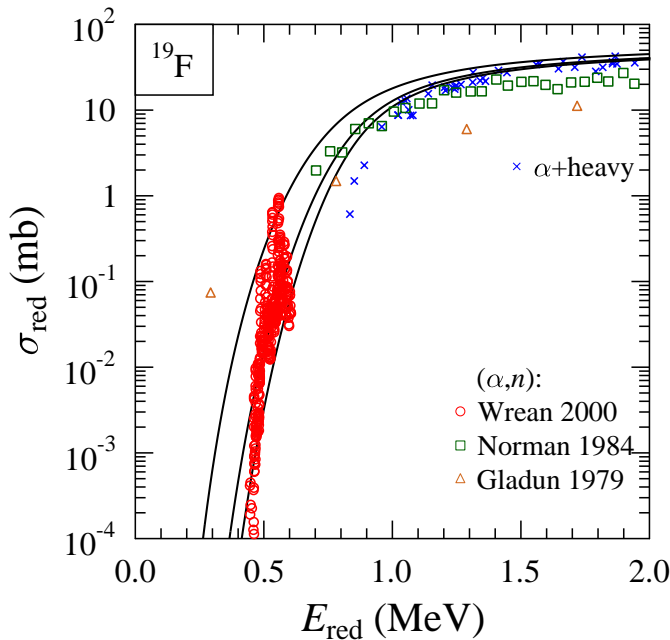


**Fig. 66.** Same as Fig. 5, but for  $\alpha$ -induced reactions on  $^{19}\text{F}$ . The experimental data have been taken from [164,165,166]. Further discussion see text.

sections. Nevertheless, from the excellent agreement of the experimental data and the StM calculations for the  $^{19}\text{F}(\alpha,p)^{22}\text{Ne}$  and  $^{19}\text{F}(\alpha,n)^{22}\text{Na}$  reactions it can be concluded that there is no evidence for a peculiar behavior of  $^{19}\text{F}$ .

## 5 Discussion

A first finding of the above presentation is that many experimental data for  $\alpha$ -induced reactions in the  $A \approx 20 - 50$  mass range show reasonable agreement. Major discrepancies between individual data sets have been discussed in the corresponding sections above. Nevertheless it should be kept in mind that in several cases absolute normalizations of the experimental data are stated with additional uncertainties of 10 – 20% which are not included in the shown error bars. New experimental data should provide absolute cross sections with small uncertainties, as has been done e.g. by Vonach *et al.* [57]. Additionally, for some reactions only one or even no data set is available. Here of course new data should provide excitation functions in small energy steps.

The general agreement between the experimental data and calculations in the StM is very good. The basic ingredient for the StM calculations is the  $\alpha$ -nucleus potential which essentially defines the total reaction cross section  $\sigma_{\text{reac}}$  for  $\alpha$ -induced reactions. As long as either the  $(\alpha,p)$  or  $(\alpha,n)$  cross section is the dominant (say greater than about 70 – 80%) contribution to  $\sigma_{\text{reac}}$ , the StM calculation is practically insensitive to all other ingredients of the StM. Fortunately, this is the case for many nuclei under

study in the  $A \approx 20 - 50$  mass region which allows a careful test of the  $\alpha$ -nucleus potential.

In the present study the simple energy-independent 4-parameter potential by McFadden and Satchler [21] has been chosen. As this potential leads to overestimation of  $\alpha$ -induced cross sections for a wide range of heavy target nuclei (above  $A \approx 60$ ) at low energies, the very good agreement between the experimental data and the StM calculation in the  $A \approx 20 - 50$  mass region is somewhat surprising. For heavy nuclei it has been suggested to add an energy dependence to the imaginary part of the McFadden/Satchler potential to avoid this typical overestimation of cross sections (e.g., [40,41]). Such an energy dependence is also expected from the theoretical side, and various parametrizations have been suggested like a Fermi-type function [40,41], the Brown-Rho parametrization [168], or a resonance-like parametrization [18]. All these parametrizations have two features in common: (i) They start from very small imaginary parts at very low energies and end at a saturation value at higher energies significantly above the Coulomb barrier; (ii) the increase is characterized by an energy where e. g. half of the saturation value is reached, and by a slope parameter. Such an energy dependence of the imaginary part reduces the total reaction cross section  $\sigma_{\text{reac}}$  towards lower energies, compared to the original McFadden/Satchler potential.

Obviously, such a reduction is not needed for the nuclei in the  $A \approx 20 - 50$  mass range. Following the discussion in McFadden and Satchler [21], it is stated that “There is a tendency for the heavier nuclei to favour smaller  $r_0$ , and for the lighter ones to favor larger  $r_0$ ”. A larger radius parameter  $r_0$  leads to increased total reaction cross sections  $\sigma_{\text{reac}}$ . Thus, strictly speaking, the 4-parameter McFadden/Satchler potential with the fixed radius parameter  $r_0 = 1.4$  fm has two shortcomings. First, the calculations should overestimate the experimental reaction cross sections  $\sigma_{\text{reac}}$  towards lower energies because of the missing energy dependence of the imaginary part. Second, the calculations should underestimate  $\sigma_{\text{reac}}$  because the adjustment of the potential to elastic scattering data in [21] requires a larger radius parameter than the fixed average value of  $r_0 = 1.4$  fm which is adopted by McFadden and Satchler. Therefore, the very good agreement between experimental data and the StM calculation using the McFadden/Satchler potential may even be considered as somewhat accidental because the missing energy dependence of the imaginary part may partly compensate the missing  $A$  dependence of the radius parameter  $r_0$ .

For some nuclei under study a good agreement between the StM calculation and the experimental data is found for the dominating channel whereas the StM calculation deviates strongly from the experimental data for the weak channel. The most prominent example for such a behavior is  $^{26}\text{Mg}$  where the dominating  $^{26}\text{Mg}(\alpha,n)^{29}\text{Si}$  cross section is well reproduced by the StM, but the  $^{26}\text{Mg}(\alpha,p)^{29}\text{Al}$  cross section is overestimated by about one order of magnitude. Such a behavior points to a deficiency in the theoretical treatment of the  $^{29}\text{Al} + p$  channel, as the  $\alpha$ -nucleus potential is confirmed by the reproduction of the  $(\alpha,n)$

channel. However, although two independent data sets [16,129] are available for the  $^{26}\text{Mg}(\alpha,p)^{29}\text{Al}$  reaction (see Sec. 4.27), both data sets have been obtained from the stacked-foil activation technique which has turned out to be not very reliable for low energies (see e.g. the huge scatter of such data for  $^{51}\text{V}$  in Fig. 6 in Sec. 4.3). A quite similar deviation for the  $(\alpha,p)$  channel can be seen for the neighboring  $^{25}\text{Mg}$  nucleus; however, here the experimental data represent only a partial cross section of the  $(\alpha,p)$  reaction (see Fig. 52 in Sec. 4.28). Interestingly, for both cases  $^{25}\text{Mg}$  and  $^{26}\text{Mg}$  the estimated  $(\alpha,p)$  cross sections from the thick-target yields in [49] show much better agreement with the StM calculations. Thus, it is not fully clear whether there is really a deficiency in the StM calculations or an experimental problem in the  $(\alpha,p)$  data of [16,129].

The agreement between experimental data and the StM calculation is limited to cases where the experimental cross section is averaged over a sufficient number of resonances in the compound nucleus. This sufficiently high level density is achieved for nuclei at the upper end of the mass range  $A \approx 20 - 50$  under study. For the lighter nuclei individual resonances become more and more visible. This obviously depends crucially on the experimental conditions like the energy spread of the beam and in particular on the target thickness. A nice example has been given for  $^{27}\text{Al}$  where thin-target data show many individual resonances whereas thick-target data from the same experiment show a smooth (i.e., non-resonant) energy dependence (see data from [108] in Fig. 48 in Sec. 4.26). As soon as the level density in the compound nucleus is not high enough, the StM calculation is only able to reproduce the general trend of the energy dependence of the excitation function, but not all the individual resonances.

The present study attempts to provide a comparison of reaction cross sections for various target nuclei at energies below and above the Coulomb barrier. For this purpose the method of reduced energies  $E_{\text{red}}$  and reduced cross sections  $\sigma_{\text{red}}$  was used [19]. It is found that the data for  $\alpha$ -induced cross sections in the  $A \approx 20 - 50$  mass range are slightly higher than the general results for  $\alpha$ -induced reactions on heavy (above  $A \approx 90$ ) targets [17,18]. The  $\sigma_{\text{red}}$  values increase relatively smoothly with decreasing target mass  $A$ . The expected range of  $\sigma_{\text{red}}$  values is indicated by three lines in all figures with reduced cross sections  $\sigma_{\text{red}}$ ; these lines correspond to the theoretical predictions for  $^{51}\text{V}$ ,  $^{36}\text{Ar}$ , and  $^{21}\text{Ne}$  (i.e., covering the mass range under study). An expected exception is the doubly-magic ( $Z = N = 20$ )  $^{40}\text{Ca}$  nucleus which shows slightly smaller  $\sigma_{\text{red}}$  compared to its neighboring nuclei (see Fig. 21 in Sec. 4.11). Surprisingly, not much differences are seen for even-even, even-odd, odd-even, and odd-odd nuclei. Unfortunately, experimental data for odd-odd nuclei are only scarcely available.

Four more significant exceptions from this generally smooth behavior of  $\sigma_{\text{red}}$  have been found. The results for  $^{40}\text{Ar}$  and  $^{36}\text{Ar}$  are far below the expected range of  $\sigma_{\text{red}}$  values. However, there are only very few data points which are based on one particular very old experiment [93]. New

data for  $^{40}\text{Ar}$  and  $^{36}\text{Ar}$  are highly desirable to illustrate this behavior. The recent results from the  $^{33}\text{S}(\alpha,p)^{36}\text{Cl}$  reaction [102] are slightly above the expected range; this discrepancy sharpens dramatically as soon as the additional cross section of the  $^{33}\text{S}(\alpha,n)^{36}\text{Ar}$  reaction (estimated from the theoretical ratio between  $(\alpha,p)$  and  $(\alpha,n)$  channel, see [20]) is taken into account. The summed  $(\alpha,p)$  and  $(\alpha,n)$  cross sections are far above the expected range for  $\sigma_{\text{red}}$ , and the energy dependence is much flatter than expected (see Fig. 37 in Sec. 4.20 and detailed discussion in [20]). Finally, the recent  $^{23}\text{Na}(\alpha,p)^{26}\text{Mg}$  data [146] are very far above the expected range, and they show a much steeper energy dependence than expected (see Fig. 57 in Sec. 4.30). As for both  $^{33}\text{S}$  and  $^{23}\text{Na}$  only one data set is available in the relevant energy range, new experimental data would be very helpful to confirm the unexpected behavior of these two nuclei.

The  $\sigma_{\text{red}}$  vs.  $E_{\text{red}}$  reduction scheme is very simple, and also other reduction schemes have been suggested. For  $^{33}\text{S}$  it was stated [20] that also the reduction scheme from [169] leads to similar conclusions.

The strong deviation between expected reduced cross sections  $\sigma_{\text{red}}$  and experimental results for  $^{40}\text{Ar}$ ,  $^{36}\text{Ar}$ ,  $^{33}\text{S}$ , and  $^{23}\text{Na}$  is correlated with a poor agreement between the experimental data and the StM calculations. From the otherwise smooth behavior of  $\sigma_{\text{red}}$  values for nuclei with  $A \approx 20 - 50$  it is obvious that it is not possible to find an  $\alpha$ -nucleus potential with smoothly varying parameters which is able to reproduce the general trend of  $\sigma_{\text{red}}$  and the lower outliers  $^{40}\text{Ar}$  and  $^{36}\text{Ar}$  and the upper outliers  $^{33}\text{S}$  and  $^{23}\text{Na}$  simultaneously.

## 6 Summary and conclusions

Reduced cross sections  $\sigma_{\text{red}}$  were derived for  $\alpha$ -induced reactions on nuclei in the  $A \approx 20 - 50$  mass range. This simple reduction scheme (reduced cross section  $\sigma_{\text{red}}$  versus reduced energy  $E_{\text{red}}$  as suggested in [19]) shows a very similar behavior for heavy-ion induced reactions in a broad energy range. It has been found earlier [17,18] that this reduction scheme works also well for  $\alpha$ -induced reactions on heavy nuclei. The present study shows that  $\alpha$ -induced reactions in the  $A \approx 20 - 50$  mass range show a trend of slightly larger reduced cross sections at low energies (below  $E_{\text{red}} \approx 1$  MeV) with decreasing target mass. However, this trend is weak and relatively smooth. Four outliers are identified:  $^{36}\text{Ar}$  and  $^{40}\text{Ar}$  with smaller  $\sigma_{\text{red}}$  values (based on early experimental data of [93]) and  $^{23}\text{Na}$  (based on [146]) and  $^{33}\text{S}$  (based on [102]) with significantly increased  $\sigma_{\text{red}}$  values.

In general, the calculation of  $E_{\text{red}}$  and  $\sigma_{\text{red}}$  allows for a quick and simple test whether the cross section of an  $\alpha$ -induced reaction for a particular nucleus behaves regularly or extraordinary. The present study provides the basis for such a comparison. From my point of view, such a test is strongly recommended for any new data on  $\alpha$ -induced reactions.

As a byproduct of the present study it was found that the reduced energy  $E_{\text{red}}$  has a simple approximate rela-

tion to the most effective energy for astrophysical reaction rates (the so-called Gamow window): e.g., for  $T_9 = 2$  the Gamow window appears around  $E_{\text{red}} \approx 0.45$  MeV for all nuclei under study in this work.

The experimental cross sections of  $\alpha$ -induced reactions in the  $A \approx 20 - 50$  mass range are compared to calculations in the statistical model. Here the cross section factorizes into a production cross section of the compound nucleus which depends on the chosen  $\alpha$ -nucleus potential, and into a decay branching of the compound state which depends on the other ingredients of the statistical model, but is almost independent of the  $\alpha$ -nucleus potential. Fortunately, for most of the nuclei under study, one particular reaction channel – ( $\alpha, p$ ) or ( $\alpha, n$ ) – is dominating which allows a strict test of the chosen  $\alpha$ -nucleus potential by comparing only the cross section of the dominating ( $\alpha, p$ ) or ( $\alpha, n$ ) channel; this test is only weakly affected by the other ingredients of the statistical model. Surprisingly it is found that the old and very simple 4-parameter potential by McFadden and Satchler [21] leads to very good agreement with most of the experimental data; i.e., the smooth energy dependence of excitation functions for nuclei in the upper half of the mass range  $A \approx 20 - 50$  is reproduced, and for the lighter nuclei under study the statistical model reproduces only the average energy dependence of the experimental excitation function which is governed by individual resonances. For the four outliers in the  $\sigma_{\text{red}}$  reduction scheme ( $^{40}\text{Ar}$ ,  $^{36}\text{Ar}$ ,  $^{33}\text{S}$ ,  $^{23}\text{Na}$ ) it is found that these nuclei also show poor agreement between the experimental data and the statistical model calculations for  $\alpha$ -induced reactions.

## Acknowledgments

I thank A. Laird for the encouragement to tackle this broad study and Z. Máté for providing the numerical data for  $^{34}\text{S}(\alpha, \alpha)^{34}\text{S}$  and  $^{50}\text{Cr}(\alpha, \alpha)^{50}\text{Cr}$ . The pleasant long-term collaboration on the  $\alpha$ -nucleus interaction with Zs. Fülöp, Gy. Gyürky, G. G. Kiss, and E. Somorjai is gratefully acknowledged. The present study benefits from the availability of experimental data in the EXFOR database – special thanks to N. Otsuka and coworkers for maintaining EXFOR. This work was supported by OTKA (K101328 and K108459).

### Note added in Proof:

According to a private communication with Alison Laird, new experiments on the  $^{23}\text{Na}(\alpha, p)^{26}\text{Mg}$  reaction have been done very recently. She points out that the “cross sections agree with NON-SMOKER, apart from at the lowest energies (below  $E_{\text{c.m.}} = 1.4$  MeV)” where the new data are even lower than the theoretical prediction. As the calculated  $^{23}\text{Na}(\alpha, p)^{26}\text{Mg}$  cross section in the StM depends essentially only on the chosen  $\alpha$ -nucleus potential, the agreement between the latest experimental data and theory also holds for the TALYS calculations in Fig. 56 (see Sec. 4.30). Thus, the status of  $^{23}\text{Na}$  may change from “outlier” to “regular behavior”.

## References

1. H. Schatz and K. E. Rehm, Nucl. Phys. **A777**, 601 (2006).
2. A. Parikh, J. José, F. Moreno and C. Iliadis, Astrophys. J. Suppl. **178**, 110 (2008).
3. F. Käppeler, R. Gallino, S. Bisterzo, W. Aoki, Rev. Mod. Phys. **83**, 157 (2011).
4. F. Käppeler and A. Mengoni, Nucl. Phys. **A777**, 291 (2006).
5. O. Straniero, R. Gallino, S. Cristallo, Nucl. Phys. **A777**, 311 (2006).
6. C. Iliadis, A. Champagne, A. Chieffi, M. Limongi, Astroph. J. Suppl. **193**, 16 (2011).
7. L.-S. The, D. D. Clayton, L. Jin, B. S. Meyer, Astroph. J. **504**, 500 (1998).
8. G. Magkotsios, F. X. Timmes, A. L. Hungerford, C. L. Fryer, P. A. Young, M. Wiescher, Astroph. J. Suppl. **191**, 66 (2010).
9. R. J. Murphy, B. Kozlovsky, G. H. Share, Astroph. J. Suppl. **215**, 18 (2014).
10. Y. Guan, L. A. Leshin, T. Ushikubo, G. J. Wasserburg, Astroph. J. **640**, 525 (2006).
11. X. Peng, F. He, X. Long, Nucl. Inst. Meth. Phys. Res. B **152**, 432 (1999).
12. D. P. Chowdhury, S. Pal, S. K. Saha, S. Gangadharan, Nucl. Inst. Meth. Phys. Res. B **103**, 261 (1995).
13. M. Soltani-Farshi, J. D. Meyer, P. Misaelides, K. Bethge, Nucl. Inst. Meth. Phys. Res. B **113**, 399 (1996).
14. A. Fenyvesi, F. Tárkányi, F. Szelecsényi, T. Takács, Z. Szücs, T. Molnár, S. Sudár, Appl. Rad. Isot. **46**, 1413 (1995).
15. S. M. Sahakundu, S. M. Qaim, G. Stöcklin, Appl. Rad. Isot. **30**, 3 (1979).
16. Y. Minai and T. Nozaki, Appl. Rad. Isot. **41**, 57 (1990).
17. P. Mohr, D. Galaviz, Zs. Fülöp, Gy. Gyürky, G. G. Kiss, E. Somorjai, Phys. Rev. C **82**, 047601 (2010).
18. P. Mohr, G. G. Kiss, Zs. Fülöp, D. Galaviz, Gy. Gyürky, E. Somorjai, At. Data Nucl. Data Tables **99**, 651 (2013).
19. P. R. S. Gomes, J. Lubian, I. Padron, R. M. Anjos, Phys. Rev. C **71**, 017601 (2005).
20. P. Mohr, Phys. Rev. C **89**, 058801 (2014).
21. L. McFadden and G. R. Satchler, Nucl. Phys. **84**, 177 (1966).
22. Gy. Gyürky, P. Mohr, Zs. Fülöp, Z. Halász, G. G. Kiss, T. Szücs, E. Somorjai, Phys. Rev. **86**, 041601(R) (2012).
23. S. J. Quinn *et al.*, Phys. Rev. C **89**, 054611 (2014).
24. P. Demetriou, C. Grama, and S. Goriely, Nucl. Phys. **A707**, 253 (2002).
25. M. Avrigeanu, A. C. Obreja, F. L. Roman, V. Avrigeanu, W. von Oertzen, At. Data Nucl. Data Tables **95**, 501 (2009).
26. M. Avrigeanu and V. Avrigeanu, Phys. Rev. C **82**, 014606 (2010).
27. V. Avrigeanu, M. Avrigeanu, C. Mănăilescu, Phys. Rev. C **90**, 044612 (2014).
28. P. Mohr, R. Longland, C. Iliadis, Phys. Rev. C **90**, 065806 (2014).
29. N. Otsuka *et al.*, Nucl. Data Sheets **120**, 272 (2014); EXFOR database available online at <http://www-nds.iaea.org/exfor/exfor.htm>.
30. G. Audi, M. Wang, A. H. Wapstra, F. G. Kondev, M. MacCormick, X. Xu, B. Pfeiffer, Chin. Phys. C **36**, 1287 (2012).
31. M. Wang, G. Audi, A. H. Wapstra, F. G. Kondev, M. MacCormick, X. Xu, B. Pfeiffer, Chin. Phys. C **36**, 1603 (2012).

32. P. N. de Faria *et al.*, Phys. Rev. C **81**, 044605 (2010).
33. A. Lépine-Szilý, R. Lichtenthaler, V. Guimaraes, Europ. Phys. J. A **50**, 128 (2014).
34. . Bredbecka, M. Brenner, K. M. Kallman, P. Manngard, Z. Mate, S. Szilagy, L. Zolnai, Nucl. Phys. **A574**, 397 (1994).
35. V. Chiste, R. Lichtenthaler, A. C. C. Villari, L. C. Gomes, Phys. Rev. C **54**, 784 (1996).
36. K. E. Rehm *et al.*, Phys. Rev. Lett. **89**, 132501 (2002).
37. P. Mohr, Proc. *Nuclear Physics in Astrophysics VII*, May 2015, York, UK, IOP Conf. Proc., to be published.
38. P. Mohr, Phys. Rev. C **84**, 055803 (2011).
39. P. Mohr, Phys. Rev. C **87**, 035802 (2013).
40. E. Somorjai *et al.*, Astron. Astrophys. **333**, 1112 (1998).
41. A. Sauerwein *et al.*, Phys. Rev. **84**, 045808 (2011).
42. W. Hauser and H. Feshbach, Phys. Rev. **87**, 366 (1952).
43. T. Rauscher, Int. J. Mod. Phys. E **20**, 1071 (2011).
44. A. J. Koning, S. Hilaire, and M. C. Duijvestijn, AIP Conf. Proc. **769**, 1154 (2005).
45. T. Rauscher and F.-K. Thielemann, At. Data Nucl. Data Tables **75**, 1 (2000); **79**, 47 (2001).
46. T. Rauscher, F.-K. Thielemann, K. L. Kratz, Phys. Rev. C **56**, 1613 (1997).
47. T. Rauscher, Astrophys. J. Suppl. **201**, 26 (2012).
48. A. Ingemarsson *et al.*, Nucl. Phys. **A676**, 3 (2000).
49. N. A. Roughton, T. P. Intrator, R. J. Peterson, C. S. Zaidins, At. Data Nucl. Data Tables **28**, 341 (1983).
50. N. A. Roughton, M. R. Fritts, R. J. Peterson, C. S. Zaidins, C. J. Hansen, At. Data Nucl. Data Tables **23**, 177 (1979).
51. C. S. Zaidins, Nucl. Inst. Meth. **120**, 125 (1974).
52. P. Mohr, T. Rauscher, H. Oberhummer, Z. Mate, Zs. Fulop, E. Somorjai, M. Jaeger, G. Staudt, Phys. Rev. C **55**, 1523 (1997).
53. V. N. Levkovskij, Middle Mass Nuclides ( $A = 40 - 100$ ) Activation Cross Sections By Medium Energy ( $E = 10 - 50$  MeV) Protons and Alpha Particles (Experiment and Systematics), Inter-vesi, Moscow, 1991.
54. A. J. Morton, A. F. Scott, S. G. Tims, V. Y. Hansper, D. G. Sargood, Nucl. Phys. **A573**, 276 (1994).
55. A. E. Vliks, J. F. Morgan, S. L. Blatt, Nucl. Phys. **A224**, 492 (1974).
56. Data base *ENDSF*, available online at [www.nndc.bnl.gov/ensdf](http://www.nndc.bnl.gov/ensdf).
57. H. Vonach, R. C. Haight, G. Winkler, Phys. Rev. C **28**, 2278 (1983).
58. V. Y. Hansper, A. J. Morton, S. G. Tims, C. I. W. Tingwell, A. F. Scott, D. G. Sargood, Nucl. Phys. **A551**, 158 (1993).
59. W. W. Bowman and M. Blann, Nucl. Phys. **A131**, 513 (1969).
60. A. Iguchi, J. At. Energy Soc. Japan **2**, 682 (1960).
61. J. Rama Rao, A. V. Mohan Rao, S. Mukherjee, R. Upadhyay, N. L. Singh, S. Agarwal, L. Chaturvedi, P. P. Singh, J. Phys. G **13**, 535 (1987).
62. N. L. Singh, S. Agarwal, J. Rama Rao, Can. J. Phys. **71**, 115 (1993).
63. N. L. Singh, S. Mukherjee, A. V. Mohan Rao, L. Chaturvedi, P. P. Singh, J. Phys. G **21**, 399 (1995).
64. A. A. Sonzogni, A. S. M. A. Romo, H. O. Mosca, S. J. Nassiff, J. Radioanal. Nucl. Chem. **170**, 143 (1993).
65. O. M. P. Bilaniuk, V. V. Tokarevskii, V. S. Bulkin, L. V. Dubar, O. F. Nemets, L. I. Slyusarenko, J. Phys. G **7**, 1699 (1981).
66. C. N. Chang, J. J. Kent, J. F. Morgan, S. L. Blatt, Nucl. Inst. Meth. **109**, 327 (1973).
67. A. J. Morton, S. G. Tims, A. F. Scott, V. Y. Hansper, C. I. W. Tingwell, D. G. Sargood, Nucl. Phys. **A537**, 167 (1992).
68. C. M. Baglin, E. B. Norman, R.-M. Larimer, G. A. Rech, AIP Conf. Proc. **769**, 1370 (2005).
69. A. J. Howard, H. B. Jensen, M. Rios, W. A. Fowler, B. A. Zimmerman, Astroph. J. **188**, 131 (1974).
70. A. A. Sonzogni *et al.*, Phys. Rev. Lett. **84**, 1651 (2000).
71. V. Margerin *et al.*, Phys. Lett. B **731**, 358 (2014).
72. T. Al-Abdullah *et al.*, Europ. Phys. J. A **50**, 140 (2014).
73. K. L. Chen and J. M. Miller, Phys. Rev. **134**, B1269 (1964).
74. V. Y. Hansper, C. I. W. Tingwell, S. G. Tims, A. F. Scott, D. G. Sargood, Nucl. Phys. **A504**, 605 (1989).
75. G. Gaul, H. Ludeckem R. Santo, H. Schmeing, R. Stock, Nucl. Phys. **A137**, 177 (1969).
76. C. W. Cheng and J. D. King, J. Phys. G **5**, 1261 (1979).
77. M. A. Buckby and J. D. King, J. Phys. G **9**, 85 (1983).
78. L. W. Mitchell, R. W. Kavanagh, M. E. Sevier, C. I. W. Tingwell, D. G. Sargood, Nucl. Phys. **A443**, 487 (1985).
79. J. J. Simpson, W. R. Dixon, R. S. Storey, Phys. Rev. C **4**, 443 (1971).
80. W. R. Dixon, R. S. Storey, J. J. Simpson, Can. J. Phys. **58**, 1360 (1980).
81. H. Nassar *et al.*, Phys. Rev. Lett. **96**, 041102 (2006).
82. C. Vockenhuber *et al.*, Phys. Rev. C **76**, 035801 (2007).
83. R. D. Hoffman *et al.*, Astroph. J. **715**, 1383 (2010).
84. D. Robertson, J. Gorres, P. Collon, M. Wiescher, H.-W. Becker, Phys. Rev. C **85**, 045810 (2012).
85. K. Schmidt *et al.*, Phys. Rev. C **88**, 025803 (2013).
86. C. Riley, K. Ueno, B. Linder, Phys. Rev. **135**, B1340 (1964).
87. C. R. Keedy, L. Haskin, J. Wing, J. R. Huizenga, Nucl. Phys. **82**, 1 (1966).
88. A. F. Scott, A. J. Morton, C. I. W. Tingwell, S. G. Tims, V. Y. Hansper, D. G. Sargood, Nucl. Phys. **A523**, 373 (1991).
89. T. Matsuo, J. M. Matuszek, N. D. Dudey, T. T. Sugihara, Phys. Rev. **139**, B886 (1965).
90. H. Oeschler, H. Schroter, H. Fuchs, L. Baum, G. Gaul, H. Ludecke, R. Santo, R. Stock, Phys. Rev. Lett. **28**, 694 (1972).
91. J. W. Nelson, J. D. Oberholtzer, H. S. Plendl, Nucl. Phys. **62**, 434 (1965).
92. A. F. Scott, C. I. W. Tingwell, V. Y. Hansper, S. G. Tims, D. G. Sargood, Nucl. Phys. **A475**, 548 (1987).
93. R. B. Schwartz, J. W. Corbett, W. W. Watson, Phys. Rev. **101**, 1370 (1956).
94. S. Tanaka, M. Furukawa, T. Mikumo, S. Iwata, M. Yagi, H. Amano, J. Phys. Soc. Japan **15**, 952 (1960).
95. D. Bucurescu, M. Ivascu, G. Semencescu, M. Titirici, Rev. Roum. Phys. **15**, 1093 (1971).
96. L. Seidlitz, E. Bleuler, D. J. Tendam, Phys. Rev. **110**, 682 (1958).
97. K. Kocher, R. Neu, F. Hoyler, H. Abele, P. Mohr, G. Staudt, P. D. Eversheim, F. Hinterberger, Phys. Rev. C **45**, 123 (1992).
98. J. L. Zyskind, J. M. Davidson, M. T. Esat, M. H. Shapiro, R. H. Spear, Nucl. Phys. **A331**, 180 (1979).
99. S. M. Qaim, M. S. Sutisna, H. Ollig, Appl. Rad. Isot. **39**, 479 (1988).
100. F. Tarkanyi, Z. Kovacs, I. Mahunka, O. Solin, J. Bergman, Radiochim. Acta **54**, 165 (1991).

101. A. F. Scott, A. J. Morton, S. G. Tims, V. Y. Hansper, D. G. Sargood, Nucl. Phys. **A552**, 363 (1993).
102. M. Bowers, Y. Kashiv, W. Bauder, M. Beard, P. Collon, W. Lu, K. Ostdiek, D. Robertson, Phys. Rev. C **88**, 065802 (2013).
103. A. Coban, M. S. Abdelmonem, F. Z. Khiari, A. A. Naqvi, A. Aksoy, Nucl. Phys. **A645**, 3 (1999).
104. J. P. Aldridge, G. E. Crawford, R. H. Davis, Phys. Rev. **167**, 1053 (1968).
105. W. A. Schier, B. K. Barnes, G. P. Couchell, J. J. Egan, P. Harihar, S. C. Mathur, A. Mittler, E. Scheldon, Nucl. Phys. **A254**, 80 (1975).
106. W. R. McMurray, D. M. Holz, I. J. van Heerden, G. Wiechers, Z. Phys. A **247**, 453 (1971).
107. C. J. Umbarger, K. W. Kemper, J. W. Nelson, H. S. Plendl, Phys. Rev. C **2**, 1378 (1970).
108. D. S. Flynn, K. K. Sekharan, B. A. Hiller, H. Laumer, J. L. Weil, F. Gabbard, Phys. Rev. C **18**, 1566 (1978).
109. W. Wühr, A. Hofmann, G. Philipp, Z. Phys. **269**, 365 (1974).
110. J. H. Gibbons and R. L. Macklin, Phys. Rev. **114**, 571 (1959).
111. M. Balakrishnan, M. K. Mehta, A. S. Divatia, S. Kailas, Phys. Rev. C **11**, 54 (1975).
112. M. Siemaszko *et al.*, J. Phys. G **20**, 1789 (1994).
113. J. Vernotte, M. Langevin, F. Takeuchi, Nucl. Phys. **A102**, 449 (1967).
114. J. W. Toevs, Nucl. Phys. **A172**, 589 (1971).
115. D. W. O. Rogers, W. R. Dixon, R. S. Storey, Nucl. Phys. **A281**, 345 (1977).
116. M. Babilon *et al.*, Phys. Rev. C **66**, 028801 (2002).
117. M. A. Buckby and J. D. King, Can. J. Phys. **62**, 134 (1984).
118. C. W. Cheng and J. D. King, Can. J. Phys. **58**, 697 (1980).
119. A. Coban, F. Z. Khiari, M. S. Abdelmonem, A. Aksoy, A. A. Naqvi, Nucl. Phys. **A678**, 3 (2000).
120. K. M. Källman, M. Brenner, V. Z. Goldberg, T. Lönnroth, P. Manngård, A. E. Pakhomov, V. V. Pankratov, Europ. Phys. J. A **16**, 159 (2003).
121. F. de S. Barros, P. D. Forsyth, A. A. Jaffe, I. J. Taylor, Proc. Phys. Soc. (London) **73**, 793 (1959).
122. J. Kuperus, Physica **31**, 1069 (1965).
123. C. Angulo *et al.*, Nucl. Phys. **A656**, 3 (1999).
124. Y. Xu, K. Takahashi, S. Goriely, M. Arnould, M. Ohta, H. Utsunomiya, Nucl. Phys. **A918**, 61 (2013).
125. P. H. Stelson and F. K. McGowan, Phys. Rev. **133**, B911 (1964).
126. B. Holmqvist and E. Ramström, Phys. Scr. **33**, 107 (1986).
127. V. V. Dyachkov, A. V. Yushkov, A. L. Shakirov, J. Instr. Exp. Techn. **56**, 521 (2013).
128. O. H. Gailar, E. Bleuler, D. J. Tendam, Phys. Rev. **112**, 1989 (1958).
129. H. J. Probst, S. M. Qaim, R. Weinreich, Appl. Rad. Isot. **27**, 431 (1976).
130. M. R. Anderson, L. W. Mitchel, M. E. Sevier, D. G. Sargood, Nucl. Phys. **A405**, 170 (1983).
131. O. Wieland, Diploma thesis, University Stuttgart, 1995 (unpublished).
132. S. Falahat, PhD thesis, University Mainz, 2010 (unpublished).
133. L. van der Zwan and K. W. Geiger, Nucl. Sci. Eng. **79**, 197 (1981).
134. A. Caciolli *et al.*, Europ. Phys. J. A **50**, 147 (2014).
135. A. Negret *et al.*, Phys. Rev. C **88**, 034604 (2013).
136. C. O. Blyth and R. Greenwood-Smith, Nucl. Phys. **A288**, 242 (1977).
137. W. Gruhle and K.-H. Möbius, Z. Phys. A **283**, 97 (1977).
138. P. G. Ikossi, K. A. Snover, J. L. Osborne, E. G. Adelberger, Nucl. Phys. **A319**, 109 (1979).
139. R. Diehl *et al.*, Nature **439**, 84 (2006).
140. L. Bouchet, E. Jourdain, J.-P. Roques, Astroph. J. **801**, 142 (2015).
141. R. A. Ward and W. A. Fowler, Astroph. J. **238**, 266 (1980).
142. R. T. Skelton, R. W. Kavanagh, D. G. Sargood, Phys. Rev. C **35**, 45 (1987).
143. E. B. Norman, T. E. Chupp, K. T. Lesko, P. Schwabach, P. J. Grant, Nucl. Phys. **A390**, 561 (1982).
144. G. Doukellis and J. Rapaport, Nucl. Phys. **A467**, 511 (1987).
145. D. P. Whitmire and C. N. Davids, Phys. Rev. C **9**, 996 (1974).
146. S. Almaraz-Calderon *et al.*, Phys. Rev. Lett. **112**, 152701 (2014).
147. F. X. Haas and J. K. Bair Phys. Rev. C **7**, 2432 (1973); Erratum: J. K. Bair and F. X. Haas, Phys. Rev. C **10**, 961 (1974).
148. H. W. Drotleff, A. Denker, J. W. Hammer, H. Knee, S. Küchler, D. Streit, C. Rolfs, H. P. Trautvetter, Z. Phys. A **338**, 367 (1991).
149. H. W. Drotleff, A. Denker, H. Knee, M. Soine, G. Wolf, J. W. Hammer, U. Greife, C. Rolfs, H. P. Trautvetter, Astrophys. J. **414**, 735 (1993).
150. M. Jaeger, R. Kunz, A. Mayer, J. W. Hammer, G. Staudt, K.-L. Kratz, B. Pfeiffer, Phys. Rev. Lett. **87**, 202501 (2001).
151. V. Kölle *et al.*, Nucl. Inst. Meth. Phys. Res. A **431**, 160 (1999).
152. R. Longland, C. Iliadis, A. I. Karakas, Phys. Rev. C **85**, 065809 (2012).
153. R. Longland, C. Iliadis, G. Rusev, A. P. Tonchev, R. J. deBoer, J. Görres, M. Wiescher, Phys. Rev. C **80**, 055803 (2009).
154. R. J. deBoer, M. Wiescher, J. Görres, R. Longland, C. Iliadis, G. Rusev, A. P. Tonchev, Phys. Rev. C **82**, 025802 (2010).
155. R. J. deBoer, A. Best, J. Görres, K. Smith, W. Tan, M. Wiescher, R. Raut, G. Rusev, A. P. Tonchev, W. Tornow, Phys. Rev. C **89**, 055802 (2014).
156. A. Denker, PhD thesis, University Stuttgart, 1994 (unpublished).
157. H.-B. Mak, D. Ashery, C. A. Barnes, Nucl. Phys. **A226**, 493 (1974).
158. W. Gruhle, Th. Bauer, T. H. Seligmann, H. H. Hackenbroich, Z. Phys. **262**, 271 (1973).
159. P. Schmalbrock, H. W. Becker, L. Buchmann, J. Görres, K. U. Kettner, W. E. Kieser, H. Kräwinkel, C. Rolfs, H. P. Trautvetter, J. W. Hammer, R. E. Azuma, Nucl. Phys. **A398**, 279 (1983).
160. J. W. Frickey, K. A. Eberhard, R. H. Davis, Phys. Rev. C **4**, 434 (1971).
161. A. G. Seamster, E. B. Norman, D. D. Leach, P. Dyer, D. Bodansky, Phys. Rev. C **29**, 394 (1984).
162. P. Mohr and A. Matic, Phys. Rev. C **87**, 035801 (2013).

163. C. Ugalde, R. E. Azuma, A. Couture, J. Görres, H. Y. Lee, E. Stech, E. Strandberg, W. Tan, M. Wiescher, Phys. Rev. C **77**, 035801 (2008).
164. P. R. Wrean and R. W. Kavanagh, Phys. Rev. C **62**, 055805 (2000).
165. E. B. Norman, T. E. Chupp, K. T. Lesko, P. J. Grant, G. L. Woodruff, Phys. Rev. C **30**, 1339 (1984).
166. V. T. Gladun and G. P. Chursin, Izv. Akad. Nauk. KazSSSR, Ser. Fiz. Mat. **14**, 82 (1979).
167. M. Balakrishnan, S. Kailas, M. K. Mehta, Pramana **10**, 329 (1978).
168. G. E. Brown and M. Rho, Nucl. Phys. **A372**, 397 (1981).
169. R. Wolski, Phys. Rev. C **88**, 041603(R) (2013).